Tribology of Sliding Contacts Within Plain Bearing Overlays Subject To Corrosion

Padmapriya Nataraj

A thesis is submitted in partial fulfilment of the requirements of
Faculty of Science and Technology, Department of Design and Engineering,
Bournemouth University for the degree of Doctor of Philosophy

October 2020

Faculty of Science and Technology, Bournemouth University

In Collaboration with

Daido Metal Co., Ltd., Ilminster, UK

Copyright Statement

Tribology of Sliding Contacts Within Plain Bearing Overlays Subject to Corrosion

Padmapriya Nataraj

Abstract

The increasing global awareness and legislative restrictions has influenced the design within Internal Combustion (IC) engines. In addition to meeting environmental requirements the specified materials should be suitable to withstand extreme operating conditions such as high combustion pressures that attains the optimum fuel economy whilst reducing the exhaust emissions.

The lead-free materials exhibit near analogous mechanical and tribological properties to the traditional lead-based materials. The plain bearings are subjected to many different laboratory-based performance tests for instance, ring-on-disc, pin-on-disc that screen candidate materials as cost effectively as possible prior to much more expensive full engine-based tests. However, it is still uncertain how these lead-free bearing materials behave in different lubrication regimes such as mixed and boundary lubrication regime. The corrosion resistance of these materials also need to be especially within used lubricant conditions.

In advance of tribology experiments a static immersion test is employed to investigate the corrosion resistance of lead-free lining and overlay materials in both new oil and degraded oil environments. The surface topography and chemical composition of the tested materials are examined using a scanning electron microscope in-built with energy dispersive x-ray spectroscopy. A digital optical microscope was also used to understand tested surface damage mechanisms. Furthermore, X-ray photoelectron spectroscopy was used to understand the chemical composition at the surface of tested materials. With aid of these characterization techniques the corrosion mechanisms of the tested materials are investigated.

A newly designed and developed test-rig module was used to investigate the tribological performance of hydrodynamic bearing shells. This test-rig simulates

automotive engine representative conditions experienced plain bearings during operation. Wear rate of these materials were explored using this new test methodology. The materials considered are tin based lead-free overlay and lead based overlays considered as a reference.

Presentations (resulted from this research project)

Industrial Presentations

1. P. Nataraj “Tribology of Sliding Contacts Within Plain Bearing Overlays Subject To Corrosion” Daido Metal Co., Ltd., Ilminster, UK, 26 July 2016
2. P. Nataraj “Comparison of corrosion behaviour of Pb-based and Pb-free linings and Overlays” Daido Metal Co., Ltd., Ilminster, UK, 28 July 2017
3. P. Nataraj “Tribological properties of Sliding Contacts of Plain Bearings by using Novel Test-rig” Bournemouth University, Poole, UK, 31October 2017
4. P. Nataraj “Tribological properties of Sliding Contacts of Plain Bearings by using Novel Test-rig” Daido Metal Co., Ltd., Ilminster, UK, 6 June 2018
5. P. Nataraj “Tribology of Sliding Contacts Within Plain Bearing Overlays Subject To Corrosion” Bournemouth University, Poole, UK, 3 November 2018

Workshops presentations/ Hands-on Training

1. Presented XPS data of corrosion tested plain bearings and Completed hands on training on CASAXPS and data processing course on 4th July 2017 UKSAF, Teignmouth, UK
2. Completed hands on training on QUASES by Prof. Sven Tougaard, Research director of QUASES-Tougaard Inc. on 6th July 2017, Teignmouth, UK

Achievements and Awards

1. PhD match funded by Bournemouth University, Poole and Daido Metal Co., Ltd., Ilminster, UK Ltd.

Table of Contents

List of Figures

List of Tables

Acknowledgements

Foremost, I would like to express my sincere gratitude to my supervisor Prof. Mark Hadfield for the continuous support of my PhD study and related research, for his patience, motivation, and immense knowledge. His guidance helped me in all the time of research and writing of this thesis report.

I would like to thank my supervisor Dr. Roya Haratian for her valuable suggestions and patience all the time of thesis writing.

Special thanks to my supervisor Dr. Yi Zhang for his guidance during this work, and for helping me to gain insights in the field of bearing materials and its applications.

I would also like to thank Daido Metal Co., Ltd. Ilminster for providing test materials and allowed me to use laboratory facilities.

I am grateful to Mr. Dave Fletcher Jones for his constant support for designing and manufacturing the tribometer test-rig for my PhD study.

I would like to thank Dr. Mayank Anand for his helpful suggestions concerning the interpretation and analysis of the data. I would like to thank project administrator Naomi Bailey for continuous support and encouragement. Further thanks and gratitude to Dr. Ignacio Tudela for his suggestions and encouragement.

I would like to thank the staff in the workshop, particularly Robert Gardiner, Stephen Fordham for their help and support in the laboratories.

I should also mention my parents, husband, son who contributed continuous support and encouragement. Finally, I appreciate help and support of colleagues and friends.

Author's Declaration

This report contains the original work of the author except otherwise indicated. This research is match funded by Bournemouth University, UK and Daido Metal Co., Ltd., Ilminster, UK. All contents of this report except materials from external referencing are subject to confidentiality.

Nomenclature

Cu	*Copper*
Pb	*Lead*
Bi	*Bismuth*
Sn	*Tin*
λ	*Film thickness*
σ	*r.m.s roughness of the two counter surfaces*
R_{q1} *and* $R_{q2}x$	*the roughness for each surface*
Al	*Aluminum*
MoS_2	*Molybdenum disulphide*
MPa	*Mega Pascal*
PVD	*Physical Vapour Deposition*
Si	*Silicon*
kN	*KiloNewton*
T	*Temperature*
t	*Time*
sec	*Second*

Abbreviations

SEM	*Scanning Electron Microscopy*
EDX	*Energy Dispersive X-ray Spectroscopy*
XPS	*X-ray Photoelectron Spectroscopy*
SCC	*Stress corrosion cracking*
PAI	*polyamide-imide*
COF	*Coefficient of Friction*
PO	*Project Objective*
JBTR	*Journal Bearing Test-rig*

Chapter 1 Introduction

1.1 Tribology

Most machine components involve the relative motion of two surfaces. Wear and friction behaviour depend on the surface properties of two interacting materials mostly in the presence of lubricant. The term 'Tribology' is defined as the science and technology of interacting surfaces in relative motion and of various subjects include friction, wear and lubrication. "Wear may be defined as the progressive loss of substance from the operating surface of a body occurring as a result of relative motion of the surface" (Ozsarac 2007). Friction and wear are not intrinsic material properties, friction coefficients and wear rates are characteristics of the whole tribosystem (Ozsarac 2007). Friction is the root cause of wear and energy loss; however, it can be controlled by a lubricant. The introduction of lubricants in tribo systems can minimize the friction and wear and moreover, the energy and material losses are reduced.

Wear is defined as the strong irreversible and dissipative interrelations between the components, but it is not an intrinsic property of material. It is rarely catastrophic although replacement of components are necessary because it reduces the operating efficiency by increasing the power loss, the oil consumption, and the rate of component replacement (Jayne 2002). The material transfer from one surface to other is more evident in dry sliding. Hence wear rates in dry sliding are three times in order of magnitude compared with a lubricated system. The load carrying capacity of the components are improved in lubricated sliding contact, where the surfaces are separated by oil film (Jayne 2002).

The effective lubrication of engine components is essential to facilitate the minimum wear and friction and lessen the impact on the environment. This task is quite difficult due to the wide range of operating conditions of the engine for instance, speed, load and temperature (Priest 2000, Taylor 1998, Summer 2019). The enhanced tribological performance of the engine bring about following benefits: reduced fuel and oil

consumption, increased engine efficiency, reduced harmful exhaust emissions, and lower the maintenance requirement such as the replacement of components and assemblies (Tung 2004). Slightest enhancement in engine efficiency can have a major consequence in world fuel economy and the environment in a long-term (Tung 2004).

The two opposing surfaces are separated by means of a lubricant or a fluid film in some cases. In some cases, the chemical film formed on the surface to produce protection during the period of boundary lubrication regime. Alkaline agents from the lubricant neutralize the acids which form in hot spots (Tung 2004). The lubricant aids the transport of the waste products away from the place where they are generated and likewise, it provides the shielding chemicals towards the site where it is required. The choice of a suitable lubricant is related to the type of engine components. For instance, the engine oil should be effective to withstand the fuel, combustion products and water especially during cold-start conditions (Tung 2004).

1.2 Lubrication regimes

The fluid film formation is not adequate to deliver complete wear protection in the time of high load and high-temperature conditions. In such cases, the additives are supportive to form a chemical film on the component surface that protects from wear and corrosion. The chemical film can be removed from the surface during severe engine conditions (Tung 2004). However, depending on the viscosity, speed, surface finish, loads, lubricant and materials, different lubrication regimes prevail as shown in fig.1.1.

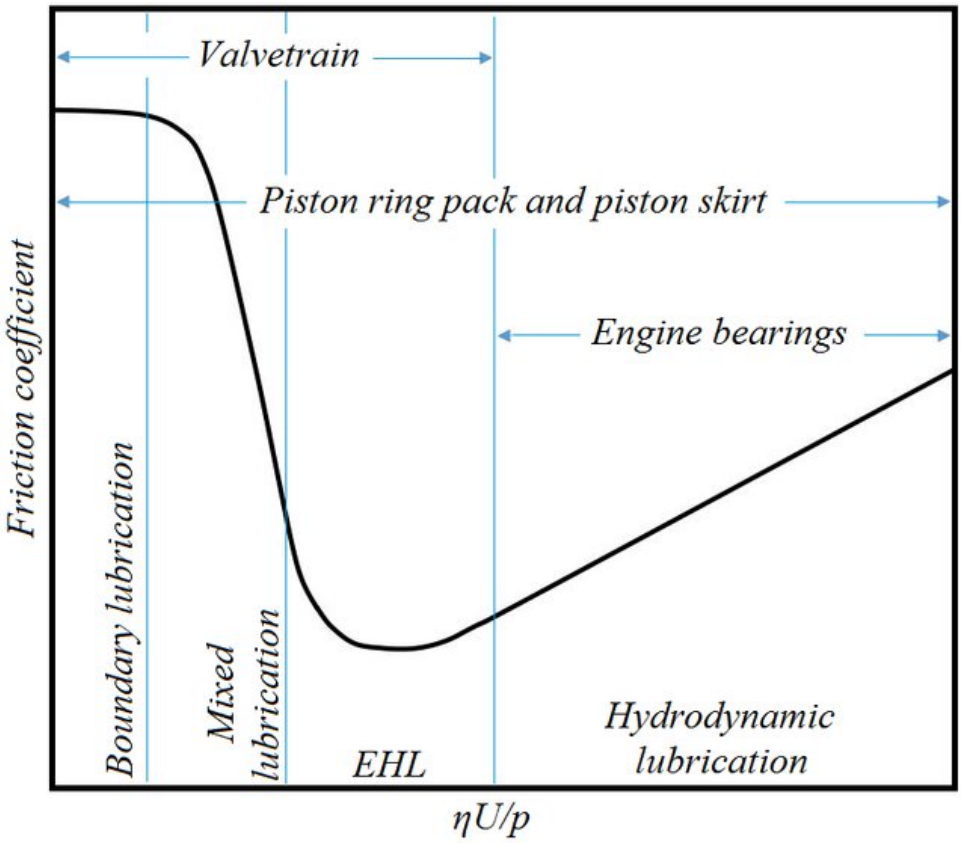

Figure 1.1 Stribeck Curve (Delprete 2020)

The stribeck curve shown in fig.1.1 explains the different lubrication regimes by means of coefficient of friction with respect the Sommerfield number (=viscosity x speed /unit load). The curve explains the possibility of more than one lubrication regime. On the top left, there is surface contact; on the bottom left, a fluid film separates the surfaces, and between these two extremes, there is intermittent or partial contact. Some components may undergo more than one lubrication regime during a single cycle. For instance, journal and thrust bearings operate in the hydrodynamic lubrication regime, with a lubricant film between the bearing surfaces, but actual metal-to-metal contact is expected to occur only at low speeds and under high loads, and when lubricants are of low viscosity.

The minimum film thickness lubricant parameter identifies the lubrication regime and is given as:

$$\lambda = h_{min}/\sigma \qquad (1)$$

where σ is the r.m.s roughness of the two counter surfaces

$$\sigma^2 = R_{q1}^2 + R_{q2}^2 \qquad (2)$$

and R_{q1} and R_{q2} are the root mean square roughness for each surface

Case 1: $\lambda > 3$ (Hydrodynamic lubrication)

The surfaces are completely separated by fluid film, asperity contacts are negligible, and friction and wear should be low.

Case 2: $1 < \lambda < 3$ (Mixed lubrication)

There is a chance of line or point contact of asperities in this regime. An increase in friction and wear may occur, predominantly if there is increase in load or decrease in sliding speed.

Case 1: $\lambda < 1$ (Boundary lubrication)

The surfaces are in contact, extreme high load or low sliding speed cause severe surface damage.

The different lubrication conditions are detailed below.

1.2.1. Hydrostatic lubrication

The bearing surfaces are separated by means of a thick film of fluid, this pressurized film formation is not caused by relative motion between the surfaces, its mainly due to the pressure from an external source. It is also known as an “externally pressurized bearing” (Bassani 1992, Rowe 2013). Both incompressible and compressible fluids are possible to use in these bearings. These bearings are mainly used in applications where zero or little relative motion between the two surfaces exist. It also used in applications where the surface contacts are strictly prohibited. Additionally, it provides stiffness to the bearings. The drawbacks of these bearings are need of high-pressure pumps and fluid cleaning equipment.

1.2.2. Hydrodynamic lubrication

The two surfaces are separated by a thick film of lubricant. The fluid film is compressed between two relative surfaces and creating enough hydrodynamic

pressure to support the load without any external pressure. Under high velocity operations they facilitate a high load carrying capacity. The converging surfaces which are in relative motion are separated by a fluid film and little wear occurs. The wear occurs mostly during start and stop conditions or the result of the presence of particles or dirt or a result of lubricant loss. The bearing life is reduced by corrosion, cavitation erosion or a dynamic load (Sun 2004, Foxwell 2007, Frene 1997).

This regime occurs when adequate oil is supplied, with enough speed to create an oil film and the generation of hydrodynamic pressure between the surfaces which are in relative motion to support the load. Here, the Coefficient of Friction (COF) is in the range between 0.001 to 0.1, depending on the working conditions (Frene 1997).

1.2.3. Elastohydrodynamic Lubrication

The counter surfaces are separated by thin film, involving the line or point contact, the pressure between the counter surfaces are much higher than the hydrodynamic lubrication. Consequently, the lubricants which form a fluid film on the surface which protect from solid-solid contact are used. This is mainly used in applications which involving heavily loaded contacts and loads act over some areas, for example point contact of rolling element bearings, line contacts of gear teeth or roller bearings. It happens in the counterparts of high geometrical conformity having low elastic modulus such as conventional journal bearings with soft liners. The COF is in the range between 0.001 to 0.2. High viscosity oils and grease are the lubricants generally used in elastohydrodynamic lubrication (Dowson 2014).

1.2.4. Mixed Lubrication

This regime occurs between hydrodynamic/elastohydrodynamic and boundary lubrication in which two lubrication mechanisms prevail. Part of the surface completely separated by fluid film and other will be in direct contact. The boundary film formation will protect the solid-solid contact. Unprotected surfaces possibly lead to cycle of adhesive wear, metal transfer and the possibility of seizure. It is also known as quasi hydrodynamic lubrication.

1.2.5. Boundary Lubrication

Boundary lubrication regime is possible during low speed or high contact pressure conditions. In this case hydrodynamic forces are unable to maintain even a thin film between sliding surfaces and direct contact occurs between asperities. The bearing interfaces during contact start–stop conditions prior to a fluid film development before hydrodynamic lubrication is developed, here boundary lubrication prevails. The COF is in the range between 0.1 to 0.25. Possible failure in this regime by means of adhesive and corrosive wear. Easily formed sheared film minimize the adhesive and corrosive wear (Zhang 2014).

1.3 Engine Bearings

The bearings are a critical part of an internal combustion engine design. The various types of bearings used within a typical engine as shown in fig 1.2.(a) & (b). For instance, main bearings which provide smooth rotation to crankshaft and protects from damage. Connecting-rod bearings are responsible for the smooth rotation of the connecting-rod between the crankshaft and the piston (Gebretsadik 2015).

Generally, the bearings are designed to transmit load with the help of a hydrodynamic fluid film. However, during start and stop conditions of the engine, the film subsides and there will be direct contact of shaft and bearing material. During steady-state operations these films exert a pressure that supports the load (Straffelini 2015). The minimum oil film thickness h_0 is essential to attain the hydrodynamic regime between the shaft and the bearing. Under these circumstances the shaft and bearing material should be stiff enough to resist deformation (Aufischer 2010).

When plain bearings operate within the hydrodynamic regime, the surfaces are separated by the oil film. In this regime, little wear takes place because of surface protection.

Wear occurs during engine start/stop conditions. Once the surface roughness become stable, wear occur at slower rate. Wear can be recognized by the sign of overlay damage, e.g., scratches on the surface. The bearing failure takes place by various reasons which include corrosion, wear, fretting, fatigue, corrosion fatigue and cavitation (Jayne 2002).

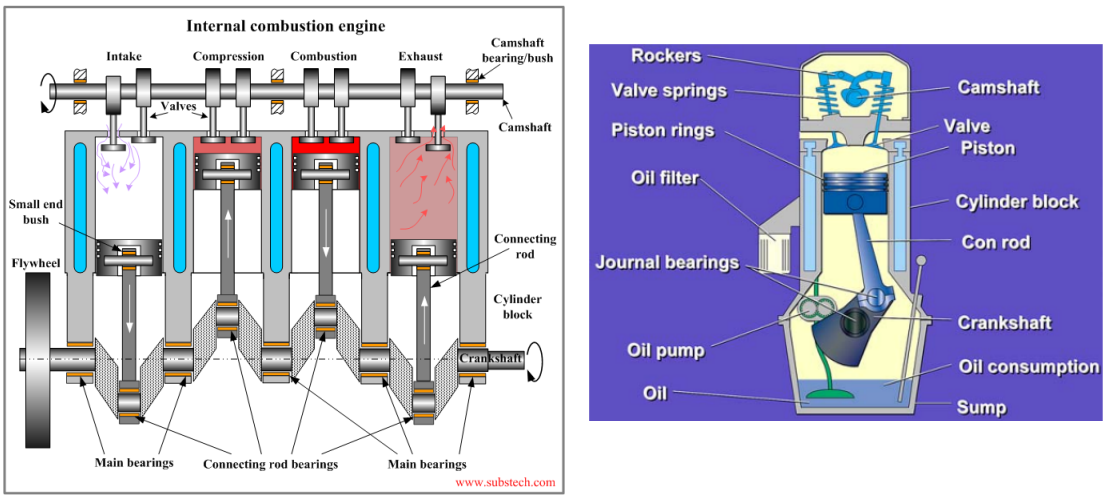

(a) (b)

Figure 1.2 (a) Schematic diagram of Internal Combustion engine (Jayne 2002)

(b) Main engine components in an internal combustion engine (Tung 2004)

1.4 Half-shell bearing

Light weight, compact and easily handled like properties leads to wide usage of these bearings in automobile engines. The dimensions are determined as per target engines. The ratio of the back-steel thickness ‘t’ and the bearing outer diameter ‘D’ t/D is 0.03 in most of the target engines (Daido Metal Handbook).

The minimum value of circumference stress σ_B upon bearing assembly and the contact pressure P_r between the housing and back steel must be maintained at about 200 MPa and 10 MPa, as well as housing rigidity (Daido Metal Handbook). In this case, fatigue

due to insufficient housing rigidity and interference, and the fretting failure is mostly reduced.

Also, the free spread diameter and interference are considered during bearing assembly. The interference forces the bearing towards the housing and the wall thickness of bearing is considered as an assembly inside diameter.

The wall thickness is total thickness which includes back steel, alloy and overlay. Bearings are generally identified based on wall thickness and the circumference length (Daido Metal Handbook). The wall thickness 'T' is determined by the ratio (t/D) and the outside diameter 'D'. Usually, $0.020 \leq t/D \leq 0.050$ (back steel thickness't'=Wall thickness 'T' – centerline alloy thickness 'A')

Oil groove is set on the thicker side of the bearing to ensure the bearing rigidity. If the t/D ratio is large, then high axial tension force is required, and this affects assembly operations and lead to additional requirement of additional material. If the t/D ratio is small, fretting may occur, or the bearing will rotate with shaft.

1.5 Degradation of lubricating oil

Generally, the lubricants are not corrosive until they become degraded. Lubricants degrade in usually due to internal contaminants causing physical and/or chemical oxidation. The presence of water within the lubricating oil can affect the wear performance of the tribo system. Water within lubricants can exist in three different forms. The primary form is known as dissolved water, the water molecules are dispersed in oil which is equivalent to the moisture in air. Dissolved water is not harmful when it is below saturation limit. The other two forms of water presence are free or emulsified water exceeding the saturation limit which is harmful to the tribosystem. The oil oxidation is a consequence of the contact of heat, air, and pressure in the lubricated oil. Water within oil can augment the oil oxidation by a few orders of magnitude. The acids are by-products of the oil oxidation can cause corrosion, hydrogen embrittlement and increase the friction and wear (Parsaeia 2016). The

contaminated oil has an effect on the strength of oil film and resulted loss of hydrodynamic film.

1.6 Research Questions

Even though Lead (Pb)-free materials are adopted over the Pb-based materials in bearing industries, there is insufficient information about their tribological performance at different operating conditions. The corrosion mechanisms of these Pb-free materials and their effect on the tribological performance is also not clear. Furthermore, the standard tribology experiments can help to screen the materials, but they do not represent the real engine conditions. Therefore, corrosion mechanisms of bearing materials and their effect on tribological performance at different lubrication regimes in simulated engine conditions needs to be investigated.

1.7 Objectives

A new test method which can evaluate the combined effects of tribological, and corrosion aspects of bearings performance is required. This is based on the absence of current bench-testing methods for plain bearings applied to internal combustion engine applications. This new test method will facilitate a better understanding of the tribological performance of bearing materials in corrosive engine environments. This is required as the current test methods are designed to evaluate only one specific bearing property and not concurrently.

This new test method will subsequently use corroded bearing samples within in a tribo-test rig. The test rig will require design, development, manufacture and be commission within the Plint TE92 HS Rotary Tribo tester at Bournemouth University. Thus, an important contribution of this research is the development of the new test-rig facility.

A newly designed and developed test-rig module will used to investigate the tribological performance of hydrodynamic bearing shells. This test-rig simulates automotive engine representative conditions experienced plain bearings during operation. Wear rate of these materials were explored using this new test methodology.

The materials considered are tin based lead-free overlay and lead based overlays considered as a reference.

Chapter 2 Literature Review

2.1 Engine bearing materials property requirement

The plain bearings are made of Copper (Cu) based alloys, Aluminium (Al) alloys, polymers, lead and/or tin-based white metals and powder metallurgy materials (Aufischer 2015). Moreover, these materials are used either in cast or wrought forms. Leaded bronzes, tin bronzes and aluminium bronzes are three types used as bearing materials. Bearing material high temperature properties are enhanced from the use of lead (Pb)-bronze, Tin (Sn)-bronze or Aluminium (Al)-bronze (Ozsarac 2007). The tensile strength is increased by adding small amounts of Zinc (Zn), Nickel (Ni) within bearing bronzes. Tin (Sn) within bronzes enhance the tensile strength, fatigue resistance and high temperature operating ability (Ozsarac 2007). To meet the required properties, the plain bearings are designed with a multilayer structure.

Plain bearings are manufactured from non-ferrous alloys, also polymer, composites and rarely ceramics are considered. They are lubricated by oil or solid lubricants depend on the applications and working conditions. As a result of legislative restrictions, lead (Pb)-based alloys are now replaced by Aluminium (Al) or Copper (Cu)-based alloys (Jayne 2002).

The selection of the suitable bearing material has a vital role in the engine performance. The resulting design should accomplish the mechanical and tribological requirements which include conformability, embeddability, wear resistance, low friction and corrosion resistance (Gebretsadik 2015).

2.1.1. Embeddability

In the case of mixed and boundary lubrication regimes, the bearing material must exhibit a good wear resistance. Debris entering through the bearing clearance can score the shaft, and the roughened shaft will cause wear within the bearing materials. Improved embeddability provided by the overlays to accommodate debris to prevent the crankshaft from damage (Gebretsadik 2015, Jayne 2002). Embeddability is

inversely proportional to the hardness and strength of bearing. However, if the embedded particles are larger in size, the bearing material deformed will protrude from the bearing surface. This protrusion alike structure in contact with the shaft has a soft and low melting phase that prevents the material transfer to avoid seizure (Jayne 2002, Aufischer 2010).

2.1.2. Conformability

Excellent conformability avoids the damage if there is any imperfect geometry on the shaft. (Gebretsadik 2015).The misalignment is either inherent nature or transient nature happened by elastic deformation or by thermal deformation, end in surface contact (Jayne 2002). Furthermore, the contact occur during engine start and stop condition while the presence of boundary or mixed regime.

2.1.3. Cavitation resistance

Cavitation erosion resistance is related to hardness although microstructure has significant influence. Cavitation erosion resistance is higher in Tin (Sn)-based white metal compared to Lead (Pb)-based white metal even though they have a similar hardness. This is perhaps due to the Cu-Sn needle like microstructure (Jayne D.T 2002). The white metals meet all the required properties as bearing materials nevertheless they can used only in slow-speed marine diesel engines.

2.1.4. Corrosion of bearing materials in lubricating oil

Sudhakar (Sudhakar 2002) investigated the corrosion failure of automobile bimetal bearings (alpha and beta brass) during storage time before assembling in engine. Stress corrosion cracking is possible in case of copper-based alloys because of exposure to ammonia, Sulphur dioxide and nitrates. The author reported bimetal perhaps picked up ammonia from surroundings and the presence of residual stress may have been caused mostly by differences in temperature resulting in differential expansion coefficients between the two phases. The author concluded that appropriate heat treatment can used to relieve these stresses. Furthermore, Stress Corrosion Cracking (SCC) is reduced or avoided by lowering the magnitude of the stress (Sudhakar 2002).

The bearing material has a steel backing with a soft overlay applied on the lining. The overlay provides the seizure resistance, good embeddability to accommodate dirt and wear debris and corrosion protection to the substrate from degraded oil. For instance, degraded oil can dissolve lead (Pb) from the substrate (Wilson 1970). The low solubility of Lead (Pb) in Copper (Cu) forms two separate phases as Lead (Pb) is corroded in degraded oil. However, the corrosion resistance of the lead (Pb) phase is improved by adding Tin (Sn) or Indium (In) within the alloy system (Wilson 1970). The pitting corrosion is possible with Tin (Sn) depleted region. The properties of electroplated overlays is different from casted and rolled metals. However, these samples are all similar in grain size, except if they've been heat-treated (Wilson 1970).

(Tichvinsky 1943) Bearing corrosion are of two types, uniform corrosion, and localized corrosion. The corrosion of all copper lead bearings was mainly uniform while all white metal alloys were localized corrosion. corrosion of tin base bearing alloy is negligible with all lubricating oil tested. While corrosion of Pb-based alloys is low and moderate, corrosion of copper-lead and cadmium-based alloys is high.

(McCloskey 1995) Bearing corrosion can be caused by corrosive compounds in the lubricant attacking the alloy in the bearing. Compounds can result from either external contaminants that are introduced to the lube oil system, or from internal contaminants that form during operation of the machine due to lube oil degradation and oxidation. Since lubricant additives have been developed to inhibit oxidation under severe operating conditions for extended periods of time, corrosion due to oxidation of the lubricant oil is no longer a common occurrence. High temperatures and exposure to air, water, or foreign materials can accelerate oxidation.

(Waukesha bearing) Copper-containing alloys, including tin-based white metal, are attacked by hydrogen sulphide in the oil.. A dark deposit, mainly copper sulphide, develops on the surface of the bearing as a result of hydrogen sulphide attack.The copper-tin compound in the lining is also depleted, weakening the material.The

phosphor bronze small end bush was corroded by sulfur as a result of decomposition of lubricating oil additives and gross pitting of the bearing surface.

2.2 Bearing Failures

The hydrodynamic fluid film bearings are expected to have a long life compared to other engine components. However, this is not the case in real engines since there is chance of other situations that interrupt bearing operational efficiency leading to premature failure.

It is essential to know about the possible failures of bearing materials in respective working conditions and take precautions to reduce or avoid it. Some of the bearing failure and corrective measures are discussed below. The following is a description of the bearing failures: Scoring due to dirt or foreign particles, faults during assembly, misalignment, inadequate lubrication etc.

2.2.1 Scoring due to dirt or foreign particles

Dirt or foreign particles entering the system is one of the causes of failure. It may lead to wear on babbitt overlays including severe scoring of the bearing and shaft material depending on many factors. These include particle size, bearing material, overlay thickness and clearance.

2.2.2 Faulty Assembly

Misassembly is another cause of many bearing failures. It happens due to inadequate or excessive assembly compressive forces, or misalignment of oil holes or bearing halves reversed. The amount of misalignment depends large extent to the loading, subsequently film thickness and the bearing length. Edge loading and excessive wear are the result of misalignment.

2.2.3 Inadequate lubrication

It can result from insufficient clearance, inadequate oil supply, blockage of oil filters, overheating of the oil cooling system, or dilution of oil by water/fuel. It prevents the bearing operating in the hydrodynamic lubrication regime and leads to metal-to-metal

contact. It will lead to rapid increase of friction and wear and subsequently wear of overlays.

2.2.4 Bond Failure

It is rare case of failure where overlay is completely separated from the backing material. The overlay is melted near the bond line at high temperature and subsequently separated because of dynamic loading. The other causes are inadequate surface preparation, surface contamination of lining material, inadequate pouring temperature, or inadequate fluxing.

2.2.5 Diffusion

Tin material used in overlays tends to diffuse towards lining material. Diffusion is time dependent process and depends on the working temperature. It will leave the surface of tin depleted region and subsequently leads to reduction in corrosion resistance and decrease in wear resistance. Nickle (Ni) and brass are commonly used barrier layer to prevent diffusion.

2.2.6 Porosity and Blisters

It will occur due to foreign inclusions, absorbed gas, powder impurities, hydrogen electroplating or lead sweating.

2.2.7 Corrosion

The bearing corrosion can result from chemical attack by corrosive compounds in the lubricant. Its particularly related to oxidation of oil. Oil oxidation may occur due to high temperature, exposure to air, water, or foreign materials. Lead is removed from the Copper -Lead (Cu-Pb) bearing alloy by attack of acid and peroxide within oxidized oil. Both Copper (Cu) and Lead (Pb) corroded materials at vulnerable and metal sulfides are present in corrosion products.

2.3 Tribology of bearing materials

The wide range of bearing materials have been used in internal combustion engine applications. The suitable material is opted based on engine operating conditions such

as speed and load. Bearing materials possess different mechanical and tribological properties; some of these properties are discussed below:

2.3.1. Lead (Pb) based materials

This is a conventional bearing material and owing to its low friction property widely used within bearing industries for extensive period (Pratt 1973). White metal bearing alloys or Aluminium-Lead (Al-Pb) alloys or Aluminium-Tin (Al-Sn) alloys are the traditional bearing materials used as linings. Lead (Pb)-based overlays provide excellent seizure resistance to avoid the seizure of crankshaft and linings and also it offers good corrosion resistance to linings from lubricating oil. Lead (Pb) based materials have excellent embeddability and conformability (Pratt 1973).

Considering the EU legislative restriction and negative impact on environment and health, the usage of Lead (Pb) based materials are now prohibited particularly in automotive applications. Subsequently Lead (Pb) free materials were adapted by bearing industries (Gerrard 2007). In addition, it was replaced due to lower tensile strength (Becker 2004) in comparison with other materials.

2.3.2. Pb-free materials

Tin, Bismuth, and bronze are Lead free materials adopted by the bearing industries (Langbein 2009). Bismuth has a melting point of 271^{o}C with mechanical and tribological properties analogous to lead (Pb). It replaced Lead (Pb) in Copper-Lead (Cu-Pb) alloys. There are some overlays that possess better tribological properties than Lead which replaced Lead (Pb)-based material for instance, Polyamide-imide containing graphite and MoS_2 (Grun 2011).

As compared to Lead (Pb) based overlays, Aluminium-Tin (Al-Sn) exhibits better wear resistance. Nevertheless, this was used as a bearing lining previously (Grun 2011).

Tin (Sn) was another proposed new bearing material. It has a melting point of 232^{o}C and its mechanical properties were comparable to Lead (Pb) and it was used in white metal alloys with different weight percent. Tin (Sn) based overlays possess excellent

resistance to cavitation, corrosion and good embeddability and conformability. However, multilayer Tin-Copper (Sn-Cu) overlays have good structural strength compared with monolayer Tin-Copper (Sn-Cu) overlays (Zhang 2016).

2.3.3. Bronze based lining materials

Langbein et al (Langbein 2009) studied seizure resistance of various bronze alloys such as CuSn4Zn1 (Copper, 4 wt% Sn, 1 wt% Zn), CuSn8Zn1 (Copper, 8 wt% Sn, 1 wt% Zn), CuSn5Zn1 (Copper, 5 wt% Sn, 1 wt% Zn). The tests were carried out at seizure load 20 MPa and fatigue load (150 MPa) and considered leaded bronze as benchmark. The load was increased stepwise till the seizure limit was reached and initially it was in running-in period. The authors conclusion of this study was CuSn5Zn1 showed better seizure resistance than others (Langbein 2009). Conformability and embeddability of these linings could be improved by overlaying with AlSn20Cu or Polymer overlays such as poly-amide-imide (PAI) with MoS2 and graphite or combination of both (Langbein 2009).

Copper-Tin (Cu-Sn) linings are solid soluble unlike Copper-Lead (Cu-Pb) alloy whereas Lead (Pb) is not solid soluble in Copper (Cu). The addition of Tin (Sn) in the bronze alloy was manufactured via powder metallurgy route possess comparable friction and wear resistance with leaded bronze (Vetterick 2010). The friction and wear properties of Tribaloy alloy reinforced with Tin-bronze composite coating were superior compared with leaded Tin-bronze alloys (Gao 2011).

2.3.4. Aluminium-Tin (Al-Sn) based bearing materials

Grun et al (Grün 2009) investigated the tribological performance of three different overlays such as PbSn18Cu2, PAI with MoS2 and graphite, Physical Vapour Deposition (PVD) coated AlSn20Cu during the running-in engine phase and during emergency conditions by using ring-on-disc test (Grün 2009). The materials PbSn18Cu2 showed superior sliding properties but load is limited due to its inferior mechanical strength. Under dynamic loading conditions the hard AlSn20-sputter

overlay coating has increased wear resistance compared with the soft overlay PbSn18Cu2. The properties of the polymeric overlay are comparable with between those materials (Grün 2009).

An addition of Silicon (Si) and Tin (Sn) in Aluminium (Al) based alloys, improve the friction and wear resistance. Amongst of all Aluminium (Al) based alloys, high silicon content improves hardness and furthermore, possesses highest wear resistance and a low coefficient of friction. Nevertheless, Al-Sn and Al-Si have superior resistance to wear compare to Al-Pb alloys (Feyzullahoğlu 2002).

2.3.5. Bismuth (Bi) based bearing materials

Lead (Pb) was replaced by Bismuth (Bi) to attain Lead (Pb) free bearing materials to conform to legislation and prevent harm to health and environment. Bismuth has similar properties to lead (Pb) in many cases for example, it forms a monotectic reaction with Copper (Cu) similar to lead (Pb), to produce low friction and excellent embeddability.

Kerr et al (Kerr 2007) investigated tribological properties of newly developed Bismuth (Bi) overlay on bronze-Bi lining with Silver (Ag) as an interlayer. The authors found that Bismuth (Bi) overlay have lower friction at higher stribeck numbers compared to Lead (Pb) based and Tin (Sn) based overlays (Kerr 2007). Wear properties of Bi is better than Pb-based material at extreme working condition and it “perhaps due to movement of Bi across the surface of the interlayer” (Kerr I 2007).

2.3.6. Polymer based bearing materials

Polymeric overlays such as polyamide-imide containing MoS2, and graphite showed better friction and wear properties compared to Pb-based overlays (Grun 2011) The low friction is mainly due to presence of graphite and MoS2 in overlay. PAI is an amorphous thermoplastic possess higher mechanical strength compared with other polymers. It is chemically inactive with diesel fuel and chemicals in engine oil. Therefore, it has resistance against thermal degradation and furthermore, the friction and wear properties can be enhanced by using solid lubricants (Grun 2011).

2.4 Wear test on bearing materials

2.4.1. Standard tests for screening bearing materials

Material design such as bearing materials, shaft materials and lubrication still rely on standard laboratory tests. The test possibilities of journal bearing system from large scale to small scale tests are shown in the Fig.2.4.1.1 (Summer 2017).

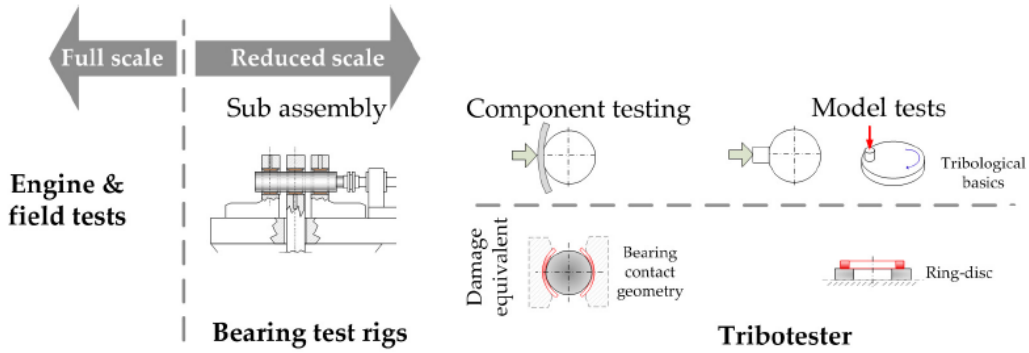

Figure 2.4.1. Test Possibilities of Plain bearings (Summer 2017)

Grun et al studied the tribological performance of different overlays (PbSn18Cu, AlSn20Cu, polymer based) and substrate (CuPb22Sn2). The tests were conducted using ring-on-disc (ASTM D3702) and novel journal bearing test rig for a different approach such as running in, stable operating, stop-start conditions. They used different counterparts such as plain and thrust bearings. The specimens were completely immersed in engine oil (Shell Rimula X 10 W). The seizure test were conducted with assistance of following parameters: sliding speed of 1.4m/s for metal bearings and 2.5 m/s for polymers, oil inlet temperature 110^{o}C, maximum load 75-120 MPa with initial step of 3.9 MPa, constant speed of 1000 rpm and time duration up to 100 hours (Grun 2011). The endurance test was conducted by using novel journal bearing test rig, the shaft rotates at 5000 rpm with sliding speed of 12.6 m/s. In this the shaft was loaded with sinusoidal load with 100Hz frequency and the test duration was 5.5 hours or two million loading cycles.

Yi Zhang et al employed ring-on-disc to study the tribological performance of monolayer and multilayer tin-copper overlays (Zhang 2016). The wear tests were

conducted using engine oil SAE10 with sliding speed of 0.013 m/s and load 12 MPa. The oil inlet temperature was 60ºC and sliding distance was about 100m. The seizure test was conducted with revolution speed of 7200 rpm at velocity 20 m/s in the lubricant VG 22. Temperature of oil inlet was 100ºC and the test was continued to failure (Zhang 2016). There have been a number of tribological tests conducted and the performance of the multilayer overlay evaluated. According to the author, fatigue strength of the multilayer tin–copper overlay is considerably better than that of the monolayer. Additionally, seizure resistance was increased from 90 MPa for the monolayer overlay to more than 100 MPa for the multilayer structure. In the ring-on-disk tribometer test, the monolayer overlay was found to wear about 16 μm, five times more than the multilayer overlay in the same conditions.

Daniel et al (Gebretsadik 2015) investigated the tribological performance of Tin (Sn)-based overlay under mixed and boundary condition by using a block-on-ring test in CETR UTM-2 tribometer and lead (Pb) based material was the reference. The tests were carried out for different rotational speeds range from 1-400 rpm with sliding speed of 0.002 m/s. The test temperature was 95ºC and the load range was between 20- 80 N (Gebretsadik 2015). Coefficient of friction (μ) decreases as rotational speed increases. Both Sn-based Pb free overlay materials exhibit a friction transition similar to that of Pb-containing materials. All tested samples show the same steady-state friction behavior. However, the Pb containing overlay shows slightly higher wear at relatively higher rotational speed. Parts of the worn surface of Pb-containing overlay exhibit compositional changes and clusters of tiny spots of material have been removed. Parts of the Sn-based overlays have abrasive wear and exposed interlayers caused by adhesive wear.

The friction and wear resistance of newly developed tribaloy alloy (tin/bronze-based composite) coating on bearing was studied under the WAMsc3 Sliding contact test along with leaded tin/bronze as reference. The test was conducted with load 50N with steps of one N and the oil was pumped only up to 300s (Gao 2011). According to the experimental results, the coated bushing with T-401/tin/bronze composite has lower

friction and higher wear resistance than the leaded tin/bronze bushing, that is, it has better tribological properties.

2.4.2 Journal Bearing Test System

Close to component test adapter conjunction with TE92 Rotary Tribometer from Phoenix Tribology were developed to investigate the wear and frictional properties of Lead-Tin (Pb-Sn) based multilayer material (Bergmann 2018). Two test strategies were developed such as start-stop and constant test strategies. Start-Stop test have three phases, initial phase author followed sliding speed of 0.38 m/s for 900 s at room temperature and the load kept constant 1.67 MPa which sets the journal bearing system in mixed lubrication condition. In Second phase, standing still system was heated to $120^{O}C$ for 900 s. The final phase was start-stop test, in which the system accelerates from 0 m/s -1.26 m/s for 5 s and decelerates for 3 s. These tests were structured with aid of loop system, each loop consist of 5 start-stop cycles. Constant test strategy followed, sliding speed of 0.23 m/s for 600s at constant load 1.06 MPa. In second phase was to heat the system to $120^{O}C$ for 900 s and additionally 300 s was added to this step to balance thermal inertia effects. Third phase consists of two loops, outer loop comprises start-stop cycle which conducted 20 times last for 10 s to create a stribeck curve. Subsequently inner loop characterizes actual load case. The shaft material 34CrNiMo6 steel and lubricant Shell Rimula 10 W were used for above test strategies. Results showed COF of individual start-stop cycle was according to Stribeck curve findings for single curve. Fast changing tribological process within test indicated sequential representation of COF is better rather than calculation of mean COF of the start-stop cycles. The friction energy resulted 173,150 J and a wear volume of 9.97 mm^3.

Florian Grun et.al investigated the tribological properties of bearings with polymeric overlay by using novel test adapter in combination of TE92 rotary tribometer from Phoenix Tribology (Grun 2013). The two half shell bearings of 120^{o} are radially pushed towards the 34CrNiMo6 steel shaft. The shaft diameter is ~48.6 mm with surface finish of Ra <0.4 µm and clearance is 1.6 per mill. The bearing width is 20mm. Shell Rimula R3 is a lubricant and Lunn-Furey contact potential circuit (CP) is used

to detect the lubrication regime. For test, the specific load is used between 0.5 and 1 MPa. The speed was raised 5 times between 30 and 1000 rpm with a constant load. The minimum value of COF for both loads was approximately 0.005. Stribeck curve was shifted to left with increase of load. Transition point from mixed to hydrodynamic regime of specific load 0.5 MPa is 275 rpm and transition point of specific load 1 MPa is 410 rpm. Author concluded that result provided in-depth understanding of bearing tribological properties.

Summer et al investigated the damage analysis (for instance wear performances, seizure and friction properties) by two test-rigs such as the ring-on disc and close-to-component test-rig (Summer 2017) discussed below.

- Ring-on-disc employed on tribometer by Phoenix technology. This test setup used the plain contact of ring and disc in axial direction which immersed in oil to imitate the real engine in boundary and mixed lubrication regime. This showed large area of contact with adequate lubrication provided by notches on the specimen. The test conducted start-stop cycle of 5 s ramp with constant load of 1.64 N/mm^2, 100^OC was set temperature. The increase of Coefficient of friction (μ) during boundary regime and observed decrease of μ in mixed lubrication regime. Again, re-increase of friction coefficient denotes the transition period of fluid regime. Soft bimetal bearing Material A showed more friction in boundary lubrication regime than tri-layer polymer coating Material B. Stribeck curve of Material B showed more expansion to the right side. Author concluded that higher the Sn content lower the friction at low speed. Friction based on lubrication oil was investigated. Fully formulated heavy duty engine oil 1 and oil2 resembles all properties of oil 1 except missing surface-active additive compound. Load 3 MPa and speed 1.4 m/s were kept constant, resulted oil formed tribofilm which showed better friction performance. summer
- The close-to-component test-rig pushed half shell bearing of 120^OC towards shaft. The Shaft diameter was ~48.6 mm with 1.6 per mill clearance in 360^O journal bearings. The wear test conducted start stop cycle with constant load

1.64 MPa at temperature 120^{O}C, ramp speed 0-1.25 m/s in 5 s duration. Trimetal with Polymer coating showed new condition of wear performance but still it showed better wear performance rather than lead trimetal bearing.

Summer et.al used ring-on-disc to explore the tribological properties of crankshaft bearing systems against varying counterpart shaft specimens and its surface characteristics under start-stop condition (Summer 2015). The shaft materials used for these investigations were forged steel and cast-iron (Becker 2004) and its performance were determined based on surface roughness for forged steel, while its microstructure for cast iron. Optimized surface finish of these shaft materials resulted minimized wear in crankshaft bearing system.

The author compared the pin-on-plate and ring-on-disc test results on model scale which evaluated the tribological properties of Cu-Sn alloy and pure aluminium bearing materials with counterpart as low carbon steel (Kartik 2012). They mentioned component scale is lack of solution for failure mechanisms and COF is not clear with respect to time, temperature, and load.

Novel coatings were introduced to enhance the friction properties based on the results of bimetal and trimetal bearing material friction mechanisms by means of journal bearing test system and ring-on-disc test methods (Summer 2019). Stribeck curve by RoD showed friction increased with decrease in velocity.

Grun et al (Grun 2013) developed the novel test-rig for a journal bearing test. The standard tribological tests were used to screen the materials although this did not represent real engine conditions. Moreover, the newly developed test-rig adopted the real engine condition. Bearings shells were radially pushed against the rotating shaft material in the presence of lubricating oil. The tests were conducted with different set of test series. Firstly, Shell Rimula R3 used as lubricant and the test oil temperature was 40^{o}C. The load was kept constant, and speed varied between 30 and 1000 rpm. Secondly, the author investigated the viscosity effect using two reference lubricants. Alike before, the load was kept constant, and speed were varied between 160 and 1000 rpm without any external heating. This test rig enables the detailed investigation of different lubrication regime (Grun 2013).

Bergmann et al (Bergmann 2014) investigated the tribological performance with the help of novel test rig Journal Bearing Adapter (JBA) which developed by Grun et al (Grun 2013).The test were conducted at various load range between 0-2 kN with different speed of 0-3000 rpm. The test carried out with different temperature 0-220^{o}C (Bergmann 2014).

Conducted literature search reveals that the plain bearings are subjected to many different laboratory-based performance tests for instance, ring-on-disc, pin-on-disc that screen candidate materials as cost effectively as possible prior to much more expensive full engine-based tests. It is still unclear how these lead-free bearing materials behave in different lubrication regimes, such as mixed lubrication and boundary lubrication. Journal bearing test system provides tribological properties of real engine conditions at reduced scale testing. Above we discussed the tribological properties of various plain bearings based on laboratory-based tests, as well as journal bearing test methods.

Chapter 3 Experimental Methodology

3.1. Plain bearing structure

Plain Bearings classified into single layer, bimetal and trimetal or multilayer depend on the material constituents as shown in fig 3.1.

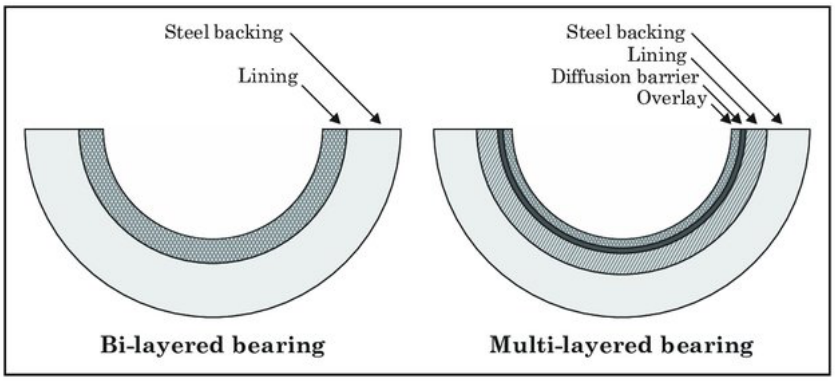

Figure 3.1. Structure of plain bearing (Tamatam 2017)

Single layer structure consists of only alloy (or lining) and this will not meet the desired properties for all applications. Bimetal structure consist of backsteel and alloy (or lining). This is used only in few applications eg., ship engines. Trimetal is overlay on the top of the bimetal structure. Various overlays are used depending on the application.

Electroplating was used to manufacture overlays. For instance, a trimetal Sn-based overlay was applied to the bronze substrate after it was cleaned with alkaline cleaner and etched with hydrochloric acid at 30 vol%. Overlay is the top layer of tri metal, which is 20 microns thick. Third layer used as a diffusion barrier for overlay with a thickness of 4 microns. Lead and bronze comprise the lining layer between an interlay and steel back with a thickness of 1 mm. The steel back provides shape and support.

3.2. Material Selection

The various bimetal and trimetal bearings were chosen for this study. The chemical composition of those bearing materials are given in Table 3.1. This plain bearing materials composition is similar to that of commercially available bearings.

Bearing materials	**Test Sample name**	**Major Chemical Composition (weight %)**
Lining	DERM 118	Sn-10%, Pb-10% and Cu (Rem)
	DERM 119	Sn-1.5%, Pb-23% and Cu (Rem)
	DERM 120	Sn-10%, Cu (Rem)
Overlays	DERM 121	Sn-10%, Cu – 2% and Pb (Rem)
	DERM 122	Bi – 100%
	DERM 123	Cu – 3% , Sn (Rem)

Table 3.1: The chemical composition of bearing materials

3.3. Experimental Strategy

In order to address the objectives an experimental strategy was planned to involve three phases as described briefly within the following sections. This strategy is visualized as a flow-diagram shown as figure 3.2.

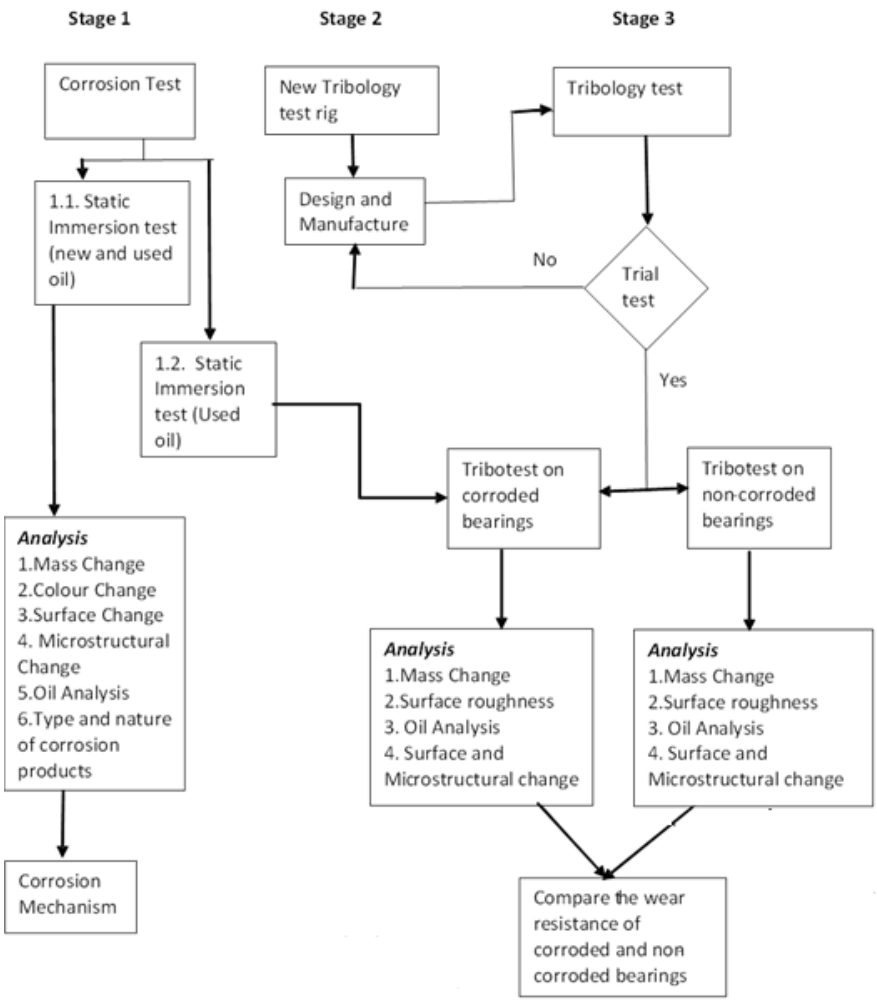

Figure 3.2. Flow chart of experimental strategy

3.3.1. Experimental Strategy – Phase one corrosion tests

This initial phase of experiments are designed to facilitate the understanding in regard to Project Objective. The concern here is to understand the corrosion mechanisms for bearing materials (overlays and linings) subject to similar environmental conditions found within a typical automotive engine (new oil, degraded oil, temperature, exposure time, and bearing material composition). These bearing samples have used later during experiments to understand the tribology and corrosion interactions. Facilities at the sponsoring company (Daido Metal Co., Ltd.) were used to conduct the corrosion tests as detailed in the transfer report. The test example shows the typical corrosion experiment parameters.

Test Example:

Aim: To understand the corrosion resistance of plain bearing materials in new and degraded oil lubricants under static conditions

Test Equipment: Standard corrosion test "ISO 10129:2006" setup at Daido Metal Co., Ltd. in Ilminster (UK)

Test Materials: Lead (Pb) based and Lead (Pb)-free plain bearing materials

Test Conditions:

Oil: Petro Canada Sentron LD 5000 (new and degraded oil)

Temperature: $120^{O}C$

Test Duration: 50, 200, 500 hours

3.3.2. Experimental Strategy – Phase two & three: The design and commissioning of a new tribology test rig

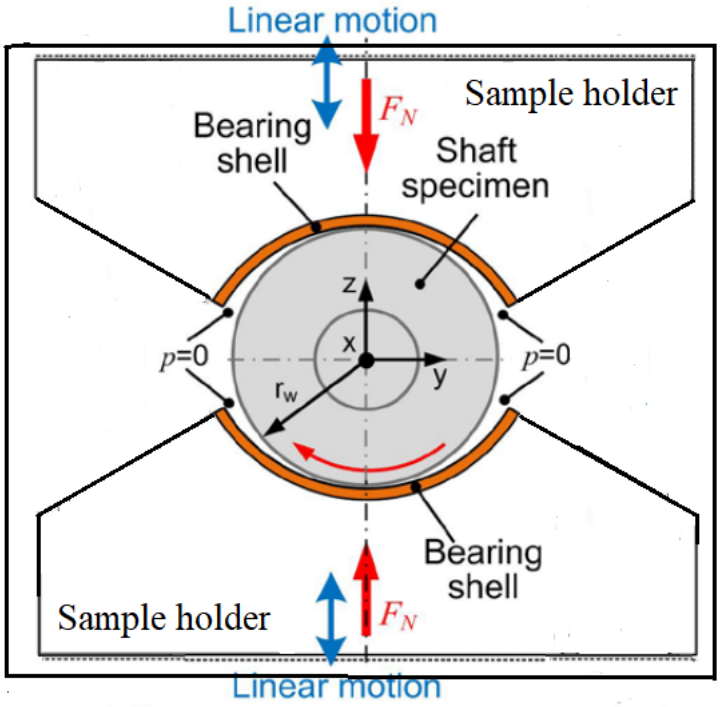

Fig. 3.3. Journal Bearing Adapter- Schematics

Figure 3.3 visualizes the novel journal bearing adapter. Two journal bearing half shells of 120° are radially pushed onto a rotating shaft specimen. The shaft diameter is ~52.75 mm. Using magnet holders, the individual sample holders can be mounted flexibly. Bearing shells have a width of 15 and 18 mm. The shaft is made of induction hardened steel and possesses a surface finish of Ra < 0.4 µm.

This phase of the experimental strategy was carried out concurrently with the corrosion tests. This has facilitated in PO 2 and PO 3 being completed. In order to assess the corrosion and tribological wear mechanisms of the hydrodynamic bearings typically found in automotive engines the surface conditions need to be replicated within laboratory conditions. This means the hydrodynamic lubrication regime, load, temperature, oil, bearing material, surface velocity all needs to be controlled. In addition it was decided important that the test rig could facilitate the working envelope of the conditions experienced within a typical engine with the facility of extending loads and controlling lubricant film thickness to produce surface failure within a

reasonable time-frame. This work involved considering different requirements and design solutions before undertaking the rig manufacture and commissioning. After a significant work schedule of design and manufacture the new test rig is now fitted to the TE92 HS tribometer and has been commissioned with the company satisfied that the failures are similar to those found within automotive engines. At present the final trials tests are being conducted to assess the differential capability of the rig to assess three different bearing materials. A typical test example is given to illustrate typical experimental parameters.

3.4. Corrosion Test

3.4.1. Specimen preparation

The Plain bearing samples were cut into angle 120^{o} by using Buehler Isomet 4000 precision saw cutting machine. The diamond blade was used to cut bearings with feed rate of 2.5-3.0 mm/min and the speed of 2500 rpm. The coatings always faced the blade to avoid damage to the coatings. Coolant were used to avoid heat during cutting operation and edges were smoothened. The samples were cleaned in ultrasonic bath contains isopropanol as a cleaning medium. Initial weight of the bearing samples were measured by using weighing scale with accuracy of 0.0001 gm. In order to observe changes in discoloration of surface after corrosion testing, bearing samples were photographed before corrosion testing.

3.4.2. Immersion test

For the tribological system "plain bearing", it is of particular interest to determine the compatibility between the bearing materials and the lubricant based on chemical and mechanical actions. Under static conditions, i.e. without simultaneous mechanical action taking place, this International Standard determines the behavior of plain bearing materials regarding corrosion caused by lubricants. The value for a single material is less informative due to greater dispersion of results that occurs when determining an increase or decrease in mass. Each result should be expressed as a mean value of three tests.

Static immersion corrosion test adopting Standard ISO 10129:2006 was carried out on various bearing materials which listed in Table 3.1 to investigate corrosion resistance and mechanism. These tests were conducted by the author during long-term location at Daido Metal Co., Ltd. in Illminster (UK). The bearing materials were manufactured by Daido Metal. The schematic diagram of corrosion test setup is shown in figure 3.4. The mass, dimensions and photographs of the test samples were recorded prior to the experiments conducted by the author.

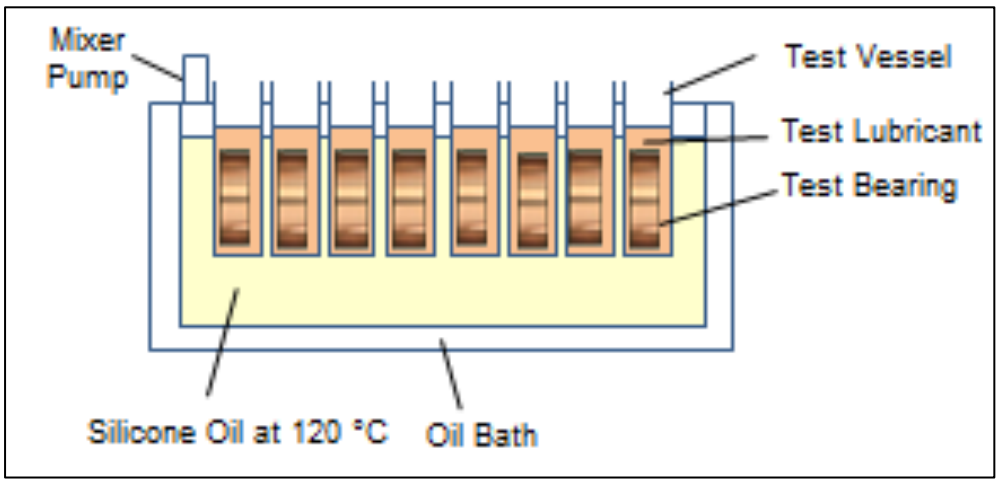

Figure 3.4. Corrosion test setup

The bearing shell test samples were weighed and immersed in a glass Beaker containing 100 ml of lubricating oil (LD5000) with chemical composition shown in Table 3.3. The bearing shell test samples were tested in both new and used oil for different time duration 50, 200 and 500 hrs. The beakers were placed in silicone oil tank at set temperature 120^{o}C. The mixer pump circulates the oil to maintain homogeneous temperature in oil tank. At the end of test, the heaters were turned off and the system was allowed to cool naturally to ambient temperature. Specimens were removed after the set test interval and cleaned with isopropanol in ultrasonic bath for removal of excess oil. They were reweighed to calculate corrosion rate and photographs were taken for visual evaluation of corrosion.

ELEMENTS	New Oil	Used Oil
IRON (ppm)	1	7
CHROMIUM (ppm)	0	1
ALUMINIUM (ppm)	1	1
COPPER (ppm)	0	1
LEAD (ppm)	0	2
NICKEL (ppm)	0	0
TIN (ppm)	0	1
MANGANESE (ppm)	0	0
TITANIUM (ppm)	0	0
SILVER (ppm)	0	0
MOLYBDENUM (ppm)	0	1
ZINC (ppm)	319	361
PHOSPHORUS (ppm)	269	291
CALCIUM (ppm)	1615	1795
BARIUM (ppm)	0	0
MAGNESIUM (ppm)	4	4
SILICON (ppm)	0	0
SODIUM (ppm)	1	3
BORON (ppm)	2	3
VANADIUM (ppm)	0	0
TBN (mgKOH/g)	4.2	3.3
TAN (mgKOH/g)	1.4	3.2

Table 3.2. Chemical composition of LD5000 new and used oil

3.4.3. Microscopic investigation

The corroded and non-corroded bearing samples were cleaned in ultrasonic bath contains isopropanol as cleaning agent to remove any oil residue, metal particles or dirt on the samples. The microstructure of the bearing samples was examined and

recorded by using NIKON ECLIPSE ME600 Microscope under 200x and 1000x magnification.

3.4.4. SEM

3.4.4.1. sample preparation

Micro sample preparation

The micro sections of corroded and non-corroded samples were prepared by using Buehler Isomet 4000 mounting press. Phenolic moulding powder were used. The standard conditions of mounting microsections were pre-set at 4 bar pressure and 175^{O}C mounting temperature. Time for preparation was around 10 minutes including cooling period of mounted microsection. Microsection sample extra edges were filed and cleaned in isopropanol and air dried the specimen.

Grinding and Polishing

The microsections were polished by using Buehler Automet-250 grinding polishing machine. The following parameters were used for grinding and polishing: Force ~25 N , 300 rpm platen speed for grinding and 150 rpm platen speed for polishing, head speed 60 rpm, relative motion comp were used for trident surface polishing and for other steps relative motion contra were used.

The following steps were followed for all samples except Pb based material. The microsections were grinded with three different CarbiMet S SiC papers such as P80, P400 and P800 for about 2 minutes with water as a lubricant. Microsections were polished on Ultrapad cloth surface with 9 micron as abrasive and metadi fluid as a lubricant. Subsequent Samples were polished on the Trident surface with 3 micron and 1 micron abrasive and metadi fluid as a lubricant. Lastly, microsections were polished on ChemoMet surface with MasterMet 2 abrasive and water as a lubricant. Samples and sample holder were cleaned in water after each step.

The following procedure is for polishing Pb based material. The microsections were grinded with three different CarbiMet SiC surface such as P80, P320, P800, P1200 for about 1 minute with water as a lubricant. After that microsections were polished on MOL cloth with 3-micron diamond suspension abrasive media and following that polished on NAP with 1-micron diamond suspension for about 2 minutes. Above mentioned parameters were used and relative motion comp for all SiC surface while relative motion contra for polishing cloth.

3.4.4.2. Surface Analysis

The microstructure of 10mmx10mm corroded and noncorroded sample surface were characterized by using JEOL 6610 LVSEM Scanning Electron Microscopy at an accelerating voltage of 15-20 keV. The samples were thoroughly cleaned in isopropanol ultrasonic bath to remove oil and metal particles. The elemental mapping and chemical composition were investigated using a Energy Dispersive X-ray Spectroscopy (EDX) which is equipped with SEM.

3.5. Tribology test on new test-rig

3.5.1. Sample preparation

The Plain bearing samples were cut into angle 120o by using Buehler Isomet 4000 precision saw cutting machine. The diamond blade was used to cut bearings with feed rate of 2.5-3.0 mm/min and the speed of 2500 rpm. The coatings always faced the blade to avoid damage to the coatings. Coolant were used to avoid heat during cutting operation and edges were smoothened. The samples were cleaned in ultrasonic bath contains isopropanol as a cleaning medium. Initial weight of the bearing samples were measured by using weighing scale.

3.5.2. Tribotest

The experiments investigated wear properties of journal bearings under gradually increased load and constant speed. The tests were conducted by using novel journal bearing test rig incorporated with TE92 tribometer from Phoenix Tribology. This test-rig was developed to exhibit wear properties of journal bearing which closely

resembles the real engine applications. Non-corroded and corroded multilayer Pb based and Pb-free journal bearings and induction hardened journal were used for wear investigations.

Test strategy carried out for considering the following parameters

Tests were conducted at constant speed of 1067 rpm at 120°C, with a load of 4 kN. In this experiment, the load was increased incrementally by 0.1 N increments at 240 s intervals, with a final step of 4 kN load running for 18000 seconds. The graph shown the Coefficient of Friction (COF) with change in load.

Chapter 4 Tribology test-rig design

A significant amount of project time to date has been deployed to the design, manufacture, development, and commissioning of a new hydrodynamic test-rig. This design will be used on the Rotary Tribometer TE92 HS. It was used for testing bearing on new and used lubricating oils, including corroded and non-corroded samples As discussed previously the main contribution to knowledge from this project will be the use of a purpose build test rig that simulates the bearing conditions within a typical automotive engine. The new hydrodynamic test rig is shown in fig 4.1 (a-d) will be used to carry out the experiments.

The Plint rotary tribometer TE92 HS was modified and shown as figure 4.1. to simulate real engine conditions. This enables the study of tribological properties and material responses of various corroded and non-corroded plain bearing materials. Two electrical resistance heaters are connected within the test adapter. A pair of 120^{o} journal bearings (machined from full size) are clamped on the sample holder as shown in figure 4.1(d) and pushed radially against the shaft which is placed at the center of the adapter containing the lubricant.

The interchangeable induction hardened journal was positioned at center of the adaptor as shown in figure 4.1(b) and it is rotated by making contact of the hub which connected with end of the spindle. Initially, the range of shaft diameter was tried to set the appropriate clearance between shaft and specimen. The bearing shell is clamped on the sample holder and self-centering mechanism aided the bearing shell to mount onto the shaft as shown in figure 4.1(b) during run with minimum deviation. The temperature sensors are placed in the adapter containing lubricant.

Bearing Clearance is one of significant parameter in bearing operation. So, it is necessary to determine the clearance with the journal and concentricity to the outside diameter. Final clearance is wholly dependent on the housing and interference between the housing and bearing shell. The misalignment can cause the edge loading in bearing

shell and hence this aspect was studied experimentally during the commissioning stage.

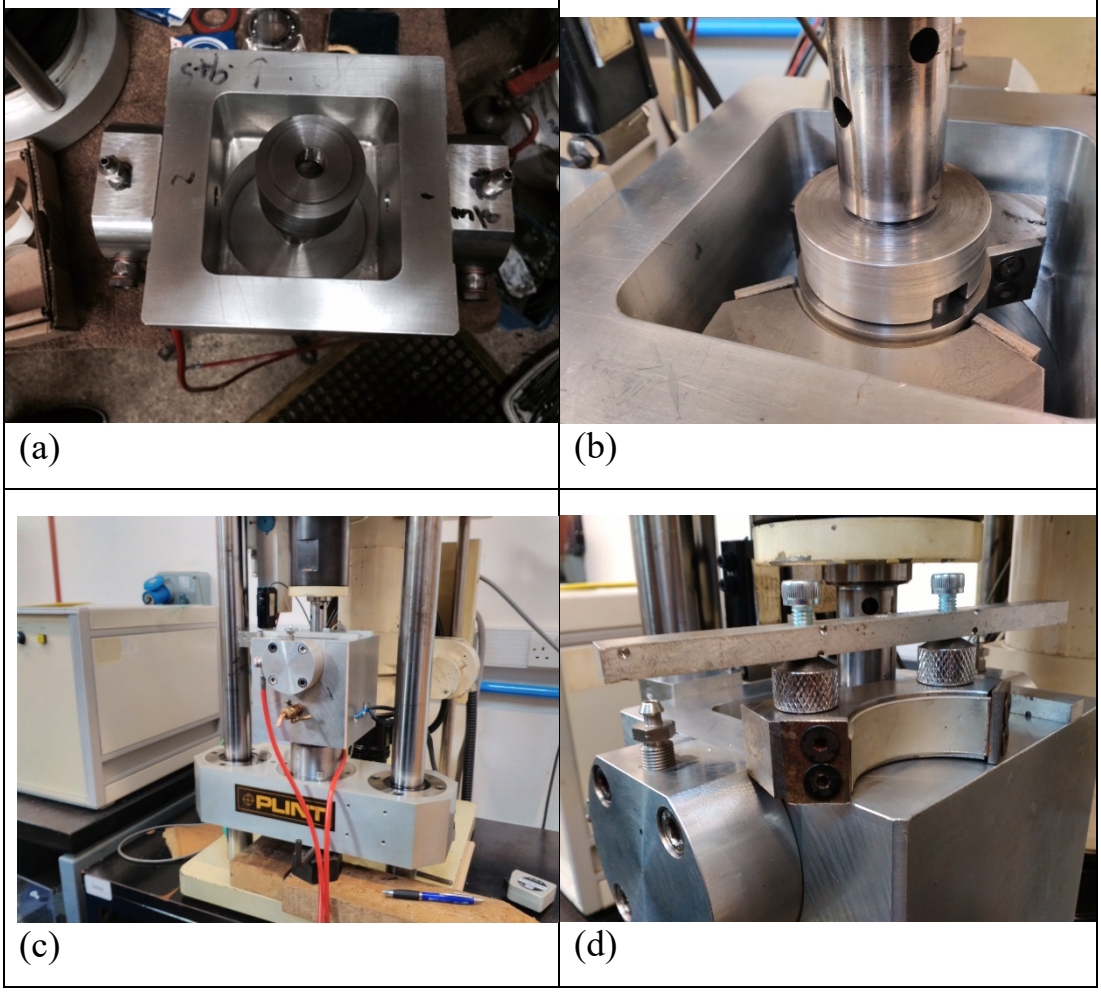

Figure.4.1. a) test adaptor with Journal at center b) bearing shell placed radially against journal shaft c) journal bearing adapter d) bearing shell with sample holder

4.1 Approach

The experimental results of tribological processes should meet real life findings. It would consider surface characteristics, chemical and physical properties of lubricant, and sliding conditions such as load, temperature, speed, contact situation, environmental conditions (Forstner 2007). Regarding bearings, it is essential to

develop reduced scale test to deliver tribological properties which is equivalent to engine bearings. Hence proposed approach is to deliver tribological properties of real engine conditions at reduced scale test.

4.2 TE92 Tribometer

The novel close-to-component test adapter is mounted on a TE92 Microprocessor Controlled Rotary Tribometer by Plint. It is versatile test machine can adopt different tribology test geometries which related to International standards. There are two interchangeable loading assemblies such as low load pneumatic bellow actuator of 2 kN and high load actuator of 10 kN, respectively. Generally, two electrical heating elements incorporated in the adapter to heat oil bath. Attached thermocouple in the oil bath is connected to the system interface which measures the system temperature. If there is sudden increase of vibration, Piezo-electric sensor which is in the machine frame will trip the circuit and stop the motor operation to avoid damage. COMPEND 2000 windows software in host PC along with Phoenix Tribology USB micro-controller interface controls and acquisition the data. Programming test sequences precedes automatic control while manual control is by using screen switches. Maximum speed limit of 10000 rpm and frictional torque is measured using transducer.

4.3 Temperature Measurement

The novel test adapter incorporates with heating elements, thermocouple is introduced from the side of the oil bath which measures the temperature of the system. The temperature is controlled by a Proportional -Integral-Derivative (PID) Software controller. The oil bath is preheated to desire temperature 120^{o}C before the start of the test and it takes around 30-40 minutes to reach the set temperature because the oil bath aluminium container is thick. The measured temperature throughout the test is system/oil temperature and is automatic control by programmed test sequences. Observed increase in temperature during test and drop to set temperature later and it could be the result of friction. Apparently, the bearing temperature during friction

should be higher than the oil bath temperature. The cooling period of oil bath after test also quite long.

4.4 Journal

The interchangeable induction hardened journal was positioned at center of the adaptor as shown in figure 3.1(b) and it is rotated by making contact of the hub which connected to the end of the spindle. Initially, the range of shaft diameter was tried to set the appropriate clearance between shaft and specimen. The bearing shell is clamped on the sample holder and self-centering mechanism aided the bearing shell to mount onto the shaft as shown in figure 3.1(b) during run with minimum deviation. Firstly, the gap in contact hub and journal coupling shown in fig 4.4.1 leads to vibrate the test-adapter during high speed test. Resulted incorrect frictional torque measurement and at some point, increase in vibration leads to trip the circuit and motor operation was stopped. To overcome that coupling of hub and journal was altered as shown in fig 4.4.1.

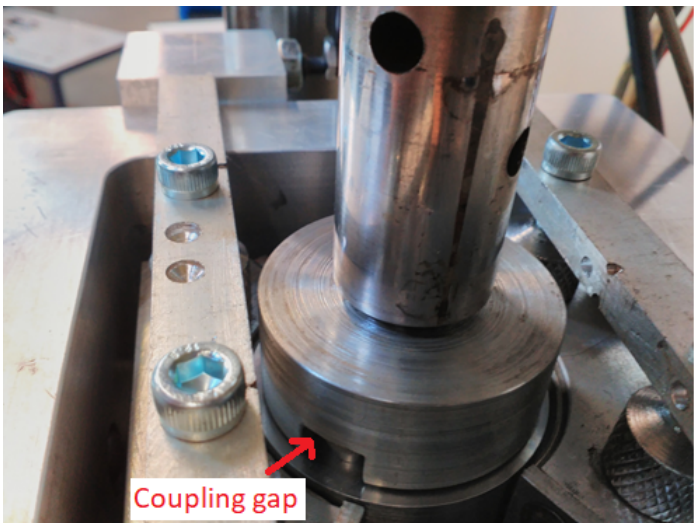

Fig.4.4.1. The coupling gap between the shaft and spindle contact hub

4.5 Oil Bath

The test rig wall is made up of Aluminium H30. As it is lightweight, it is easy to handle and less energy consumption Excellent when increasing load of the rig. Heat conductivity of Aluminium assist to reach desired test temperature as quick and drain away the heat quickly. The material can withstand at harsh engine oil environment due to its corrosion resistant property. It can withstand the test speed and high load as it possesses good shock and sound absorption quality. Oil drainpipe was introduced at bottom of the actuator to drain the oil after each test. After drained the oil via pipe, the leftover oil is wiped out with blue roll and made it ready for next test.

4.6 Load Assembly

Load assembly consist of high load pneumatic actuator bellow of 10 kN and hydraulic pressure load setup as shown in fig 4.6.1. The cylinder is filled with engine oil and the piston is operated manually to push bearing against the shaft and removal of bearing away from the shaft after completion of test. The load assembly is connected to the adapter on both sides attached to load pin which introduced behind the specimen holder which pushes the bearing against the shaft. Preload 15N was applied to aiding the alignment of bearing with shaft.

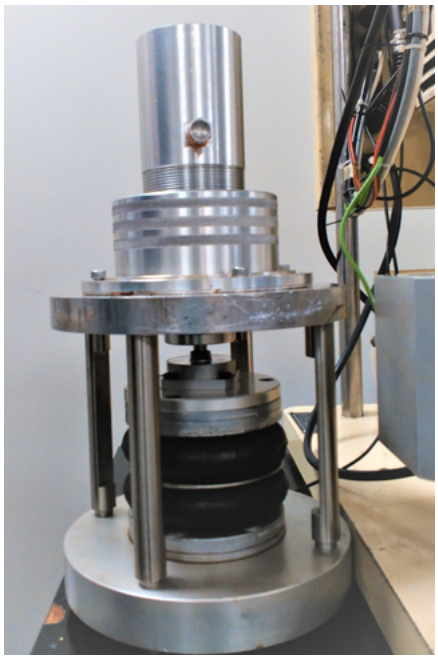

Fig 4.6.1. Hydraulic load pressure setup with 10 kN load actuator

4.7 Bearing Holder

Bearing holder contains dimple on its back to attach to the load pin. 120^{O} bearing is fastened to the holder with an aid of a screw on each side. Magnetic handle attached to the bearing holder assist the holder to sit at proper place and removed the magnetic holder once preload is applied to the bearing.

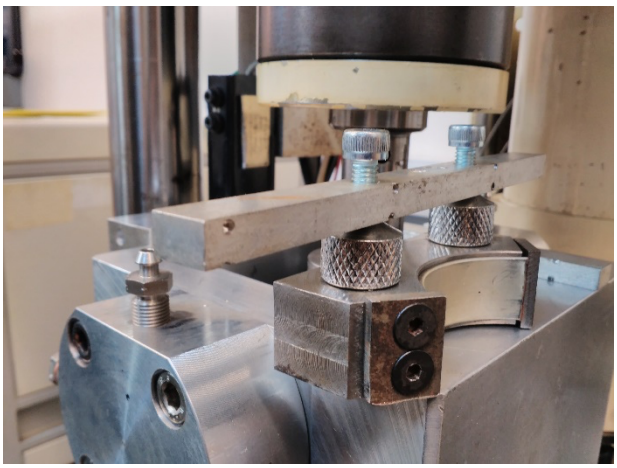

Fig 4.7.1. Bearing holder with magnetic handle

4.8 Test-rig

Test-rig comprises oil bath, height adjusting spring support and hydraulic load setup with a combination of Tribometer TE92. The oil bath is filled with LD5000 engine oil, both shaft and bearings were immersed completely to ensure proper lubrication. The load unit consist of load cell 10kN and hydraulic setup which is filled with engine oil. The heating elements were connected at side of the oil bath and drainpipe is set to remove the oil after each test. The load applied on the bearing holder pushes bearing towards the shaft which connected to the driving shaft. Normal load Pn and COF was calculated based on the geometry and applied force Fn.

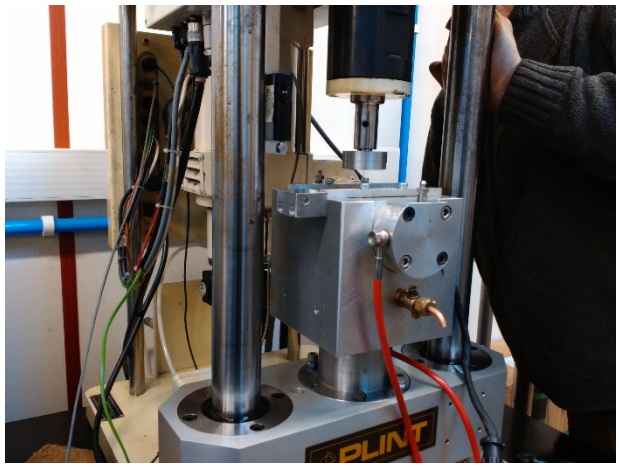

Figure 4.8.1 Test-rig with combination of Tribometer TE92

4.9 The test-rig wall

The test rig wall is made up of Aluminium H30. As it is lightweight, it is easy to handle and less energy consumption Excellent when increasing load of the rig. Heat conductivity of Aluminium assist to reach desired test temperature as quick and drain away the heat quickly. The material can withstand at harsh engine oil environment due to its corrosion resistant property. It can withstand the test speed and high load as it possesses good shock and sound absorption quality.

4.10 Journal

It is induction hardened steel with diameter of 52.75 mm with similar material to the internal combustion engine journal. The diameter is chosen on trial and error based method to obtain appropriate oil clearance. As it is interchangeable, it can be replaced with new journal if test demands.

4.11 Sample holder

The sample holder is made up of steel, the bearing is attached to the sample holder with adjusting bolts on the holder as shown in the fig4.7.1. The bearing is free to align with shaft and the magnet is used to adjust the position of the bearing with respect to the shaft. the sample holder has dimple on the back, and it is attached to loading pin, it is used to apply load on the bearing towards journal by hydraulic pressure.

In engines the high load is on the lower bearing in the housing. But here the bearing is cut into 120o to obtain high load on both the bearings, so we can use both bearings for studying wear mechanisms. However, trial test results showed that high load is not always on the center of the bearing and it depends on the bearing alignment with respect to the journal.

4.12 Bearing length

The dimension in the axial direction including chamfered section is the bearing length and this influence the load performance. While the effective bearing length excludes the chamfered section and oil grove. Bearing length ‘L/D’ is the ratio of the bearing load and the outside diameter. Generally, L/D is between 0.25 and 0.5, while 0.3 or higher is recommended. If it is too large, lead to increase in misalignment , uneven adherence of bearing and housing ,etc. If it is too small, lowers the load resistance so load must be reduced. The effective bearing length should be smaller than the bearing length to prevent the seizure or excessive loading on the shaft.

4.13 Height

The bearing is firmly fit to the housing to prevent fretting between the bearing outside diameter and housing inside surface, and the interference is required to measure the height of the bearing. The outer diameter of the bearing cannot be measured under free conditions. Therefore, the height is measured with applied measurement loads and the height gauge is fit firmly against the bearing.

The height is determined based on the bearing hoop stress σ_B and contact pressure P_r. The height is measured by considering the housing rigidity, housing material, temperature (Daido metal).

When the height increases, excessive stress may occur in the housing when the height is too small, fretting, migration, etc., may occur during operation. The measurement load is depending on the pressure stress.

Pressure stress during measurement=measurement load (Wall thickness- Alloy thickness) x bearing length.

Chapter 5 Results and Discussions

5.1 Mass Change

The mass changes of the bearing shells are important as a measure of surface damage resulting from corrosion tests conducted as described in section 3.1. The mass changes on lining and overlay materials designated from section 3.1 are shown as Table 5.1 and 5.2. These results presented mass changes of the bearing materials after corrosion tests in new and used oil over the periods of 50, 200 and 500 hours. On assessment of these tables, mass changes within coated materials were relatively small. Significant mass changes were observed in lining materials. Furthermore, in few a cases mass gain was observed due to oil adsorption.

Substrates:	**Pb-free**		**Pb-based (Sintered)**		**Pb-based (Cast)**	
Designation:	**DERM 120**		**DERM 119**		**DERM 118**	
Test Time	**New oil**	**Used oil**	**New oil**	**Used oil**	**New oil**	**Used oil**
50h	-54	-24	-31	1517	-5	871
200h	26	87	6	6986	53	1494
500h	-11	80	38	14710	136	2980

Table 5.1. Mass change (mg/cm^2) of substrates after corrosion tests (Linings)

Coatings	Pb-free		Pb-free		Pb-based	
Designation	**DERM 123**		**DERM 122**		**DERM 121**	
Test Time	**New oil**	**Used oil**	**New oil**	**Used oil**	**New oil**	**Used oil**
50h	-0.004	-0.045	-0.043	-0.186	-0.018	0.054
200h	-0.028	-0.03	-0.007	-0.04	0.09	0.148
500h	-0.032	-0.058	0.152	-0.139	0.075	0.24

Table 5.2. Mass change (mg/cm^2) of coatings after corrosion tests (Overlays)

The sample (DERM120) results shown in figure 5.1 indicates the Copper-Tin (Cu-Sn) lining material gained mass. It is comparatively small in both new and used oil, besides there is possibility of oil film formation on the surface during corrosion test. There was significant mass change in case of another lining material (sample DERM119) which is Lead (Pb) a based sintered material within used oil. The mass loss increased as the test duration increased. In addition, lead (Pb) is prone to corrosion within acid nonetheless deteriorated oil contains organic acids. The sample (DERM 118) is a lead (Pb) based cast lining material is also showing a mass loss in case of used oil but not as much compared with sampleDERM119. However, Tin (Sn) weight percentage in sample DERM118 is greater and this can enhance the corrosion resistance of the lead (Pb) phase within the Cu-Pb alloy.

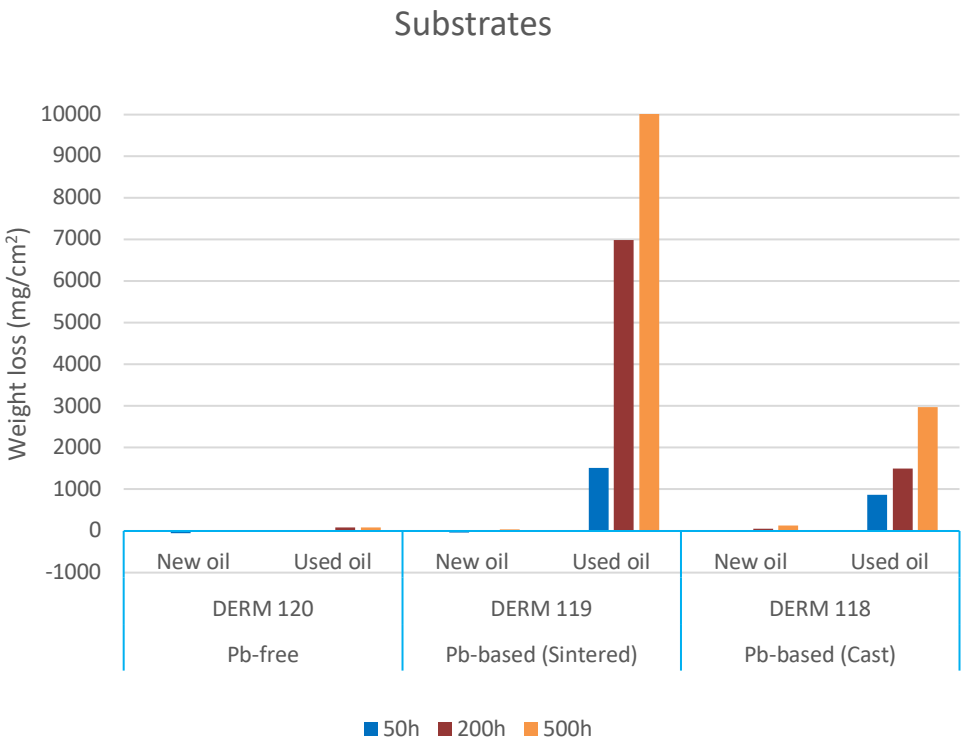

Figure 5.1. Weight loss of different lining materials in both new and used oil

Fig 5.2. showed that weight loss of coatings with respect to test duration in both new and used oil. When weight loss of coatings is compared to substrates, no significant changes are seen in the graph. The weight loss in coatings were negligible.

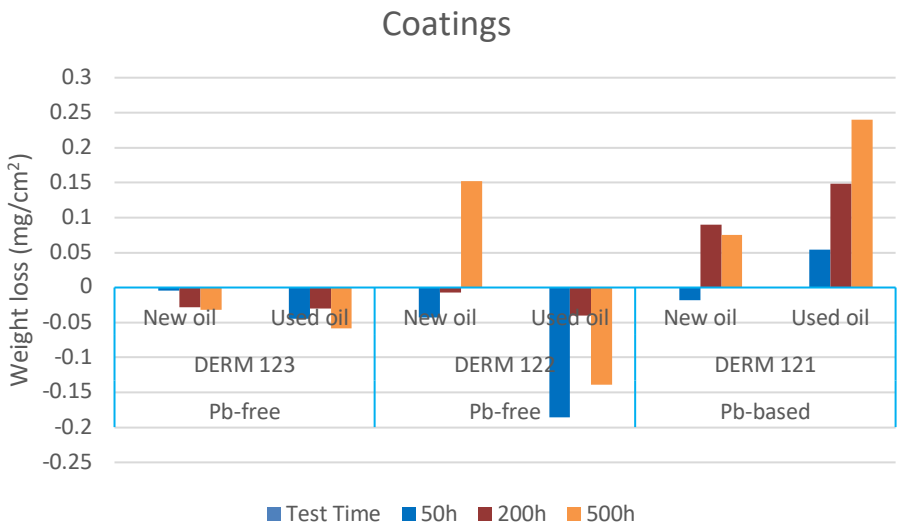

Figure 5.2. Weight loss of coatings in both new and used oil

5.2. Visual Evaluation

The photographs of DERM119, DERM120 and DERM118 before and after static immersion test were shown in Fig.5.3. The photographs in fig 5.3. shown that discoloration of DERM 119 was quite significant in case of deteriorated oil. Initially it was lustrous pink in color turned to be yellow at 50 h and subsequently it turned to be dull and light brown in color at 200 and 500 hrs.

The discoloration take place as a result of test samples reaction with lubricating oil. The discoloration due to corrosion, high temperature or prolonged immersion in oil.

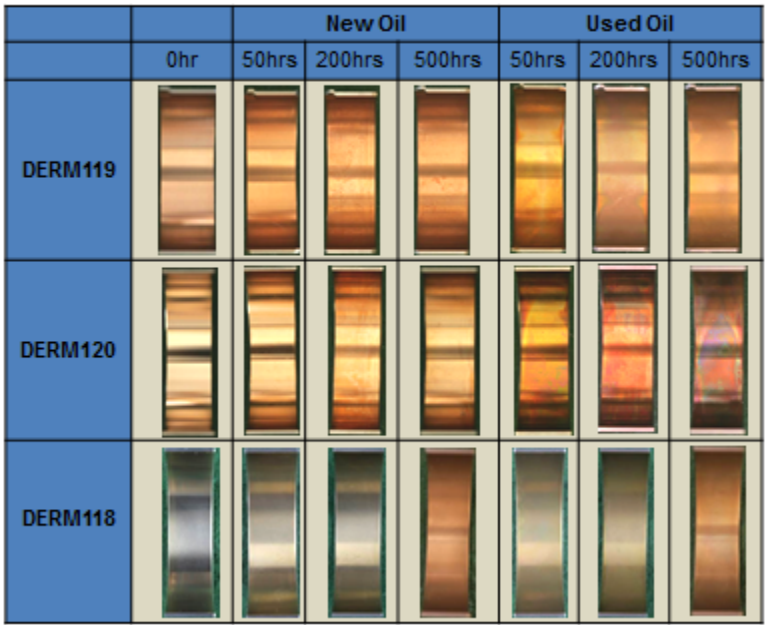

Figure 5.3. The photographs of tested and untested bearing lining materials

The visual comparison of untested and tested samples in both new and used oil is given in fig 5.3 and 5.4.DERM119 was lustrous pink in colour and turn down to yellow and followed by non-lustrous brown after tested in new oil but it seemed severe in case of deteriorated oil. Pb-based lining material in new oil was more resistant to corrosion attack compared to used oil. DERM120 was appeared to be bright and no significant colour change after tested in new oil but the tested samples in used oil seemed blackened and it was severe corrosion in the long test duration 200hrs and 500 hrs in

deteriorated oil. The appearance of the DERM118 changed after long duration 500 hrs in both used and new oil.

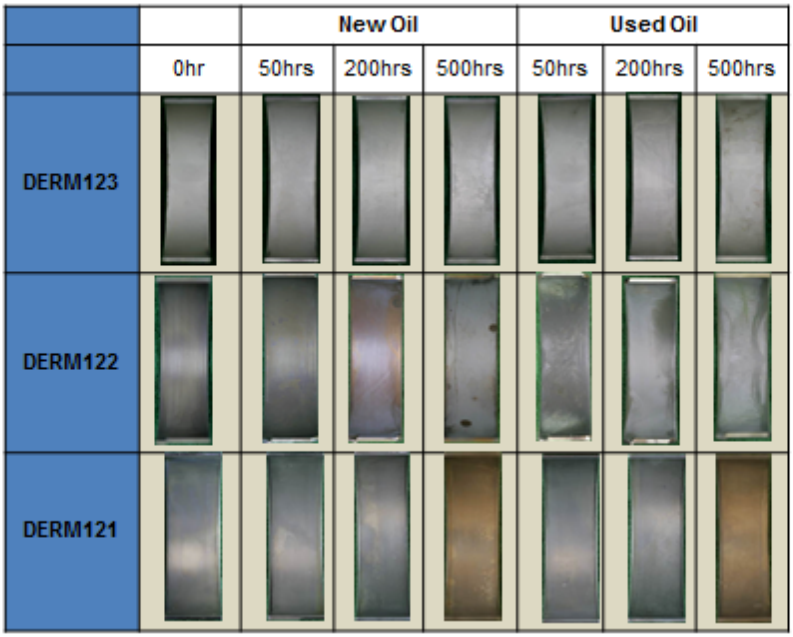

Figure 5.4. The photographs of tested and untested bearing overlays

Sn-based coated material DERM123 shown excellent corrosion resistance in both new and deteriorated oil. Appearance of Bi coated DERM121 changed after tested 200hrs in new oil but there is no significant change in case of used oil. Discoloration of Pb-based coated samples DERM122 observed after 500 hrs tests in both cases. There was no appearance change observed before 200 hrs.

5.3. Cross-sectional and Surface Analysis

5.3.1. Pb-based lining material

Sample DERM119

Lead in copper-lead and bronze-lead alloys were insoluble in solid state and it form different phases . Thus, pure, and unalloyed phase of Pb are more susceptible to corrosion in weak organic acids. The corrosion test was carried out on DERM119 for different time duration 50 h, 200 h and 500 h respectively in both new and used oil.

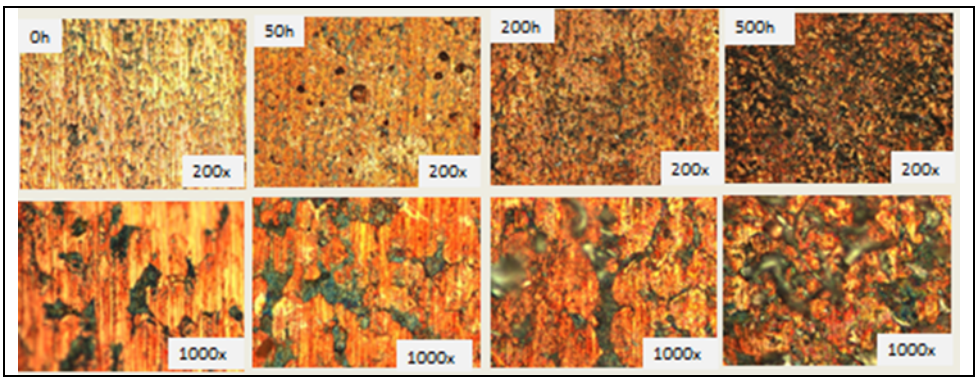

Figure 5.5. Optical images of DERM119 at different corrosion test duration in new oil

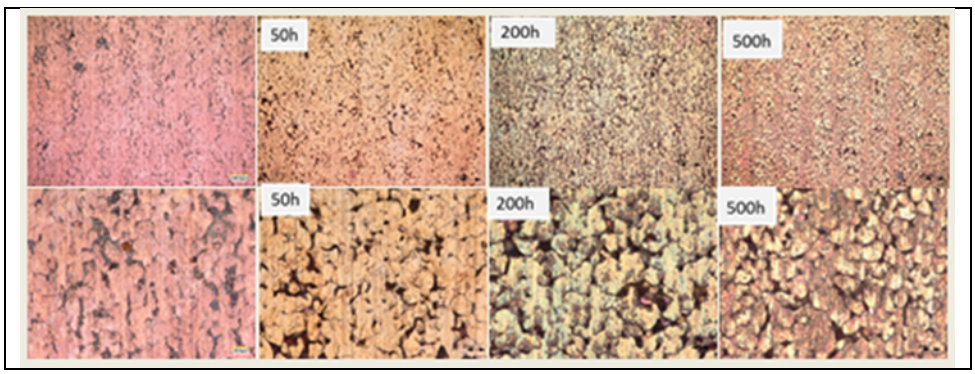

Figure 5.6. Optical images of DERM119 at different corrosion test duration in used oil

New oil doesn't contain any organic acids and there is no evidence of corrosion of DERM119 in new oil. Generally, Pb in degraded oil form lead oxides which is thick

yellow deposit and disappeared after certain period (Wilson 1970). The photographs in fig. 5.5 show significant discoloration of DERM 119 in the case of deteriorated oil. According to the surface morphology shown in Fig.5.6 and the cross sectional and elemental mappings of Fig.5.8 and 5.9, the Lead has moved out of the Cu matrix. The oil samples were analyzed to determine the dissolved Pb in oil and it is tabulated in table 5.3. The severity of disappearance of lead from Cu matrix was more as test time increases moreover, it appeared to be uniform depth in corrosion. The graph fig.5.10 showed linearity between the depth of corrosion and test duration, hence corrosion of Pb in Cu matrix is a function of time.

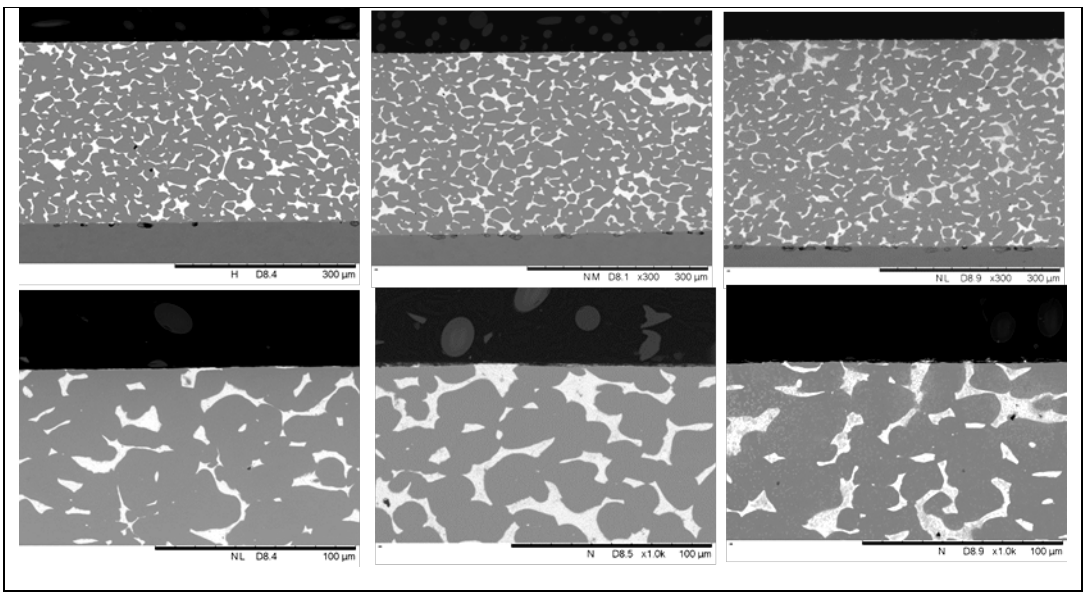

Figure 5.7. The cross-sectional SEM images of DERM119 after corrosion test in new oil at 50 hrs,200 hrs and 500 hrs (300X and 1000X magnification)

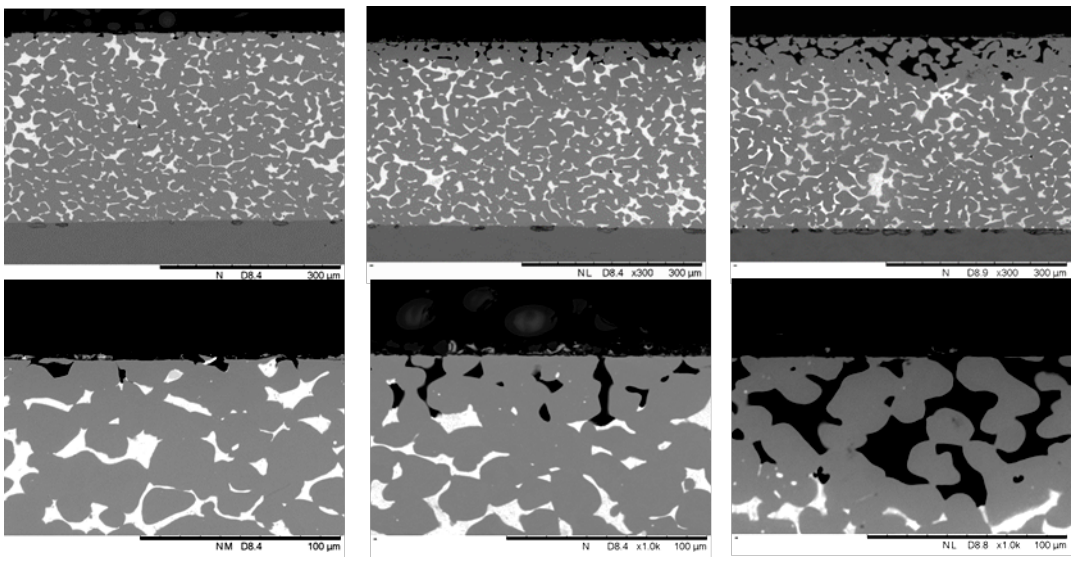

Figure 5.8. The cross-sectional SEM images of DERM119 after corrosion test in used oil at 50 hrs,200 hrs and 500 hrs at magnification 300 X and 1000X

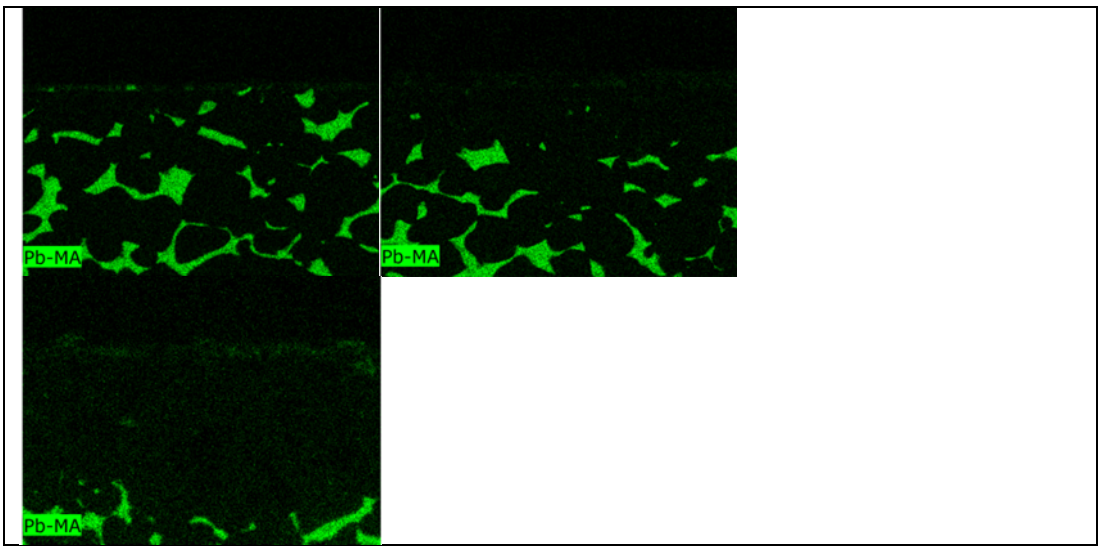

Figure 5.9. Elemental mapping of Pb after tested in engine oil at 120oC at 50h , 200h and 500h

Test time (in hrs)	Depth of Pb disappearance (in µm)	Average depth (in µm)
0	0.0	0.0
50	10.6 10.9 6.38	9.3
200	30.6 32.7 34.8	32.7
500	63.0 63.8 74.6	67.1

Table 5.3. Depth of lead disappearance at different test duration

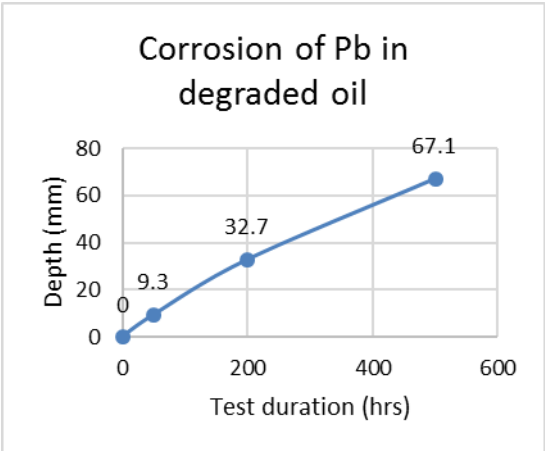

Figure 5.10. Depth of Pb disappearance with respect to test duration in used oil

To check the oil composition, acid number and base number, titration method were used. The oil analysis result for DERM119 after tested in used oil for 50 h, 200 h and 500 h are given in Table 5.4. Pb content in oil increased with increase in test duration in oxidized oil.

Oil	Lead (ppm)	Copper(ppm)	TBN (mgKOH/g)	TAN (mgKOH/g)
Used oil 0h	2	1	3.3	3.2
DERM119 U50 h	242	9	3.7	3.1
DERM119 U200 h	1109	42	2.5	3.3
DERM119 U500 h	2177	78	3.7	3.6

Table 5.4. Presence of lead and copper in used oil

(McCloskey 1995) When lubricants become corrosive due to an accumulation of acids and peroxides, lead is removed from copper-lead bearing alloys. Sulphur compounds are usually the corrosive element when both copper and lead are attacked. In internal combustion engines, sulphur compounds can originate from the fuel system, leaks in centrifugal compressors' lubricating systems, or as a result of extended operation at high temperatures. To guard against such corrosion, some bearing designs utilize an overlay over the copper alloy bearing.

The result suggests that the possible corrosion mechanisms of Cu-Pb alloy in degraded oil are:

Pb in open atmosphere readily form PbO on its surface. Generally, it is insoluble in lubricating oil, but it is soluble in degraded oil which contains organic acids. PbO reaction with weak organic acids is given in the following equation.

$PbO + 2RCOOH \rightarrow (RCOO)_2\, Pb + H_2O$ (3) (Kumar 2013).

As said in literature, the peroxide formation in degraded oil would be a reason to formation of lead oxides. Eventually, lead oxides dissolve in degraded oil and left the voids in Cu-Pb alloy substrate. However, it was difficult to say that lead or lead oxide react with organic acids in degraded oil (Kumar 2013).

Other possibilities are Pb dissolve in organic acids as the reaction given below

$$Pb + 2RCOOH \rightarrow (RCOO)_2\, Pb + H^2 \quad (4)$$

Both mechanisms were possibly functioning on the DERM119 in used oil. Oil was analyzed to prove the presence of dissolved Pb from the substrate.

Sample DERM118

Fig.5.13 and 5.14 shows the polished cross section of DERM 119 of both untested sample and tested sample of 50 h,200 h and 500 h in new and used oil. It consists of steel backing and lining. The lining has the soft phase Pb distributed throughout in Cu matrix along with little Sn content. The tested samples in new oil showed similar features alike untested sample. However, samples from used oil showed Pb disappearance from the surface. The depth of Pb disappearance increases with increase in test duration and it is justified by the cross section shown in fig 5.14.

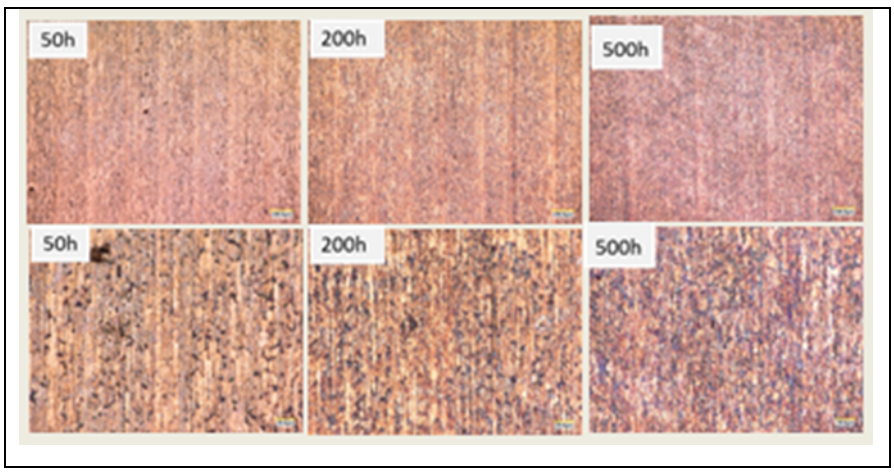

Figure 5.11. Optical images of DERM118 at different test duration in new oil

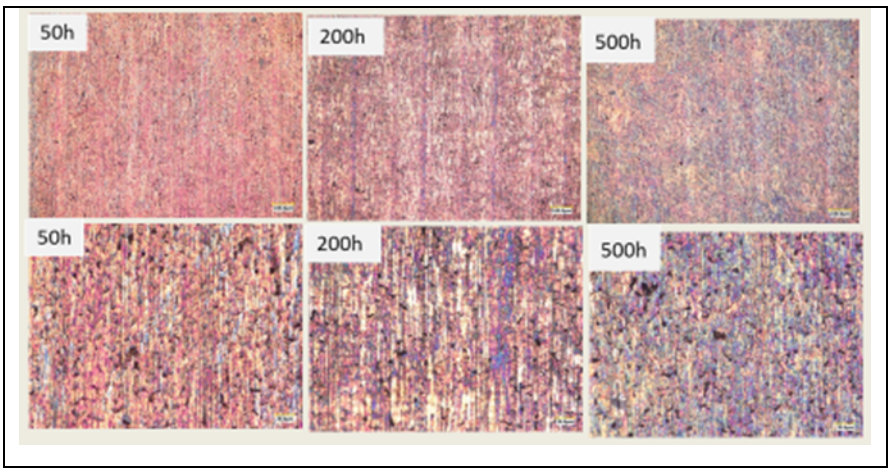

Figure 5.12. Optical images of DERM118 at different test duration in used oil

Low melting point Pb forms a discrete phase in the Cu matrix as in DERM119. Additionally, it is a cast alloy and has a higher Sn content than sintered DERM119. Sn dissolves in the Pb phase and enhances the corrosion resistance of leaded Cu alloys. Fig. 5.11 and 5.13 show the cross-sectional and surface analysis of DERM118 tested in new oil for 50, 200 and 500 hrs. These samples did not exhibit any significant differences except discoloration.

The cross-sectional analysis showed the Pb disappearance from the surface and the corrosion was non-uniform. Similar corrosion mechanisms as shown in eqn (3) & (4) prevail. Non-uniformity perhaps due to the presence of Sn. The chances of diffusity of Sn in copper is high. Sn depleted region possibly prone to corrosion. Fig.5.15 the graph showed the severity of corrosion with respect to exposure time.

The test sample DERM118 anticipated to have similar corrosion mechanisms alike another Pb-based sample DERM119. The cross sectional and surface analysis of DERM118 tested in used oil shown in Fig 5.14 and 5.12. revealed that Pb phases disappeared from the surface. As discussed above, the peroxide and organic acids could dissolve Pb phase.

(Tichvinsky 1943) Bearing corrosion are of two types, uniform corrosion, and localized corrosion. The corrosion of all copper lead bearings was uniform.

In degraded oil, uniform corrosion occurs in copper lead bearings.

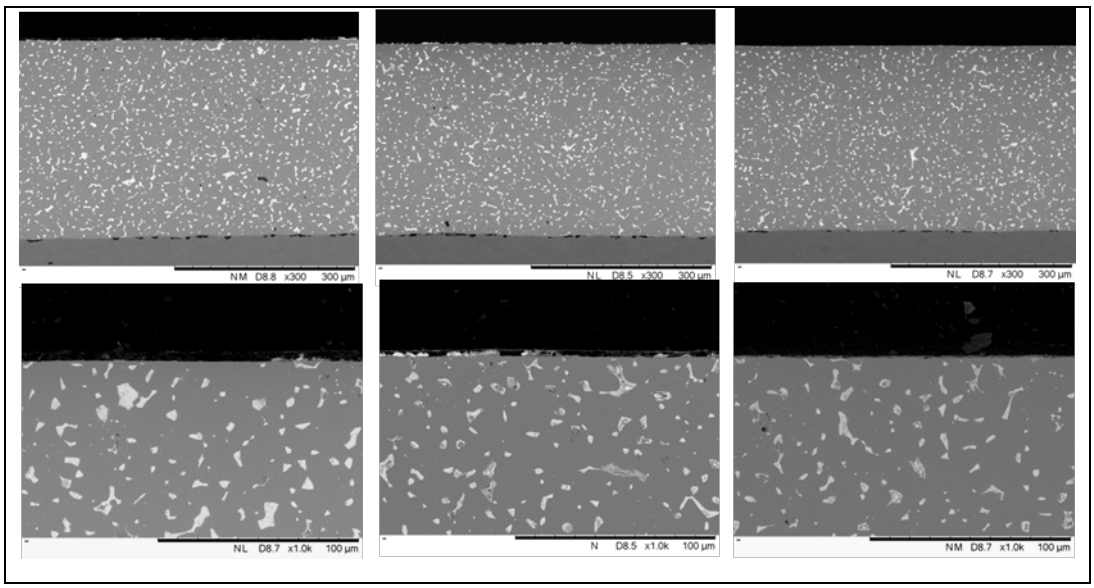

Figure 5.13. The cross-sectional SEM images of DERM118 after corrosion test in new oil at 50 hrs,200 hrs and 500 hrs (300X)

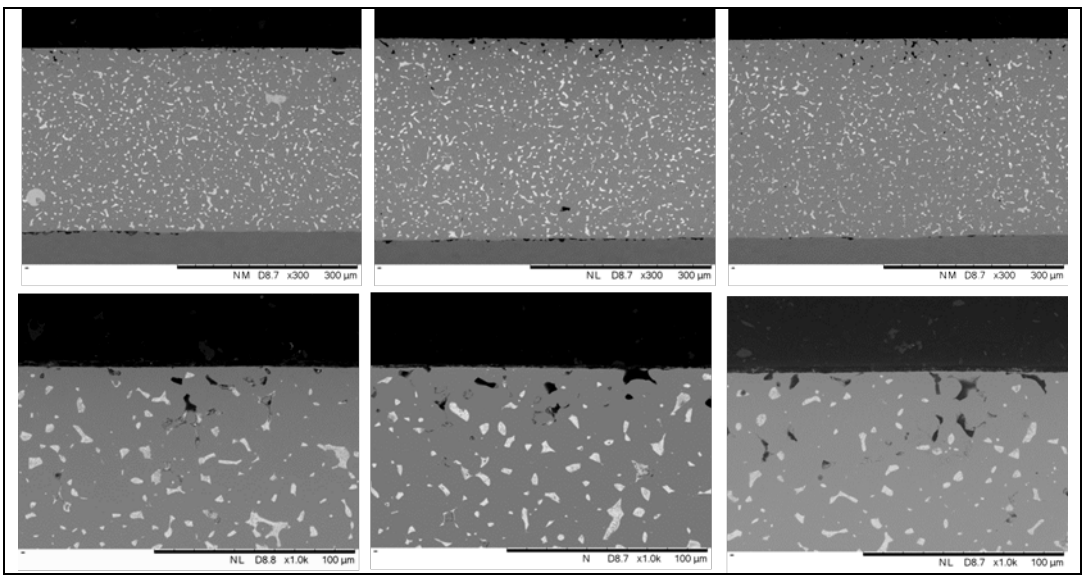

Figure 5.14. The cross-sectional SEM images of DERM118 after corrosion test in used oil at 50 hrs,200 hrs and 500 hrs (500X and 1000X)

Test time (in hrs)	Depth of Pb disappearance (in µm)	Average depth (in µm)
0	0.0	0.0
50	5.56 22.1 9.04	12.23
200	21.0 24.4 15.7	20.37
500	43.6 33.7 33.0	36.77

Table 5.5.

Depth of lead disappearance at different test duration

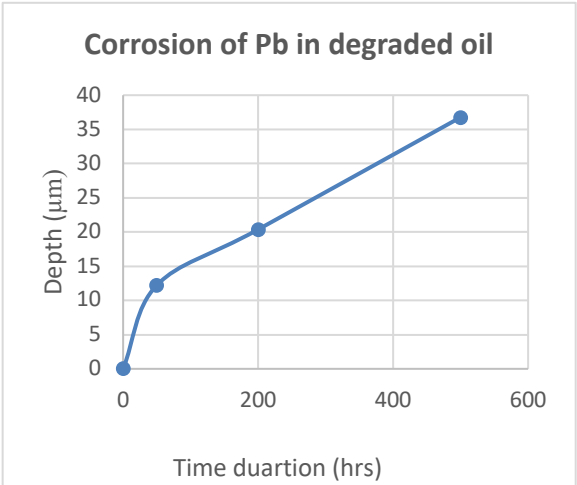

Figure 5.15. Depth of Pb disappearance with respect to test duration in used oil

5.3.2. Lead (Pb) based coated material (DERM 121)

The corrosion tests from the lead (Pb) based coated samples were considered. Figures 5.16 and 5.17 show the optical micrographs of lead (Pb) based coatings at different time intervals after static immersion corrosion test within new and used oil (120^{O}C). Lead (Pb) based electroplated coatings on the surface of a Copper-Lead (Cu-Pb) alloy (DERM 119) lining material. Black spots or areas are observed (figures 5.16 and 5.17) within all tested samples for both new and used oil results. However, these areas are not as severe in case of new oil.

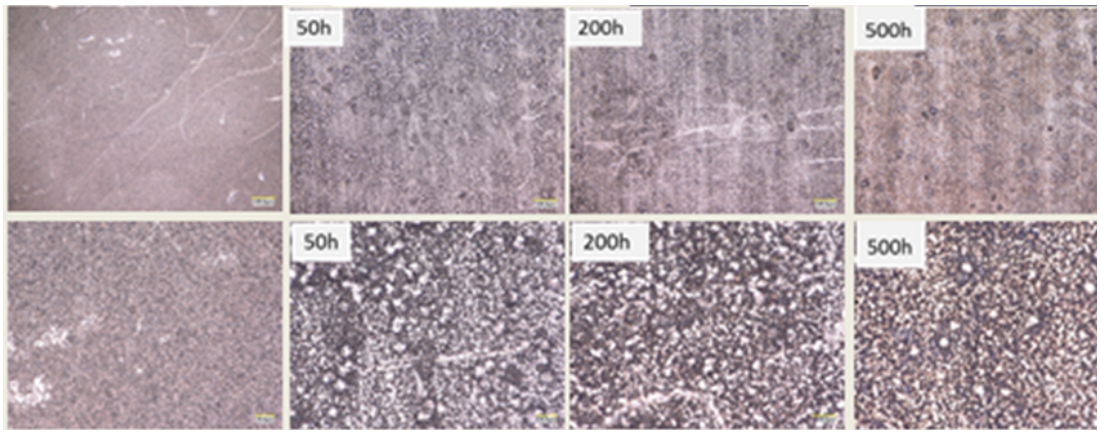

Figure 5.16. Optical images of DERM121 at different test duration in new oil

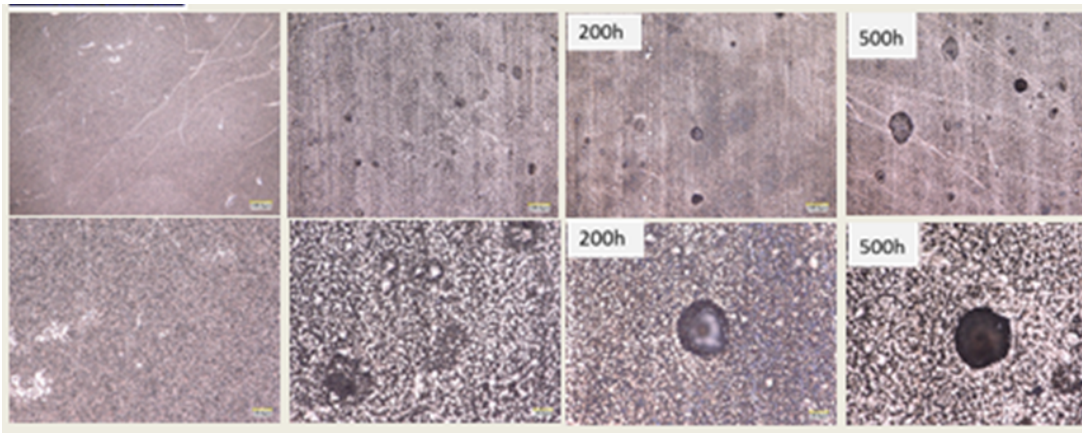

Figure 5.17. Optical images of DERM121 at different test duration in used oil

The microstructure on the cross-section of the coated lead-Tin (Pb- Sn) sample (DERM 121) is shown in Figure 5.18 (new oil) and 5.19 (used oil). These cross-sections are produced post corrosion tests (120^{O}C) in both new oil and used oil. The cross-sections (figures 5.18 and 5.19) show no evidence of corrosion attack on this trimetal bearing material.

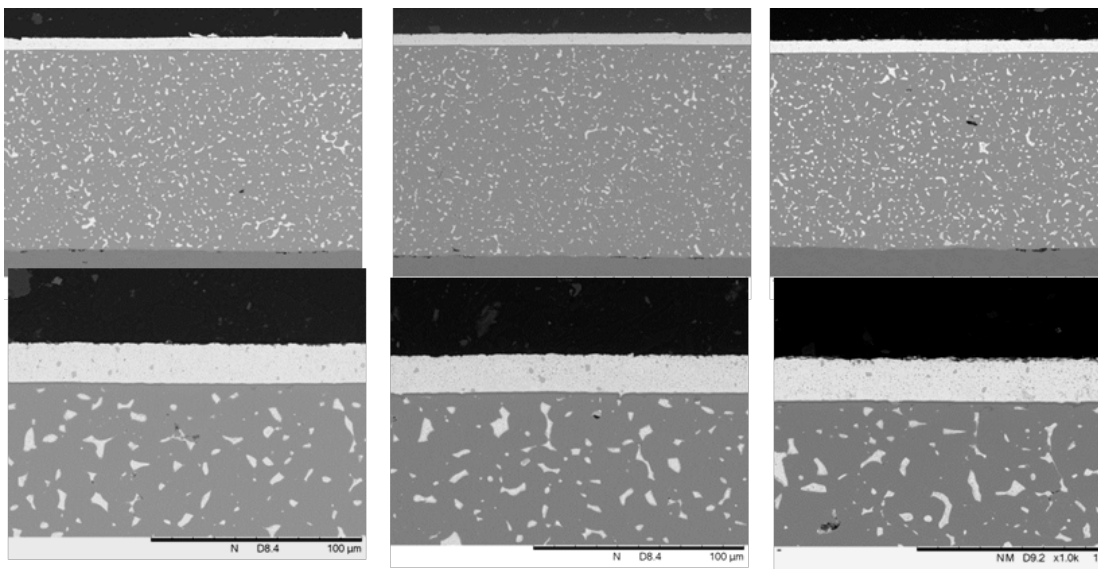

Figure 5.18. Cross-sectional SEM images of trimetal bearing material (DERM121) after corrosion test in new oil at 50, 200 and 500 hours at magnification 500X and 1000X

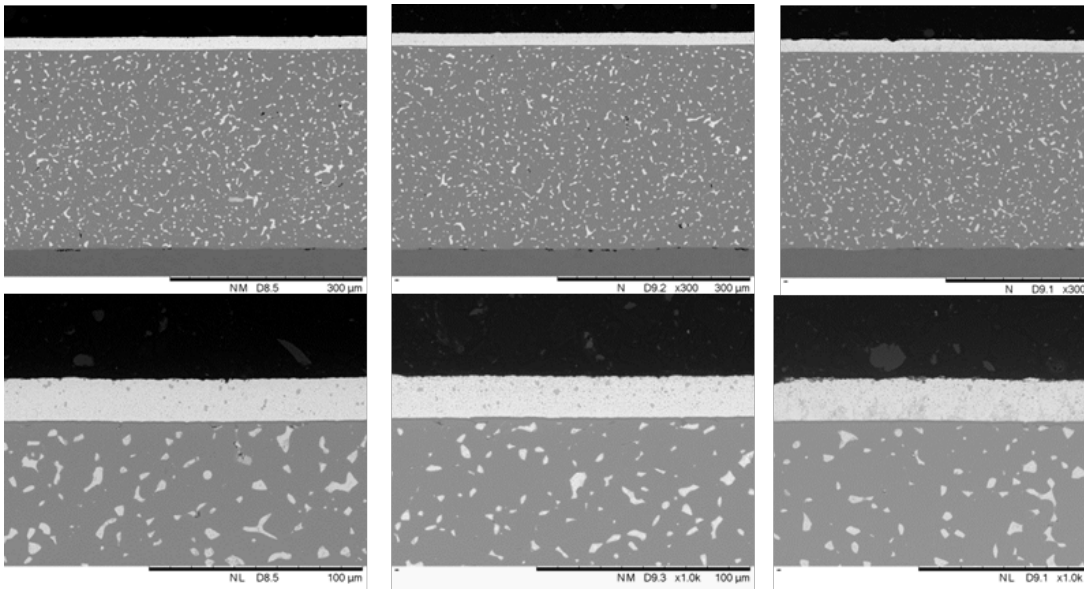

Figure 5.19. Cross-sectional SEM images of trimetal bearing material (DERM121) after corrosion test in used oil at 50, 200 and 500 hours at magnification 500X and 1000X

In terms of the surface, the black spots or areas were investigated in more detail to identify damage mechanisms. Samples that were tested in used oil were the subject of further investigation due to the severity of surface damage compared to samples tested in new oil. The investigations using digital optical microscopy (section 3.1) are illustrated in figures 5.20 (2D), figures 5.21-5.23 (3D). The blackspots along with observed pits were observed first in the 50 hour test sample. The severity of pits increased with increase in test duration in degraded oil. The copper-lead (Cu-Pb) lining was visible after 200 and 500 hours test samples and shown in figure 5.21-5.23. Interestingly after detailed observations, protrusions or raised edges are found around pit edges given Figures 5.21 - 5.23.

(Waukesha bearing) Copper-containing alloys, including tin-based whitemetal, are attacked by hydrogen sulphide in the oil..A dark deposit, mainly copper sulphide, develops on the surface of the bearing as a result of hydrogen sulphide attack.The copper-tin compound in the lining is also depleted, weakening the material.The phosphor bronze small end bush was corroded by sulfur as a result of decomposition of lubricating oil additives and gross pitting of the bearing surface.

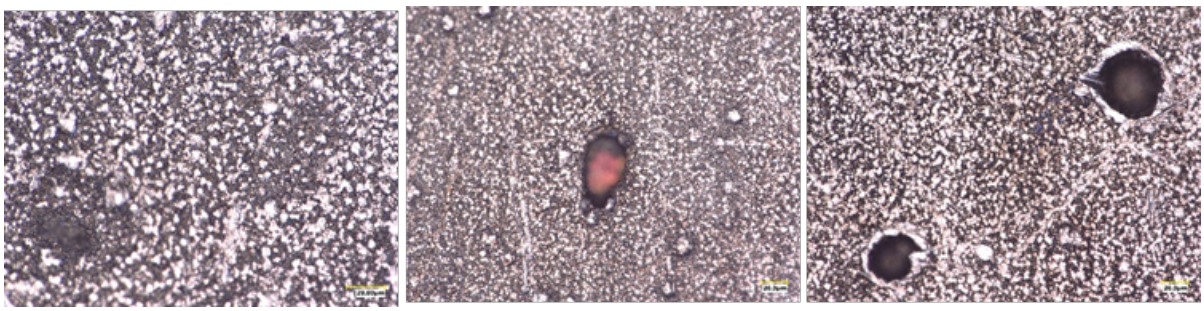

Figure 5.20. Two dimensional optical images of lead based coating (DERM 121) after 50, 200 and 500 hours at magnification 1000X tested in used oil

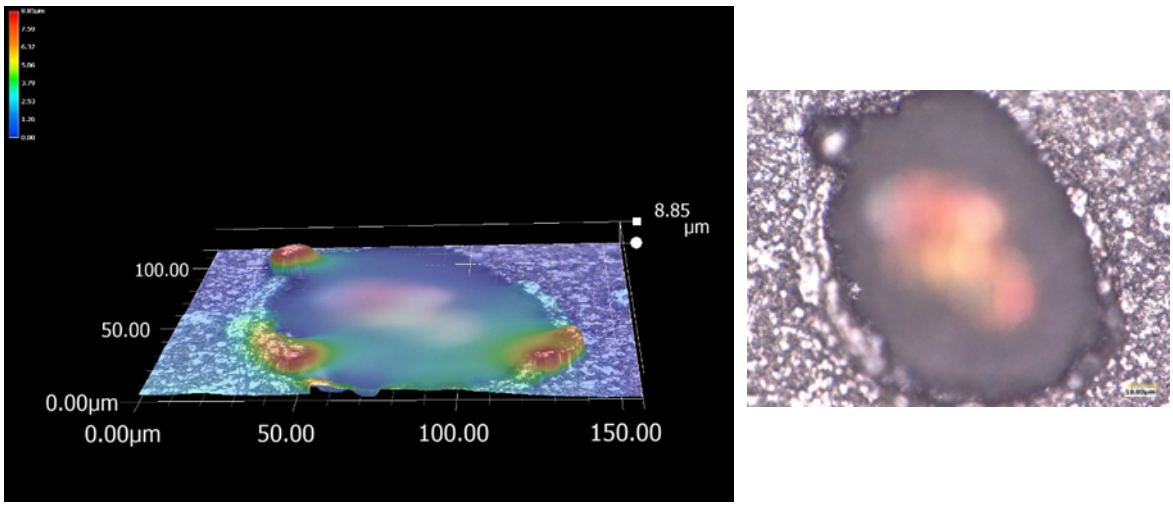

Figure 5.21. Three-dimensional optical image of lead based coating (DERM 121) after 50 hours tested in used oil

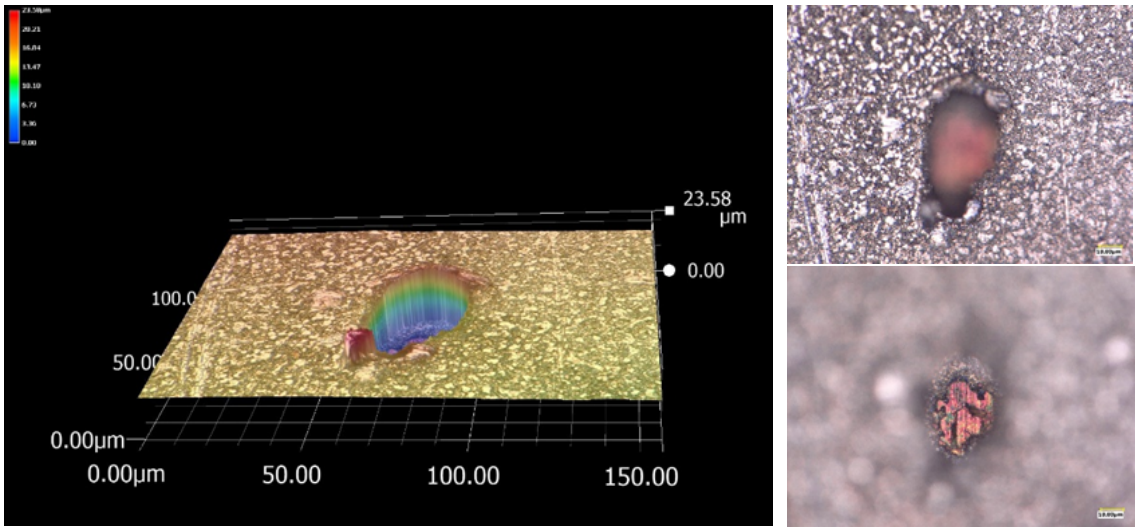

Figure 5.22 Three-dimensional optical image of lead based coating (DERM 121) after 200 hours tested in used oil

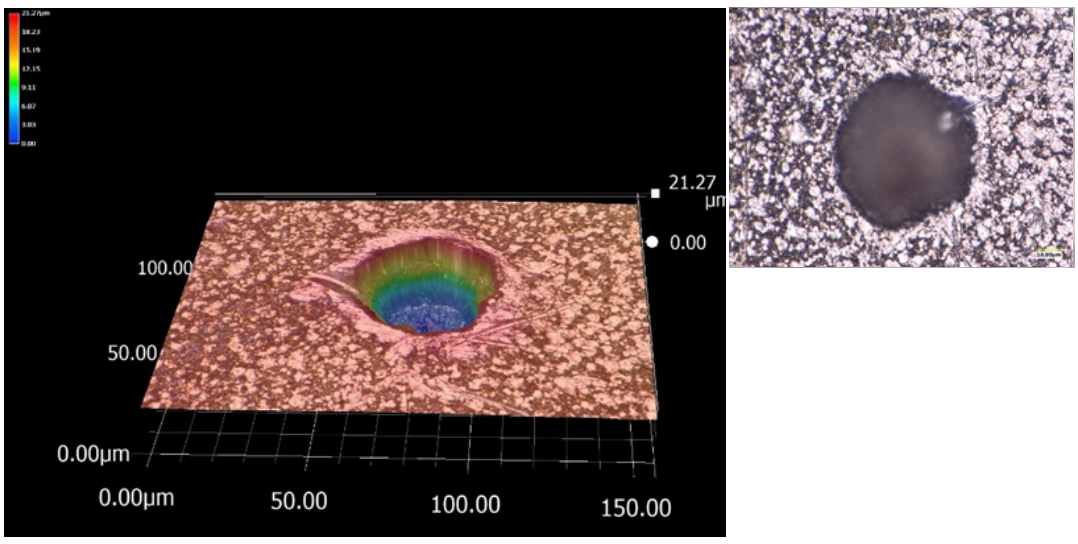

Figure 5.23. Three-dimensional optical image of lead based coating (DERM 121) after 500 hours tested in used oil

A chemical analysis of the actual surface was conducted to investigate the mechanisms of surface damage of the test sample (500 hours) within the used oil. Section 3.1 describes the Xray Photoelectron Spectroscopy (XPS) analysis used for this surface analysis. Figure 5.24 illustrates the X-ray spectra of lead coating on the surface. The experimental parameters of the XPS showed the peak position at 136.5 eV identified as lead (Pb). At the peak position of 138.4 eV shows a much more consistent identification with Pb (II) compound, either PbS or PbO. A strong Tin (Sn) signal at 486.4 eV confirmed the presence of Tin (Sn) on the surface.

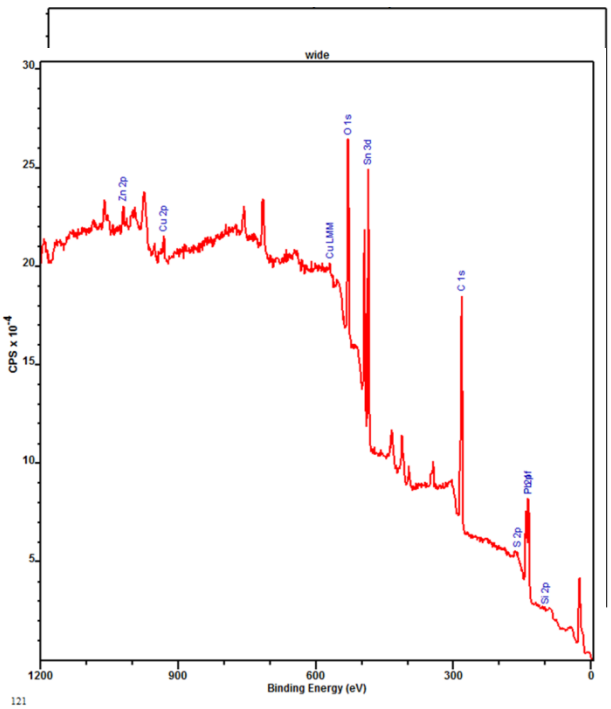

Figure 5.24. XPS spectra of lead Tin Coating (DERM121)

5.3.3. Lead–Free Lining Material: Copper-Tin (DERM120)

Copper-Tin (Cu-Sn) alloy is a lead (Pb) free lining material. The corrosion test described in section 3.1 was carried out on the sample for different test durations of 50, 200 and 500 hours (in both new and used oil). The optical micrographs of the samples tested in new and used oil is given in figures 5.25 and 5.26.

The optical micrographic images shown in Figures 5.25 and 5.26 reveal that little evidence of corrosion takes place in new oil but in the case of used oil the surface appearance changed and discolouration occurs. Additionally, the mass change was negligible as compared to the lead (Pb)-based lining material (section 5.1). Here, corrosion is observed to progress in degraded oil and the surface discolouration increases significantly after 500 hours. It is assumed at this stage that the surface is composed of copper oxide. The blackening phenomenon noted in visual examinations after testing in degraded oil is also present and compares with results from section 5.2.

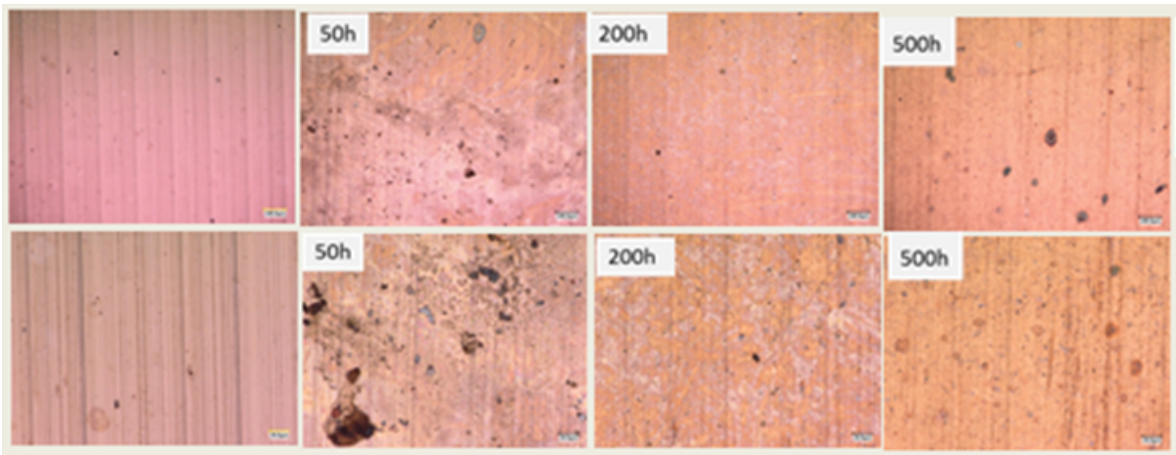

Figure 5.25. Optical images of copper-tin alloy (DERM 120) surfaces at different corrosion test durations in new oil

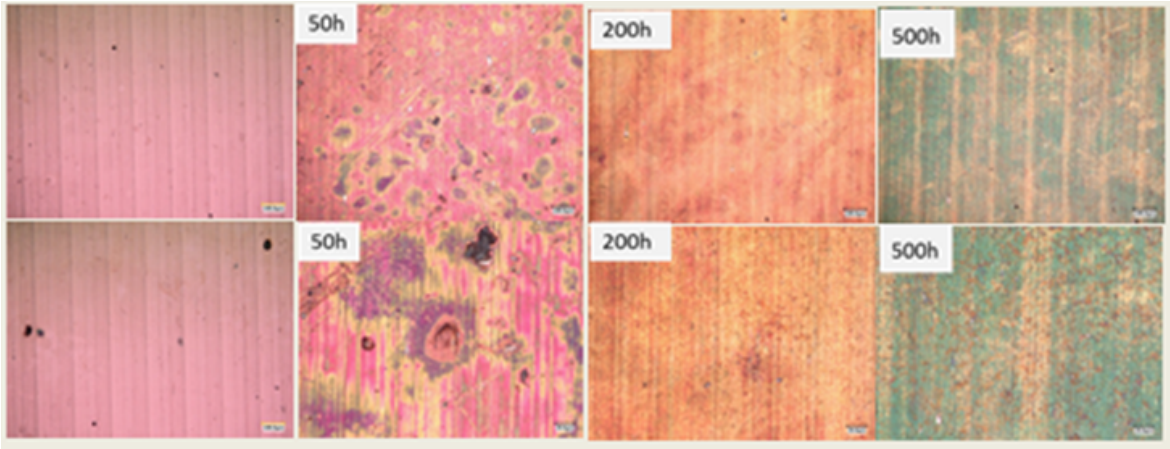

Figure 5.26. Optical images of copper-tin alloy (DERM 120) surfaces at different corrosion test durations in used oil

Cross-sections of the samples shown in figures 5.25 and 5.26 were prepared to investigate further the corrosion mechanisms and the subsurface damage. The cross-sectional images are shown in figures 5.27 and 5.28. This subsurface investigation did not produce any further information concerning the surface reactions.

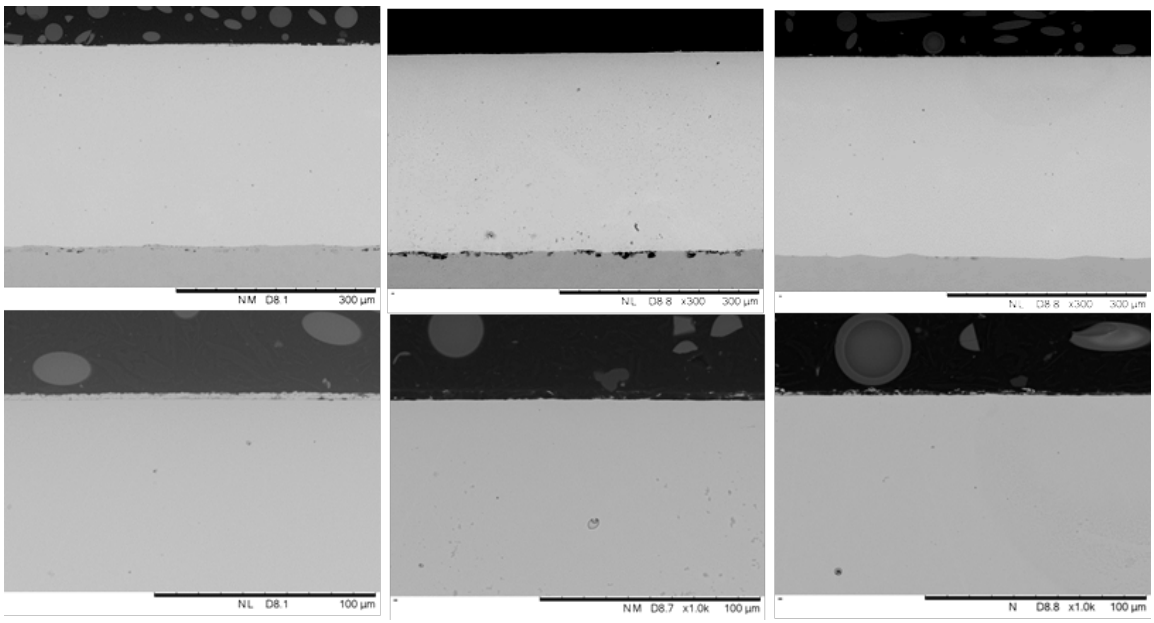

Figure 5.27. Cross-sectional SEM images of copper-tin alloy lining (DERM120) after corrosion tests in new oil after 50, 200 and 500 hours at magnification 500X and 1000X

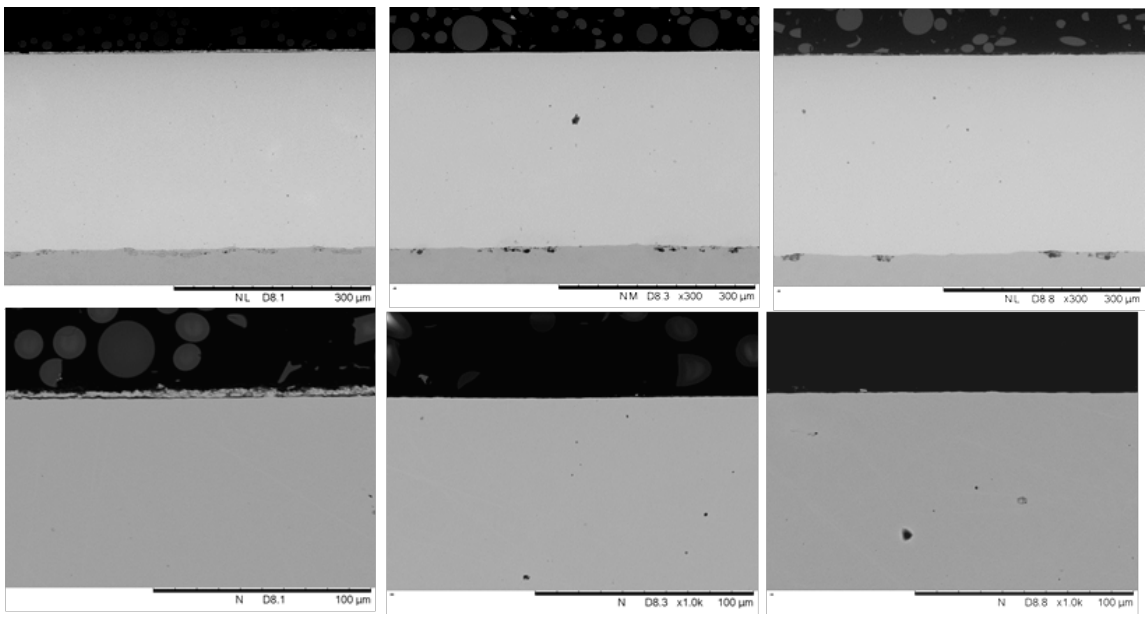

Figure 5.28. Cross-sectional SEM images of copper-tin alloy lining (DERM120) after corrosion tests in used oil after 50, 200 and 500 hours at magnification 500X and 1000X

The microscopy examination produced colour changes with suspected copper oxide features. To confirm this assumption, an XPS surface investigation was conducted. The results from the XPS analysis are shown in figure 5.29. Here, after curve-fitting, the peak spectra at 932.1 eV is identified as metallic copper and an oxidized copper at 934.3 eV. It is assumed that this initially indicates Cu (II) or Cu (I) compounds on the surface. It can be postulated that due to the weak satellites (figure 5.29) that Cu (I) is the more likely compound on the surface.

A negligible amount of tin (Sn) was observed in the XPS spectra of the copper-tin (Cu-Sn) surface, shown in figure 5.29. This absence of Tin (Sn) leads to the conclusion that surface Copper Oxides (CuO) identified previously have formed completely on the surface. This Copper Oxide (CuO) surface layer masks the Copper-Tin (Cu-Sn) lining surface of this material.

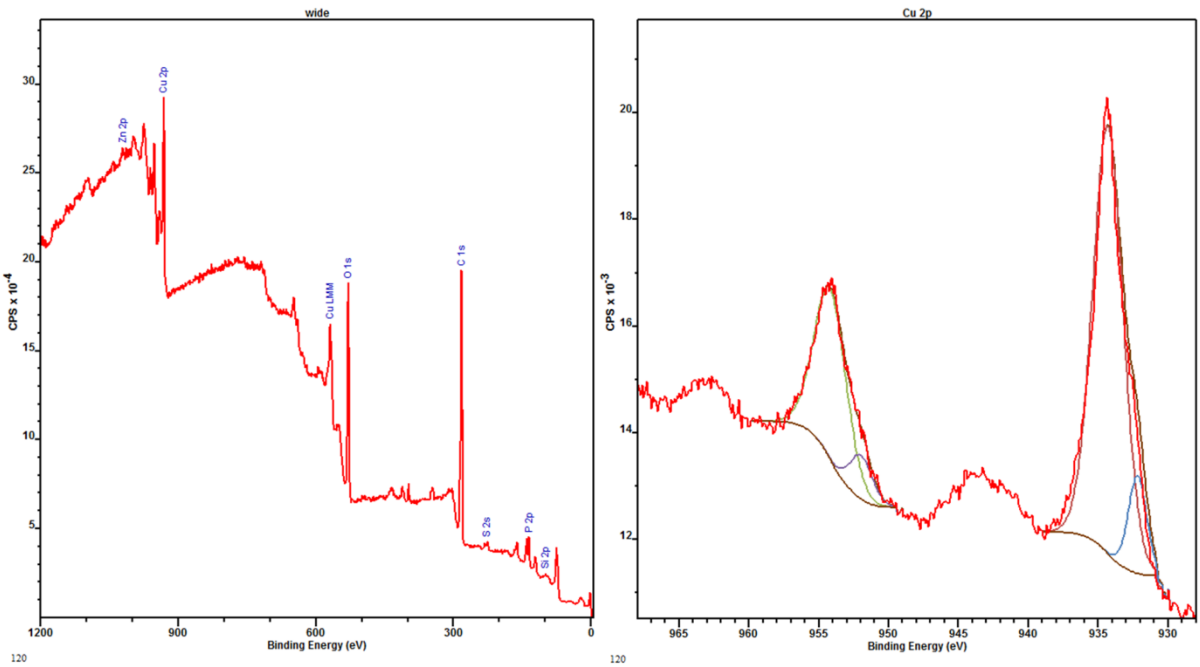

Figure 5.29. The XPS spectra of the copper-tin (Cu-Sn) surface

5.3.4 Lead (Pb)-free coatings

a) Bismuth (Bi) coating (DERM 122)

This material (DERM 122) comprises a dual layer coating of Silver (Ag) as a lower layer and Bismuth (Bi) as the top layer. The samples here are corrosion tested in a new and used oil environment for 50, 200 and 500 hours. The initial images using optical micrographs are shown in figures 5.30 and 5.31. It can be seen that the untested samples in both new and used oil tests have different colours to the tested samples (orange to blue).

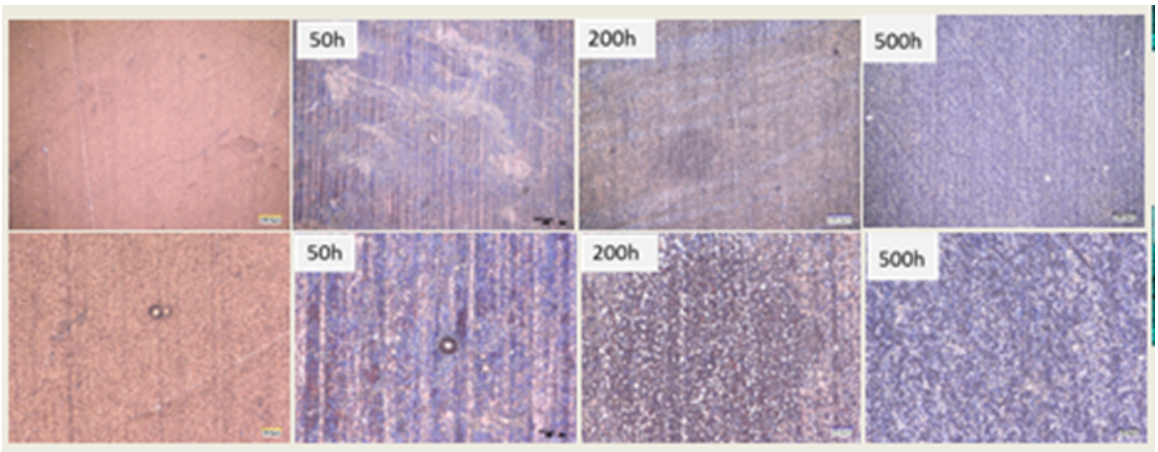

Figure 5.30. Optical images of Bismuth on Silver Coating (DERM 122) surfaces at different corrosion test durations in new oil (300X and 1000X).

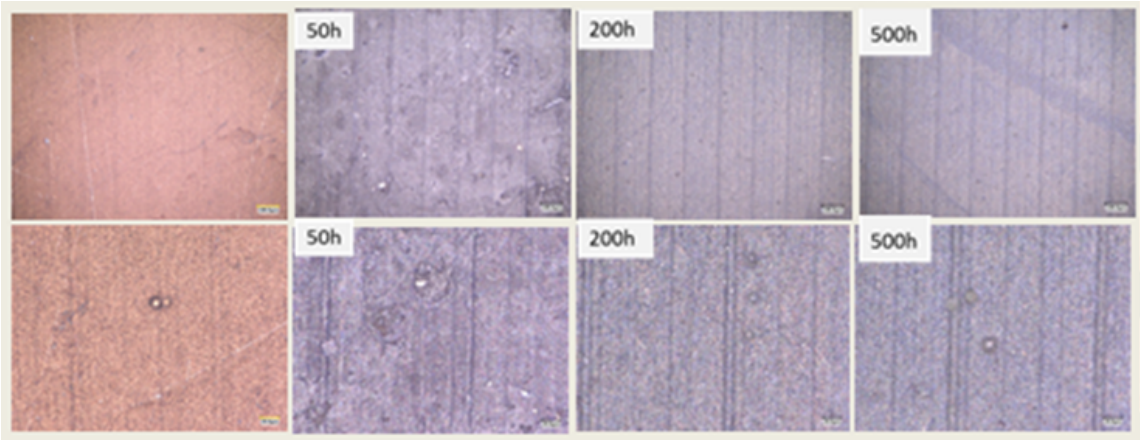

Figure 5.31. Optical images of Bismuth on Silver Coating (DERM 122) surfaces at different corrosion test durations in new oil (300X and 1000X).

Cross-sectional analysis is conducted of the samples (figure 5.30 and 5.31) to determine any further damage mechanisms due to the corrosion tests in new and used oil. The images of cross-sections are shown in figures 5.32 and 5.33. Here, in the case of new oil, it is observed that discontinuous layers exist on the surface after 500 hours testing (figure 5.32). In the case of used oil (figure 5.33), this layer has developed as continuous on the 500 hours test sample.

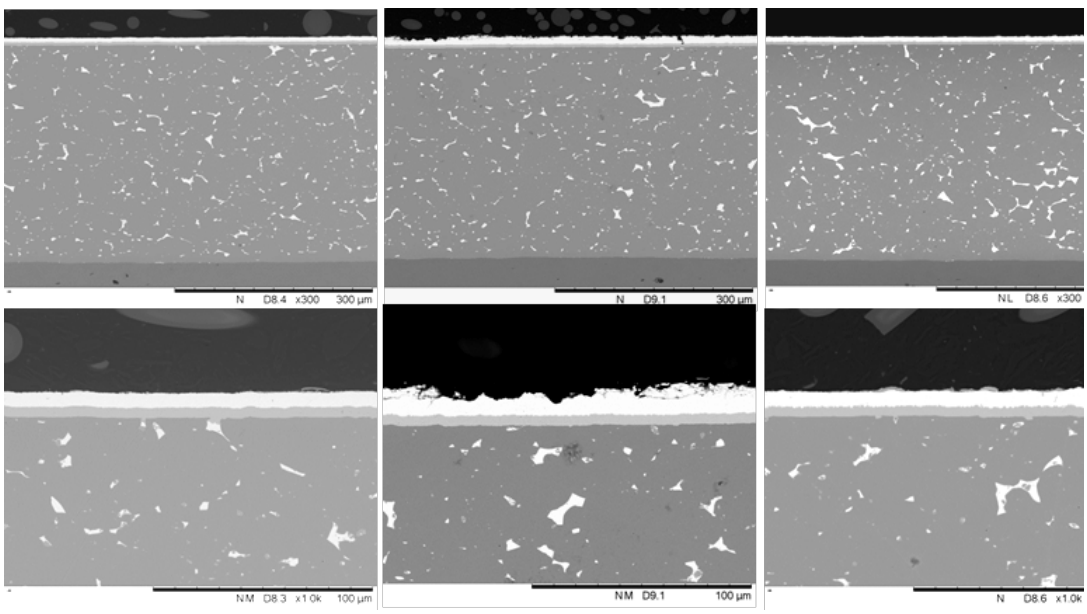

Figure 5.32. Cross-sectional SEM images of Bismuth on Silver Coating (DERM122) after corrosion test in new oil after 50, 200 and 500 hours (500X and 1000X)

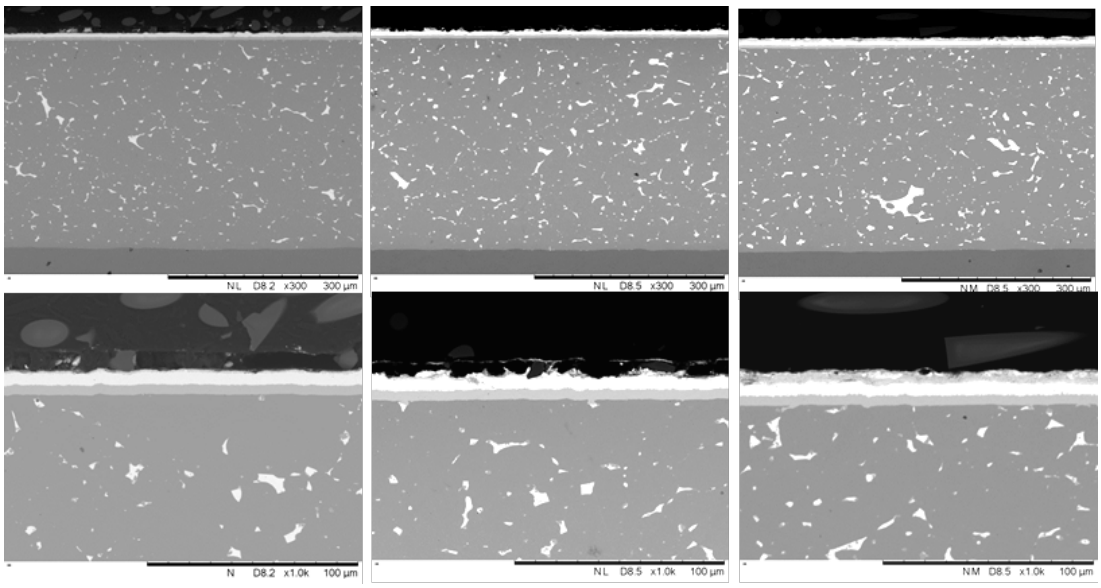

Figure 5.33. Cross-sectional SEM images of Bismuth on Silver Coating (DERM122) after corrosion test in used oil after 50, 200 and 500 hours (500X and 1000X)

Elemental mapping using EDS via the SEM was also conducted of the surfaces shown in figures 5.30 and 5.31. Here, no Silver (Ag) was observed near the surface layer in the case of used oil corrosion tests. Silver was however, detected on the surface on the new oil tests after 200 and 500 hours duration. To examine these interesting observations and identify the mechanisms involved it was decided to use XPS techniques on these samples. XPS studies (figure 5.34) confirmed the presence of Bismuth oxide on the surface.

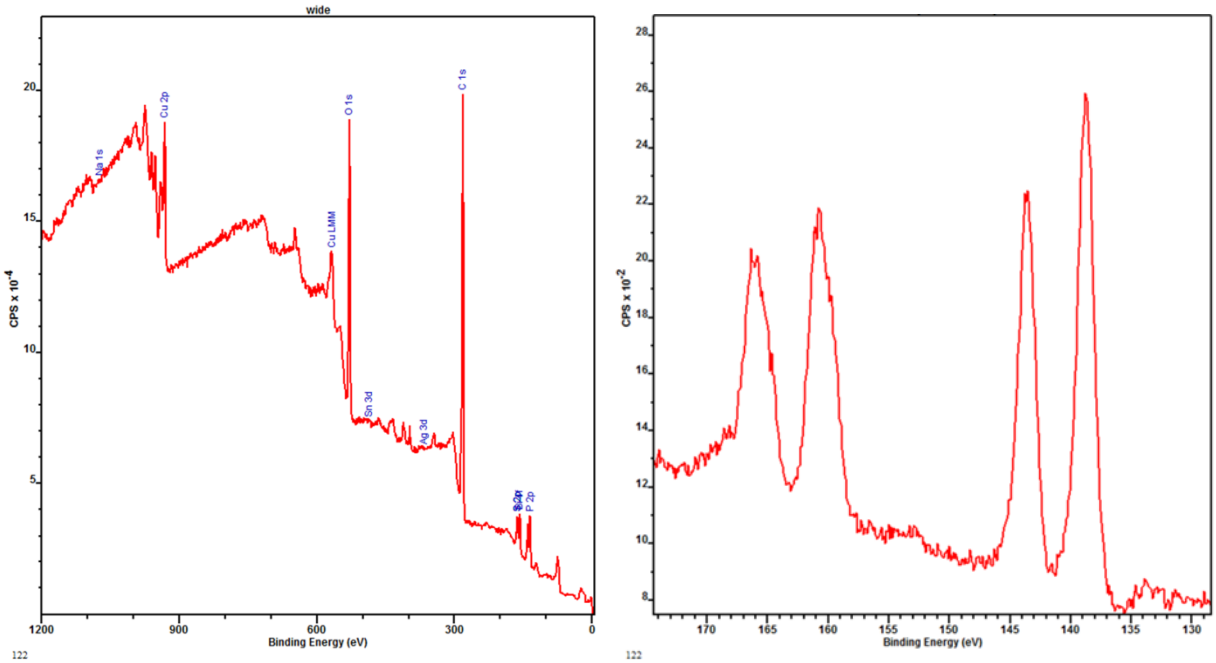

Figure 5.34. Xray Photoelectron Spectroscopy (XPS) of Bismuth on Silver Coating (DERM122) showing the spectra for used oil after 500-hour test.

The analysis of this sample leads to a possible mechanism of corrosion. The oxide layer observed is only at the 500 hours corrosion test in used oil. Here, Bismuth reacts with hydrogen peroxide and form a Bismuth (III) oxide on the surface is given below:

$$2Bi + 3H_2O_2 = Bi_2O_3 + 3H_2O \quad (5)$$

b) Tin (Sn) coating (DERM 123)

A Tin (Sn) coating containing a three percent Copper (Cu) was investigated as an alternative material selection. This is a complex structure of material layers including Tin - Copper (3%), an intermediate layer of nickel, another layer of Tin-Copper (3%), another intermediate layer of nickel the Copper-Lead lining material. This material is subjected to corrosion tests using the same methodology as previously described

(section 3.1). The optical micrographs shown as figures 5.35 (new oil) and 5.36 (used oil) indicate no colour changes present.

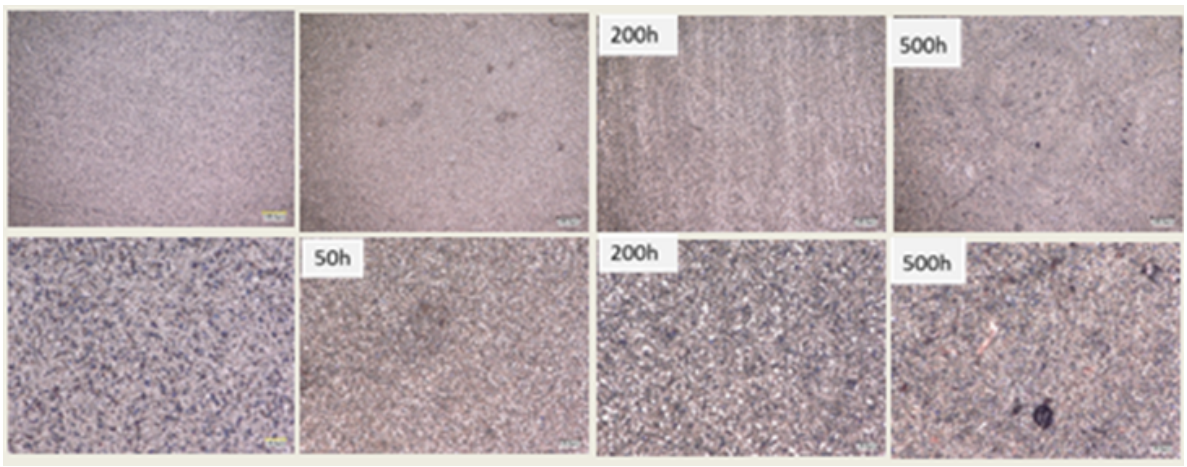

Figure 5.35. Optical micrograph images of Tin (Sn) coating (DERM 123) surfaces at different test durations (0, 50, 200 and 500 hours) in new oil (X300, X1000)

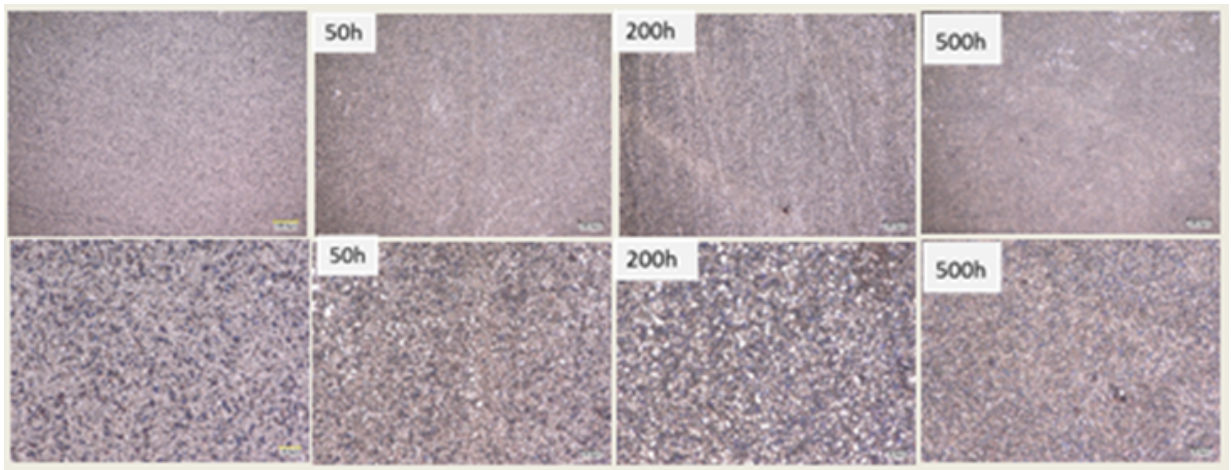

Figure 5.36. Optical micrograph images of Tin (Sn) coating (DERM 123) surfaces at different test durations (0, 50, 200 and 500 hours) in used oil (X300, X1000)

Although little evidence of surface change was detected from the surface observations (figures 5.35 and 5.36) a SEM cross-sectional analysis was conducted for completeness. Here figures 5.37 and 5.38 show the results from the cross-sectional SEM images that show the coating material of Tin (Sn) (DERM 123). According to cross-sectional and surface analysis, there is no change in appearance, and there is also no evidence of corrosion in both new and used oil tests.

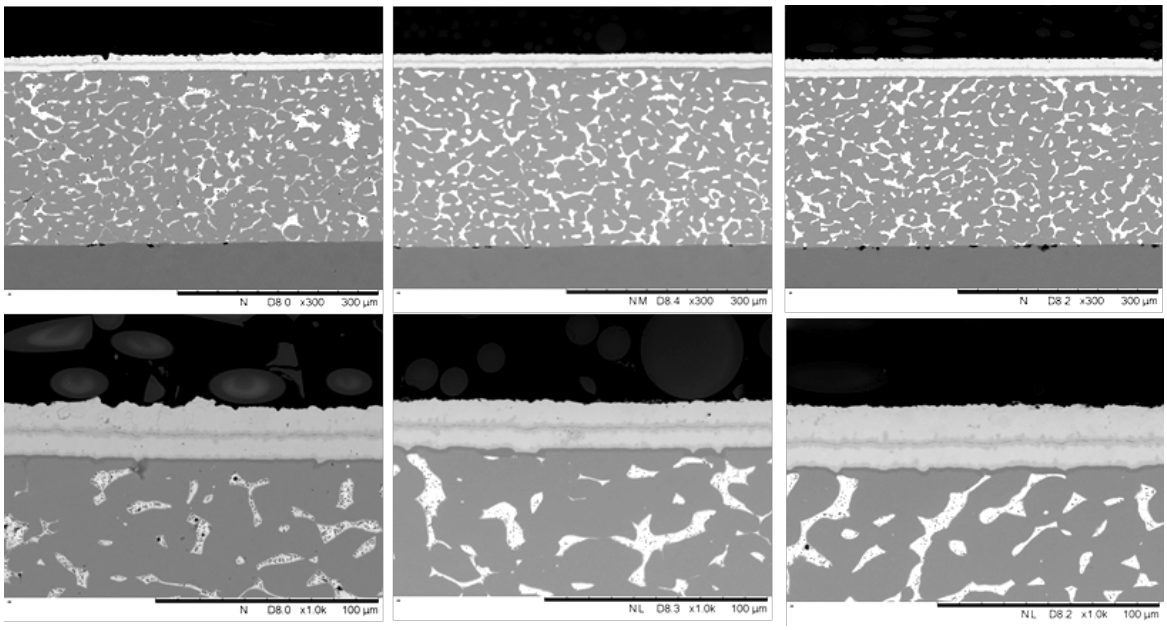

Figure 5.37. The cross-sectional SEM images of DERM123 after corrosion test in new oil after 50 hrs,200 hrs and 500 hrs at magnification 500X and 1000X

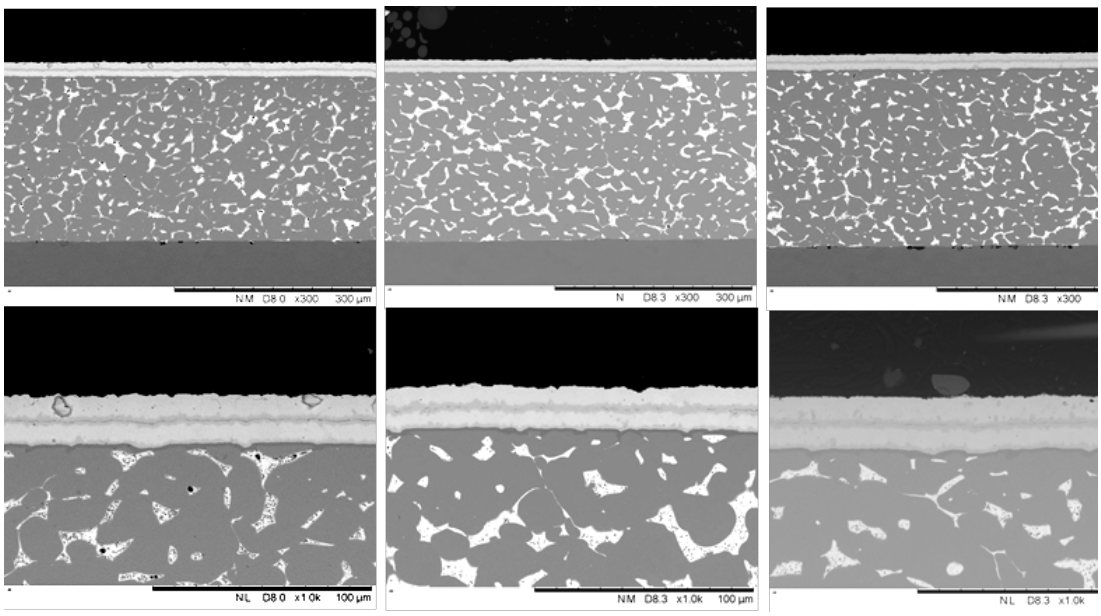

Figure 5.38. The cross-sectional SEM images of DERM122 after corrosion test in new oil after 50 hrs, 200 hrs and 500 hrs at magnification 500X and 1000X

5.4 Tribotest

In this study, corroded and non-corroded Pb-based overlays such as DERM121, DERM124 and Pb-free overlay DERM123 were tested under a novel test rig. The test material was selected after corrosion analysis. As compared to overlays, lining materials will have poor tribological properties, and most applications employ plain bearings with overlays. During the development and optimization of the test-rig and parameters, a large number of trials were performed as follows to check the shaft diameter with respect to the bearing diameter

- heating element operation & time taken to heat the oil bath
- temperature effect on test parameters by varying temperatures say $80^{O}C$, $100^{O}C$, $120^{O}C$
- to check the load effect on materials
- to test the hydraulic load setup operation
- To optimize the probe position of test-rig to measure the torque

- The contact hub and shaft coupling issues

Considering the above reason and time limit only corroded and non-corroded three materials were tested.

The bearing holder is not attached to test-rig and so it was allowed the bearing to align freely with shaft. The preload was applied to move the bearing close to the shaft. During Start of the test, it always observed quite rise of COF and it depend on the alignment of the bearing with respect to shaft. The test was programmed by using COMPEND software to control and collect data during test. The coefficient of friction was calculated using the formula:

$$Coefficient\ of\ friction\ (\mu) = Friction\ force \div Normal\ load$$

$$Torque(Nm) = Friction\ force(N) \times Friction\ radius(m)$$

The frictional torque is measured using a force transducer.

5.4.1 Pb-free Overlay

Sample DERM123 Non-corroded

Since the initial running in phase is short in duration and has a minimal contribution to the energetic effort, it is negligible in terms of overall wear. During preloading, the sample is moved closer to the shaft to prevent misassemble. In fact, wear progresses as soon as the start-stop cycle begins after the heating phase. A steady run of temperatures indicates that the system operates under stable thermal conditions throughout the entire test period. In accordance with the frictional behaviour, the resulting friction energy behaves. For the initial cycles, the amount of energy gained shows a steep incline, but as the test continues, the amount of added energy decreases.

Fig. 5.4.1.1 illustrates the decrease in coefficient of friction (COF) with increasing load. With an increase in load, COF increased at the beginning, showing boundary

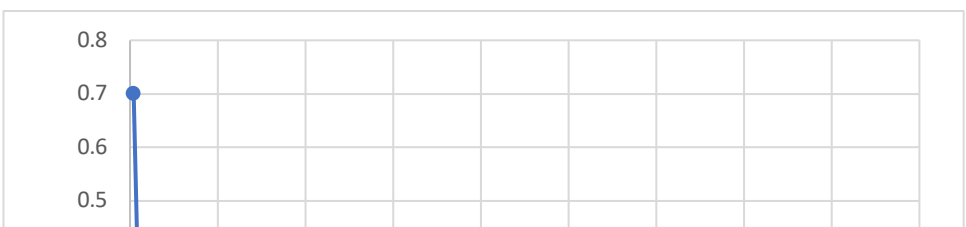

lubrication regime, but gradually decreased, indicating mixed lubrication prevailed. In the hydrodynamic film region, COF was stable and low.

Fig.5.4.1.1. Constant speed strategy: The Coefficient of friction with varying load

Fig 5.4.1.2. shows that temperature rised during start of the test and fallen gradually below set temperature 120^{O}C. The temperature become stable once COF was low and stable. The increase in temperature is due to friction.

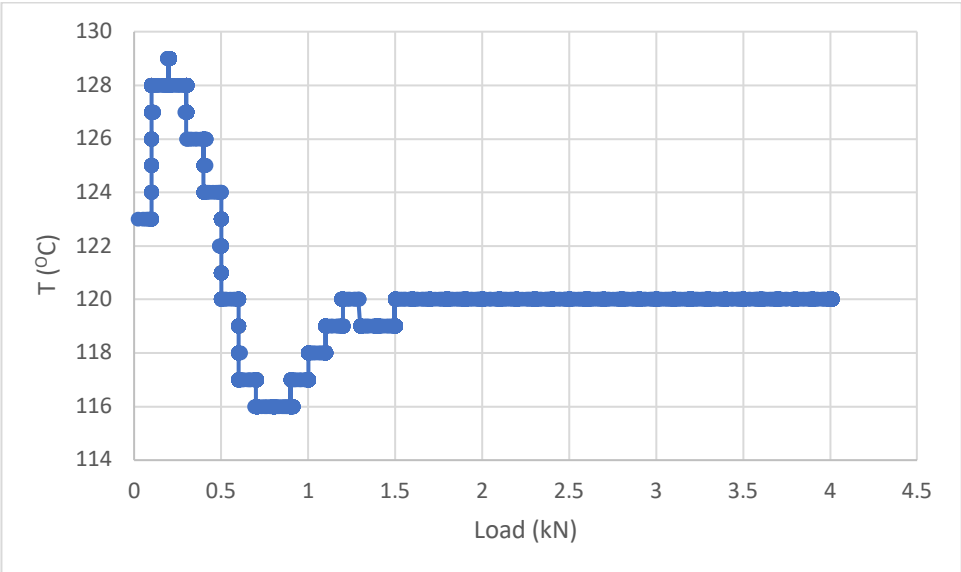

Fig.5.4.1.2. Change of set temperature with respect to load

Sample DERM123 Corroded

During Start of the test, it always observed the boundary lubrication regime. From section 5.3.3 Sn overlay showed excellent corrosion resistance and was expected tribological properties should be similar to the non-corroded sample. Therefore, the COF rise between 1 kN and 1.5 kN should be result of alignment of the bearing. Fig. 5.4.1.3. resulted high COF during start of the test, then decreased as like other materials. But there was unexpected increase of COF after the mixed lubrication region.

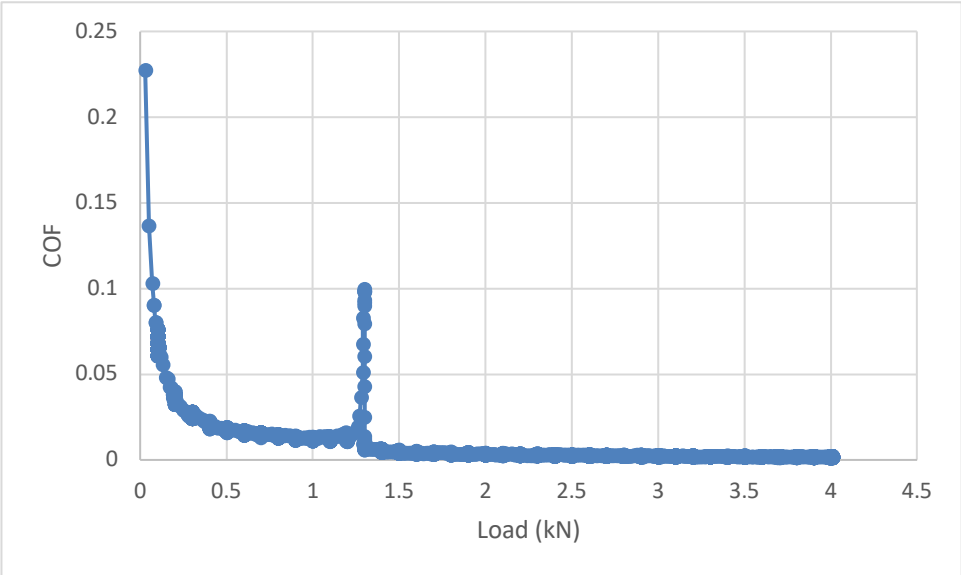

Fig.5.4.1.3. Constant speed strategy: The Coefficient of friction with varying load

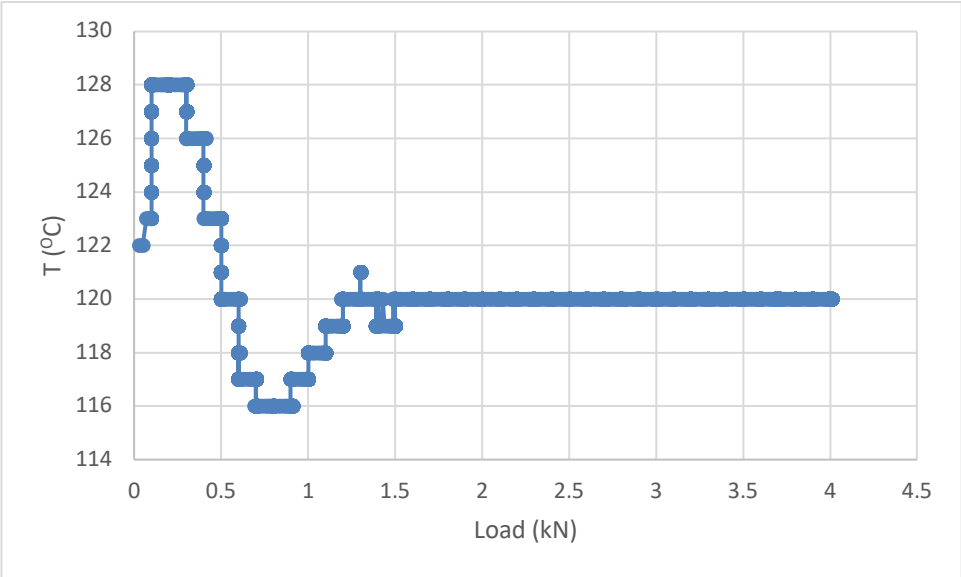

Figure 5.4.1.4 Temperature changes with effect of load

The temperature variation with increase in load shown in the fig 5.4.1.4. Temperature increased to 128^{O}C and dropped to 116^{O}C, later increased and reached desired temperature 120^{O}C. COF increased between load 1 kN and 1.5 kN in the fig. 5.4.1.3 equivalent increase in the temperature at same region. It confirmed that temperature changed from set temperature was due to friction. Friction leads to increase in the temperature.

An impression of the overall wear process of the top sliding material is given in Fig 5.4.1.5. The asperity peaks of the initially rough surface level due to solid contact with the shaft specimen. This results in a polished shiny smooth surface as depicted in Figure 5.4.1.5.

Fig.5.4.1.5. The Pb-free bearing overlay after test

5.4.2 Pb-based Overlay

Sample DERM121 non-corroded

The Coefficient of friction of the DERM121 at constant speed of 1068 rpm at temperature 120^{O}C with respect to increasing load from 0.1N to 4 kN is shown in the fig 5.4.2.1. The graph showed COF decreased from the initial jump of COF and it showed slight fluctuation whenever load increased. After certain load hydrodynamic fluid film formed and COF reduced to low.

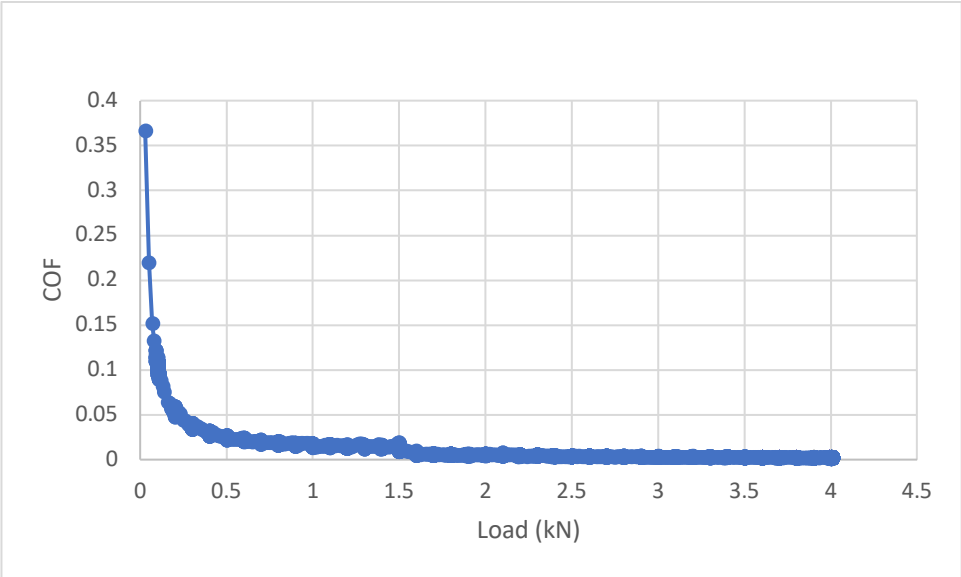

Figure 5.4.2.1. Constant speed strategy: The Coefficient of friction with varying load

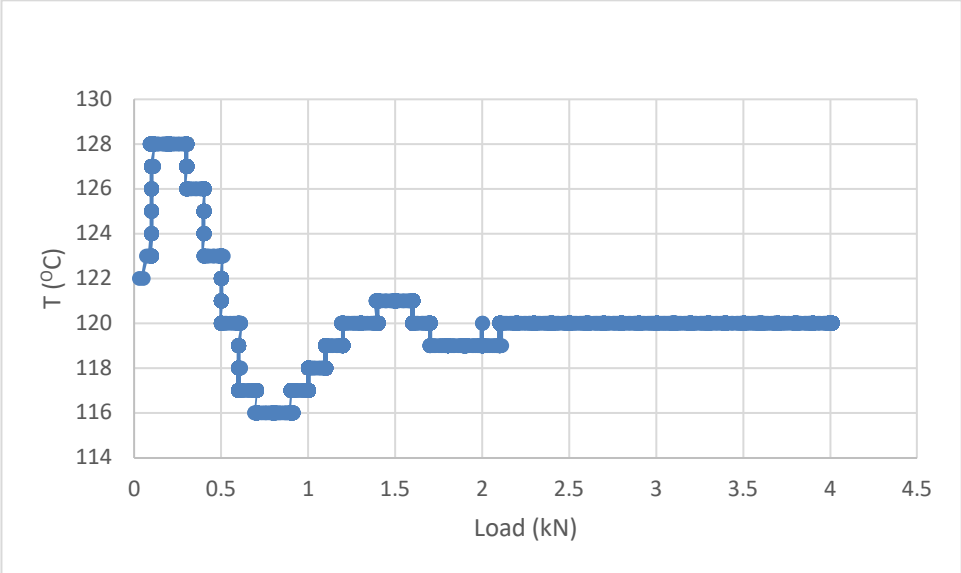

Fig.5.4.2.2. Change of set temperature with respect to load

The fig.5.4.2.2 showed the variation of the set temperature 120^{O}C with load. The program was set that the test will start once the temperature 120^{O}C is reached. The temperature was increased above set temperature during start of the test and after it fallen below the set temperature and subsequently reached again to 120^{O}C. Initially it

observed there was fluctuation in the set temperature caused by increase in COF but once COF is low and steady the temperature also maintained at 120^{O}C.

Sample DERM121 Corroded

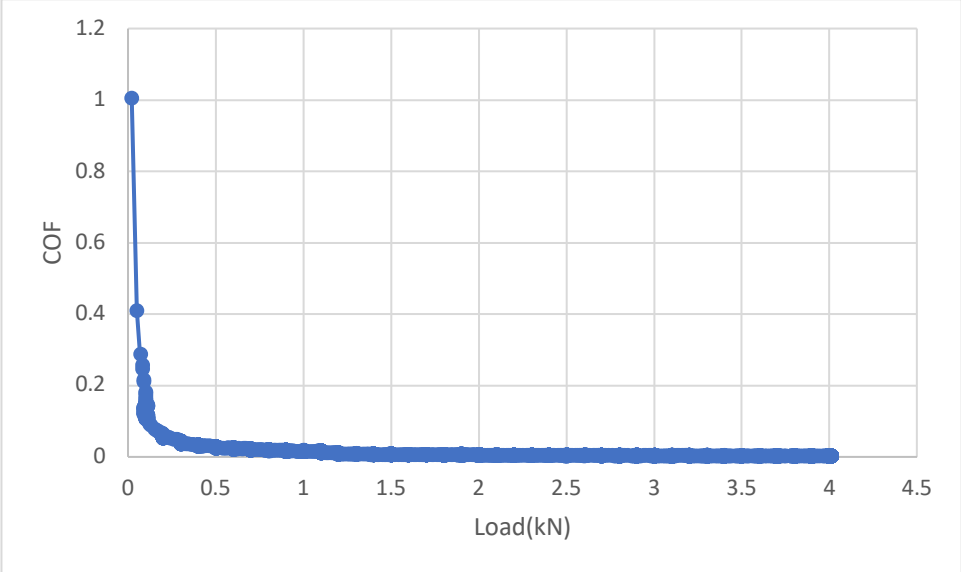

Fig.5.4.2.3. Constant speed strategy: The Coefficient of friction with varying load

The fig 5.4.2.3 showed the Coefficient of friction increased during start and decreased to maintain as low throughout the test running in. Corrosion test in used oil resulted the missing of Pb particles from the surface of Pb based overlay. Expected more friction rather than non-corroded DERM121, the graph showed high COF during start as compared to non-corroded one. But COF is not constant for all 3 tests of corroded DERM121 and again it depends on free alignment of bearing against shaft. The sample picture showed the high pressure is not always at centre, sometimes happened at the edges.

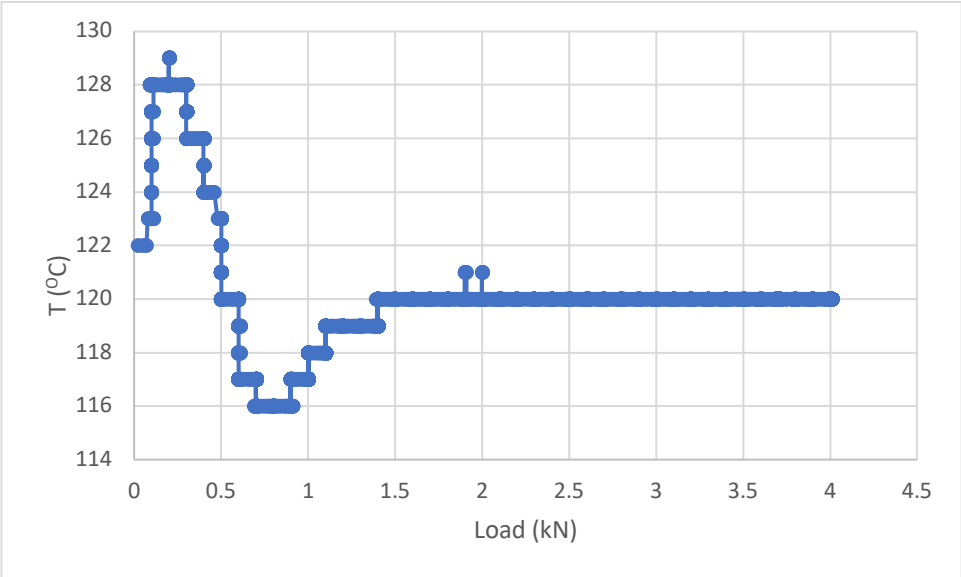

Fig.5.4.2.4. Change of set temperature with respect to load

The temperature was increased initially then gradually decreased as like other materials and later it reached the set temperature.

Fig.5.4.2.5. Pb-based bearing overlay material after test

Figure 5.4.2.5. shows the overall wear process for the top sliding material. Due to solid contact with the shaft specimen, the asperity peaks of the initially rough surface level out. Figure that shows a shiny surface where there was solid contact. As the protective hard phase layer wears off, the COF sinks proportionately to the amount of residual Pb-based matrix that contributes to the solid contact. In the process of wear, the topmost sliding layer does not change in material composition but constantly wears away. Wear also occurs in areas that are completely worn away and show contact with the adjacent Cu-based lining material. Consequently, there are low friction losses and a decreased inclination of the wear curve.

Sample DERM124 Non-corroded

The fig 5.4.2.6. showed slight increase in coefficient of friction after mixed lubrication region prevails and later reduced. The upper and lower samples showed the high pressure was not always happened at the centre of bearing , it completely depend on the bearing contact with shaft material.

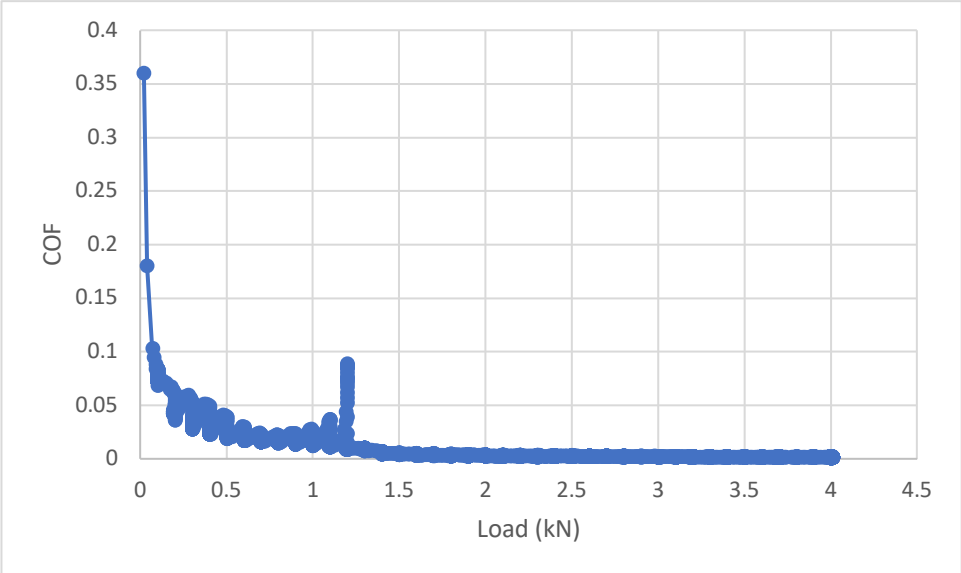

Fig.5.4.2.6. Constant speed strategy: The Coefficient of friction with varying load

The temperature has increased wherever increase in Coefficient of friction as shown in the fig.5.4.2.7. During hydrodynamic film region the temperature have maintained

the input temperature. In all developed Journal bearing test-rig which discussed in the section 2.4.2 the temperature at the back of the bearing have measured along with oil bath temperature.

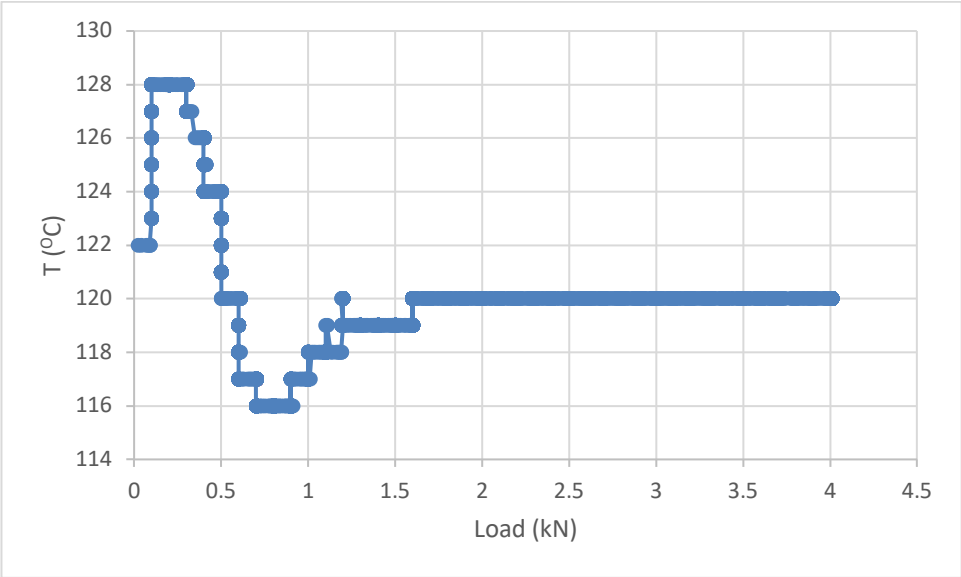

Fig.5.4.2.7 Change of set temperature with respect to load

CHAPTER 6 CONCLUSIONS

As a result of corrosion tests conducted on the materials prior to tribological experiments, the following preliminary conclusions are made:

1. It was found that the corrosion of lead phases in sintered (DERM 119) and cast (DERM 118) copper-lead alloy lining materials occurred only in used deteriorated oil. Surface and cross-sectional analysis of these corrosion test materials have confirmed the disappearance of lead (Pb) phases from the copper matrix. Further oil analysis revealed that the presence of lead (Pb) and copper (Cu) in oil samples. Corrosion of lead in used oil was found to be a time-dependent process.

2. Copper-tin alloy (DERM120) lining material showed good corrosion resistance as compared to copper-lead (DERM 119 and DERM 118) alloy lining materials. However, XPS analysis revealed that the presence of copper oxide on the surface after 500 hour testing in used oil.

3. Pitting corrosion occurred on lead-tin (DERM 121) overlays after testing in used oil. Cross-sectional and surface analysis confirmed that the corrosion does not affect the lining material beneath the overlays.

4. Tin overlays (DERM 123) exhibits excellent corrosion resistance in both new and used oil as compared to other test materials.

5. Silver (Ag) was diffused near the surface in bismuth overlay (DERM 122) material after testing in new oil. Bismuth oxide was found on the surface after 500 hours test in used oil.

6. Severe corrosion was observed only after testing in used deteriorated oil. Lead-free materials demonstrated good corrosion resistance. Overlays exhibit good resistance to corrosion as compared to lining materials.

As a result of tribological performance of tested material the following conclusions were made:

1. For the initial cycles, the amount of energy gained shows a steep incline, but as the test continues, the amount of added energy decreases.

2. In combination with the comprehensive surface analysis chain, the used test methodology is capable of resolving the wear process of journal bearing specimens. A detailed analysis of the process of wear and its effect on tribological behavior could be accomplished using this methodology.

4. To differentiate the material wear performance, increased test duration or start/stop cycle, increased load should be tried.

5. The SEM images (appendix) confirm the poor wear resistance of Pb-based overlays, and the good wear resistance of Sn-based overlays.

References

Adams, M.J., Romeo, M.J. and Rawson, P., 2007. FTIR analysis and monitoring of synthetic aviation engine oils. *Talanta*, *73*(4), pp.629-634.

Aufischer, R., 2010. *Diesel Engine Bearings for a Lead Free Future* (No. 2010-32-0060). SAE Technical Paper

Aufischer, R., Walker, R., Offenbecher, M., Feng, O. and Hager, G., 2015, November. Friction Reduction Opportunities in Combustion Engine Crank Train Bearings. In *Internal Combustion Engine Division Fall Technical Conference* (Vol. 57281, p. V002T07A008). American Society of Mechanical Engineers

Bassani, R. and Piccigallo, B., 1992. *Hydrostatic lubrication* (Vol. 22). Elsevier.
Rowe, W.B., 2013. *Hydrostatic and hybrid bearing design*. Elsevier.

Becker, E.P., 2004. Trends in tribological materials and engine technology. *Tribology International*, *37*(7), pp.569-575.

Bergmann, P., SUMMER, F., GRÜN, F., GÓDOR, I., OFFENBECHER, M. and LAINÉ, E., 2014. Tribological Investigations of Journal Bearings by means of a close to component Test Methodology. In *Proceedings of Symposium der ÖTG* (pp. 113-121).

Bergmann, P., Grün, F., Gódor, I. and Herbst, K., 2016. Methodology Development for Numerical Evaluation of Wear in Tribological Contacts. *Design of Machines and Structures*, *6*(1), pp.5-14.

Bergmann, P., Grün, F., Summer, F., Gódor, I. and Stadler, G., 2017. Expansion of the metrological visualization capability by the implementation of acoustic emission analysis. *Advances in Tribology*, *2017*.

Bergmann, P., Grün, F., Gódor, I., & Hager, G. Simulative Investigations of a Close-to-Component Journal Bearing System and Comparison with Test Data. *1. Hugh Spikes, Imperial College, UK: Stress-assisted thermal activation in Tribology 2. Wilfried J. Bartz, Technische Akademie Esslingen: High Performance Lubricants-From Mineral to Synthetic Base Oils 3. Achim Feldermann, RWTH Aachen University, Germany: CFD Modeling of Elastohydrodynamic Lubrication Using Reduced FE-Models*, 59.

Bergmann, P., Grün, F., Summer, F. and Gódor, I., 2018. Evaluation of wear phenomena of journal bearings by close to component testing and application of a numerical wear assessment. *Lubricants*, *6*(3), p.65.

Daido Metal Co., Ltd., *Book of Engineering Data Required to Design Plain Bearings for Automobile Engines*

Delprete, C. and Razavykia, A., 2020. Piston dynamics, lubrication and tribological performance evaluation: A review. International Journal of Engine Research, 21(5), pp.725-741.

Dowson, D. and Higginson, G.R., 2014. Elasto-hydrodynamic lubrication: international series on materials science and technology. Elsevier.

Feyzullahoğlu, E. and Şakiroğlu, N., 2010. The wear of aluminium-based journal bearing materials under lubrication. *Materials & Design (1980-2015)*, *31*(5), pp.2532-2539.

Fowell, M., Olver, A.V., Gosman, A.D., Spikes, H.A. and Pegg, I., 2007. Entrainment and inlet suction: two mechanisms of hydrodynamic lubrication in textured bearings.

Frene, J., Nicolas, D., Degueurce, B., Berthe, D. and Godet, M., 1997. *Hydrodynamic lubrication: bearings and thrust bearings*. Elsevier.

Gao, F., Liu, R. and Wu, X.J., 2011. Tribaloy alloy reinforced tin–bronze composite coating for journal bearing applications. *Thin Solid Films*, *519*(15), pp.4809-4817.

Gebretsadik, D.W., Hardell, J. and Prakash, B., 2015. Tribological performance of tin-based overlay plated engine bearing materials. *Tribology International*, *92*, pp.281-289.

Gerrard, J. and Kandlikar, M., 2007. Is European end-of-life vehicle legislation living up to expectations? Assessing the impact of the ELV Directive on 'green'innovation and vehicle recovery. *Journal of Cleaner Production*, *15*(1), pp.17-27.

Grün, F., Gódor, I. and Eichlseder, W., 2009. Fundamentals of optimizing aluminium-based journal bearing materials. *Proceedings of the Institution of Mechanical Engineers, Part J: Journal of Engineering Tribology*, *223*(5), pp.777-785.

Grün, F., Gódor, I., Gärtner, W. and Eichlseder, W., 2011. Tribological performance of thin overlays for journal bearings. *Tribology international*, *44*(11), pp.1271-1280.

Grün, F., Krampl, H., Schiffer, J., Moder, J., Gódor, I. and Offenbecher, M., 2013. Tribometric development tools for journal bearings-A novel test adapter. In *Proceedings of the 5th World Tribology Congress, WTC 2013* (pp. 1117-1120).

Jayne, D.T., Shanklin, J.R. and Stachew, C.F., 2002. *Controlling the corrosion of copper alloys in engine oil formulations: antiwear, friction modifier, dispersant synergy* (No. 2002-01-2767). SAE Technical Paper.

Kawagoe, K., Kanayama, H., Desaki, T. and Fuwa, Y., 2003. *New conceptual lead free overlays consisted of solid lubricant for internal combustion Engine bearings* (No. 2003-01-0244). SAE Technical Paper.

Kerr, I., Priest, M., Okamoto, Y. and Fujita, M., 2007. Friction and wear performance of newly developed automotive bearing materials under boundary and mixed lubrication regimes. *Proceedings of the Institution of Mechanical Engineers, Part J: Journal of Engineering Tribology*, *221*(3), pp.321-331.

Kumar, R.V., Yang, J. and Sonmez, S., 2013. Relevance of reaction of lead compounds with carboxylic acid in lead recovery from secondary sources. *J Powder Metall Min*, *2*(107), p.2.

Langbein, F., Loidl, M., Eberhard, A. and Mergen, R., 2009, January. Slide bearing types for combustion engines designed for upcoming emission regulations. In *Internal Combustion Engine Division Fall Technical Conference* (Vol. 43635, pp. 533-541).

Lepper, K., James, M., Chashechkina, J. and Rigney, D.A., 1997. Sliding behavior of selected aluminum alloys. *Wear*, *203*, pp.46-56.

McCloskey, T.H., 1995. Troubleshooting Bearing And Lube Oil System Problems. In *Proceedings of the 24th Turbomachinery Symposium*. Texas A&M University. Turbomachinery Laboratories.

Moder, J., Bergmann, P. and Grün, F., 2018. Lubrication Regime Classification of Hydrodynamic Journal Bearings by Machine Learning Using Torque Data. *Lubricants*, *6*(4), p.108.

Ozsarac, U., Findik, F. and Durman, M., 2007. The wear behaviour investigation of sliding bearings with a designed testing machine. *Materials & design*, *28*(1), pp.345-350

Parsaeian, P., Ghanbarzadeh, A., Wilson, M., Van Eijk, M.C., Nedelcu, I., Dowson, D., Neville, A. and Morina, A., 2016. An experimental and analytical study of the effect of water and its tribochemistry on the tribocorrosive wear of boundary lubricated systems with ZDDP-containing oil. *Wear*, *358*, pp.23-31.

Pondicherry, K.S., Grün, F., Gódor, I., Bertram, R. and Offenbecher, M., 2013. Applicability of ring-on-disc and pin-on-plate test methods for Cu–steel and Al–steel systems for large area conformal contacts. *Lubrication Science*, *25*(3), pp.231-247.

Pratt, G.C., 1973. Materials for plain bearings. *International Metallurgical Reviews*, *18*(2), pp.62-88.

Priest, M. and Taylor, C.M., 2000. Automobile engine tribology—approaching the surface. *Wear*, *241*(2), pp.193-203.

Straffelini G., 2015. Tribological Systems. Friction and Wear: Springer; pp.237-276.

Sudhakar, K.V., 2002. Failure analysis of automobile bimetal bearings. *Engineering Failure Analysis*, *9*(2), pp.221-225.

Summer, F., Grün, F., Schiffer, J., Gódor, I. and Papadimitriou, I., 2015. Tribological study of crankshaft bearing systems: Comparison of forged steel and cast iron counterparts under start–stop operation. *Wear*, *338*, pp.232-241.

Summer, F., Bergmann, P. and Grün, F., 2017. Damage equivalent test methodologies as design elements for journal bearing systems. *Lubricants*, *5*(4), p.47.

Summer, F., Grün, F., Offenbecher, M. and Taylor, S., 2019. Challenges of friction reduction of engine plain bearings–Tackling the problem with novel bearing materials. *Tribology International*, *131*, pp.238-250.

Sun, J. and Changlin, G., 2004. Hydrodynamic lubrication analysis of journal bearing considering misalignment caused by shaft deformation. Tribology International, 37(10), pp.841-848.

Tamatam, L.R., 2017. Tribological performance of different crankshaft bearings in conjunction with textured shaft surfaces.

Taylor, C.M., 1998. Automobile engine tribology—design considerations for efficiency and durability. *Wear*, *221*(1), pp.1-8.

Tichvinsky, L.M., 1943. CORROSION of BEARING ALLOYS. SAE Transactions, pp.69-77.

Tung, S.C. and McMillan, M.L., 2004. Automotive tribology overview of current advances and challenges for the future. *Tribology International*, *37*(7), pp.517-536.

Vetterick, G., Anderson, I. and Besser, M., 2010. Novel Lead-free Bronze Bearing Materials Produced by Powder Metallurgy Processing. *Minerals, Metals and Materials Society/AIME, 420 Commonwealth Dr., P. O. Box 430 Warrendale PA 15086 USA.[np]. 14-18 Feb*.

Wilson, R.W. and Shone, E.B., 1970. The corrosion of overlay bearings. *Anti-Corrosion Methods and Materials*.

Zhang, C., 2014. Understanding the wear and tribological properties of ceramic matrix composites. In *Advances in ceramic matrix composites* (pp. 312-339). Woodhead Publishing.

Zhang, Y., Tudela, I., Pal, M., Kerr, I., 2016. High strength tin-based overlay for medium and high speed diesel engine bearing tribological applications. *Tribology International*, 93:687-95.

Appendix-I : Corrosion test

EXPERIMENTAL DETAILS

Corrosion Test Conditions:

Test duration 50, 200, 500 hrs
Test temperature 120 °C

Corrosion Test Plan:

Test duration (Hrs)	DERM119		DERM123		DERM122		DERM120		Test Status
50	New Oil	Used Oil	New Oil	Used Oil	New Oil	Used Oil	New Oil	Used Oil	Completed
200	New Oil	Used Oil	New Oil	Used Oil	New Oil	Used Oil	New Oil	Used Oil	Completed
500	New Oil	Used Oil	New Oil	Used Oil	New Oil	Used Oil	New Oil	Used Oil	Completed

Corrosion Test Setup:

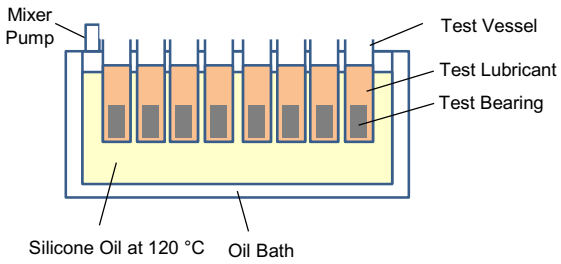

Report includes:

1. Weight loss evaluation.
2. Visual evaluation, including photographs.
3. Surface and cross-sectional analyses using SEM-EDX.
4. Oil analysis

DAIDO METAL

Weight loss measurements -Substrates

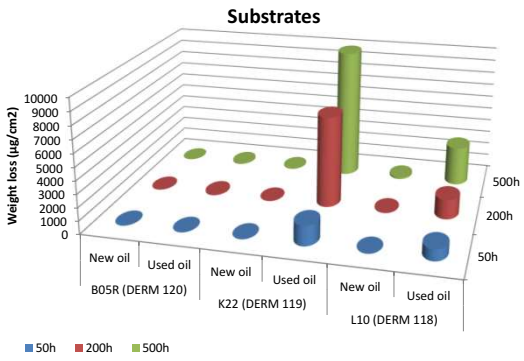

Substrates	Pb-free		Pb-based (Sintered)		Pb-based (Casted)	
µg	B05R (DERM 120)		K22 (DERM 119)		L10 (DERM 118)	
	New oil	Used oil	New oil	Used oil	New oil	Used oil
50h	-54	-24	-31	1517	-5	871
200h	26	87	6	6986	53	1494
500h	-11	80	38	14710	136	2980

DAIDO METAL

Weight loss measurements -Coatings

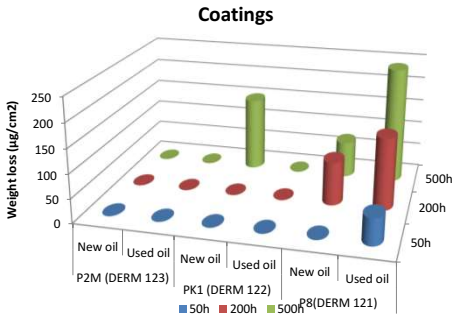

Coatings µg	Pb-free		Pb-free		Pb-based	
	P2M (DERM 123)		PK1 (DERM 122)		P8(DERM 121)	
	New oil	Used oil	New oil	Used oil	New oil	Used oil
50h	-4	-45	-43	-186	-18	54
200h	-28	-30	-7	-130	90	148
500h	-32	-58	152	-139	75	240

DERM119

APPEARANCE CHANGE (DERM119 after 50hrs)

	Before test	After test
New Oil	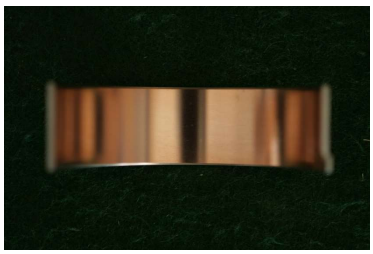	
Used Oil		

DAIDO METAL

5

APPEARANCE CHANGE (DERM119 after 200hrs)

	Before test	After test
New Oil	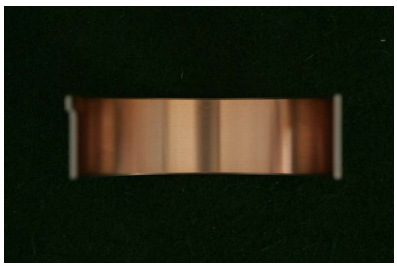	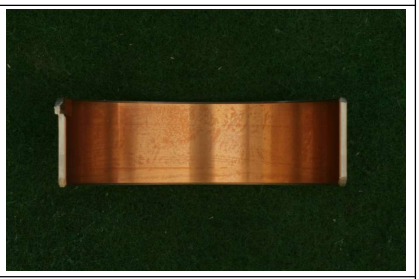
Used Oil	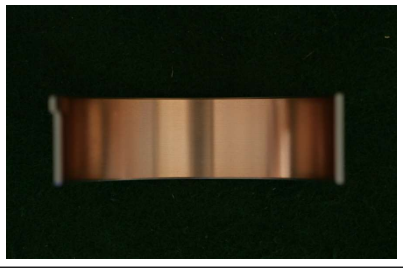	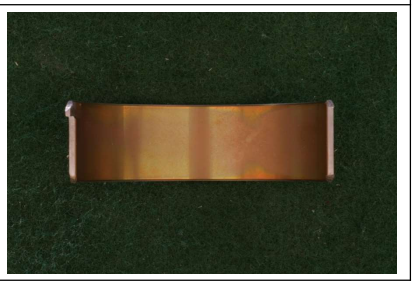

DAIDO METAL

6

APPEARANCE CHANGE (DERM119 after 500hrs)

	Before test	After test
New Oil	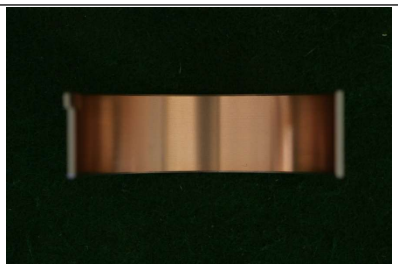	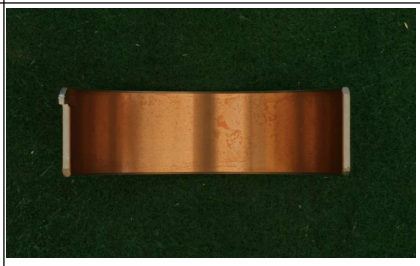
Used Oil		

DAIDO METAL

7

CROSS-SECTIONAL ANALYSIS (DERM119 after 50,200,500 hrs)

New Oil (MAG: X300)

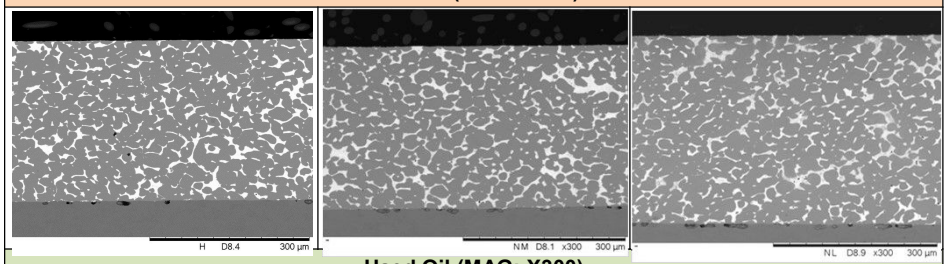

Used Oil (MAG: X300)

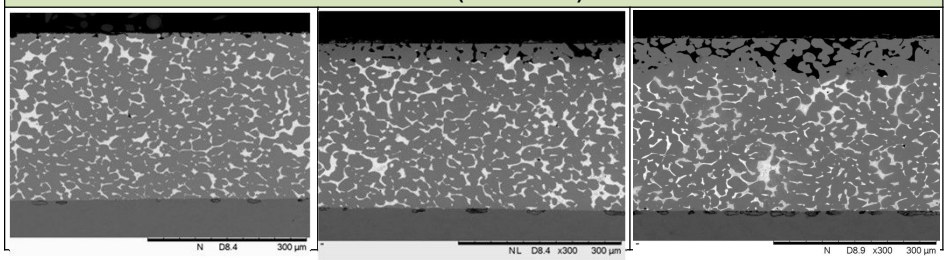

DAIDO METAL

8

CROSS-SECTIONAL ANALYSIS (DERM119 after 50,200,500 hrs)

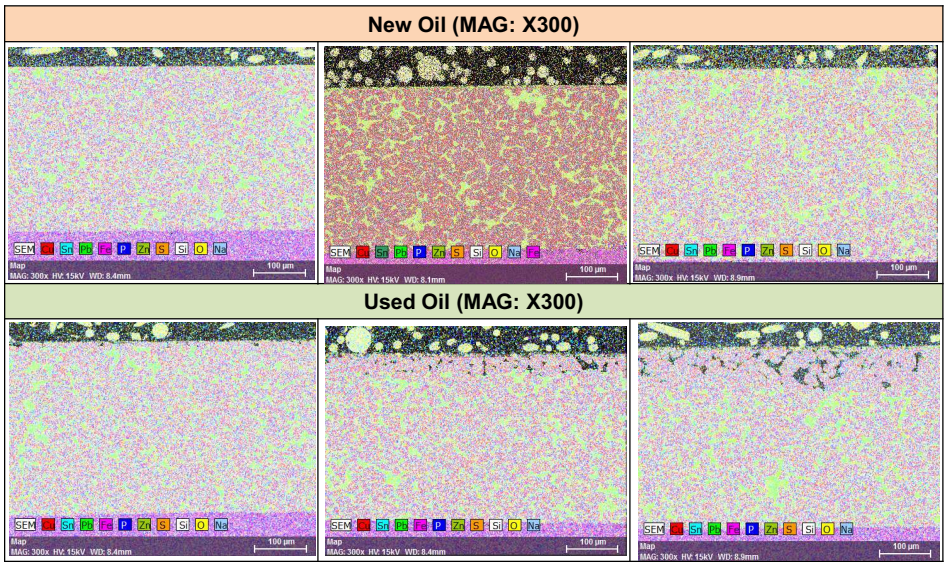

DAIDO METAL

9

DERM119 after 50,200 & 500 hrs
(NEW OIL 300X)

29-10-2020

DAIDO METAL

10

50 hrs

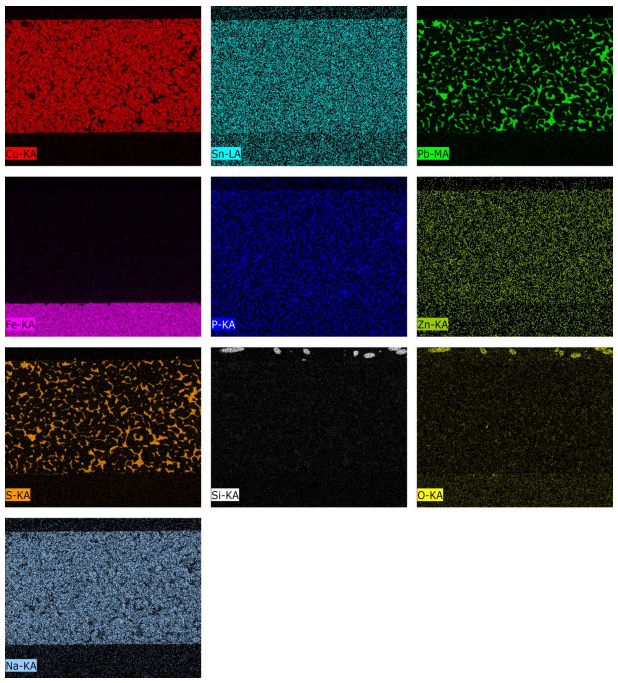

DAIDO METAL

11

200 hrs

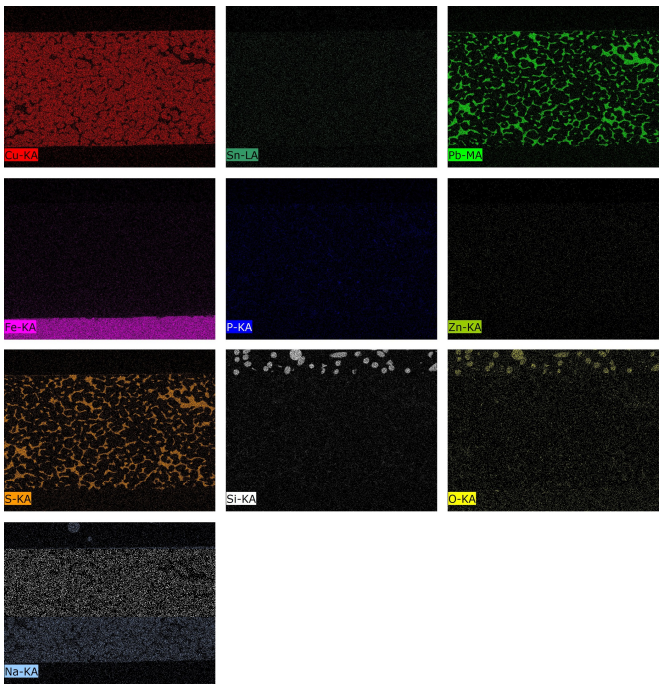

DAIDO METAL

12

500 hrs

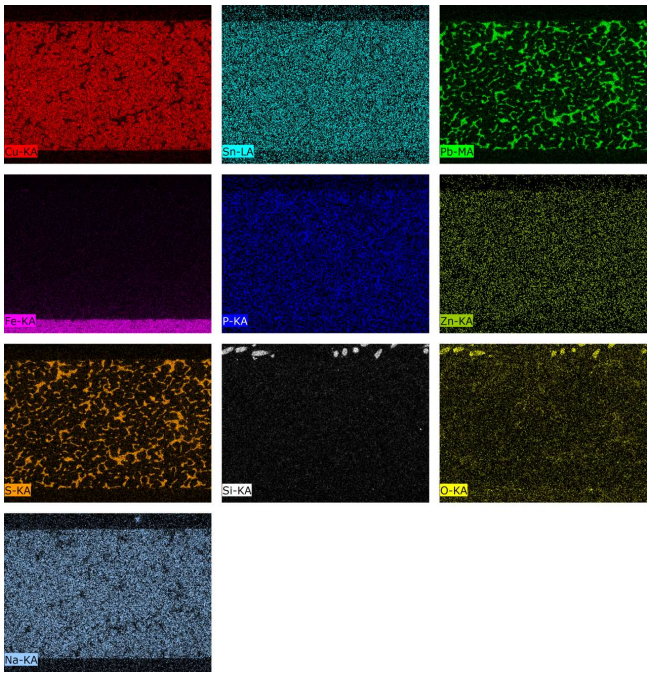

DAIDO METAL

13

DERM119 after 50,200 & 500 hrs
(USED OIL 300X)

29-10-2020

DAIDO METAL

14

50 Hrs

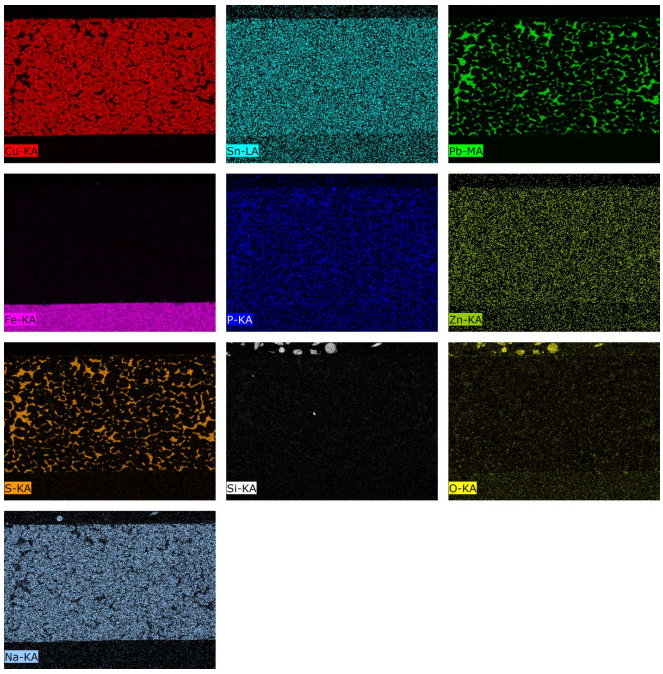

29-10-2020

DAIDO METAL

15

200 hrs

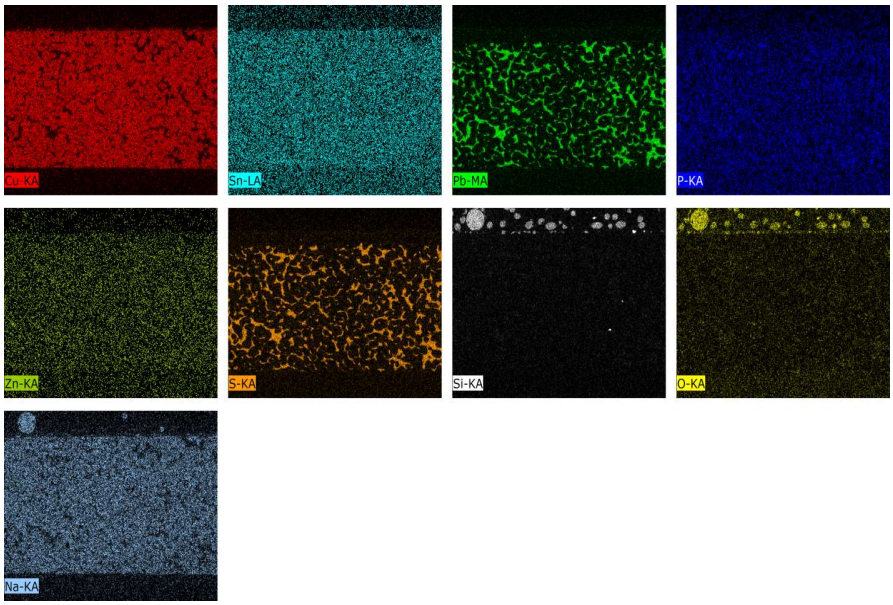

29-10-2020

DAIDO METAL

16

500 hrs

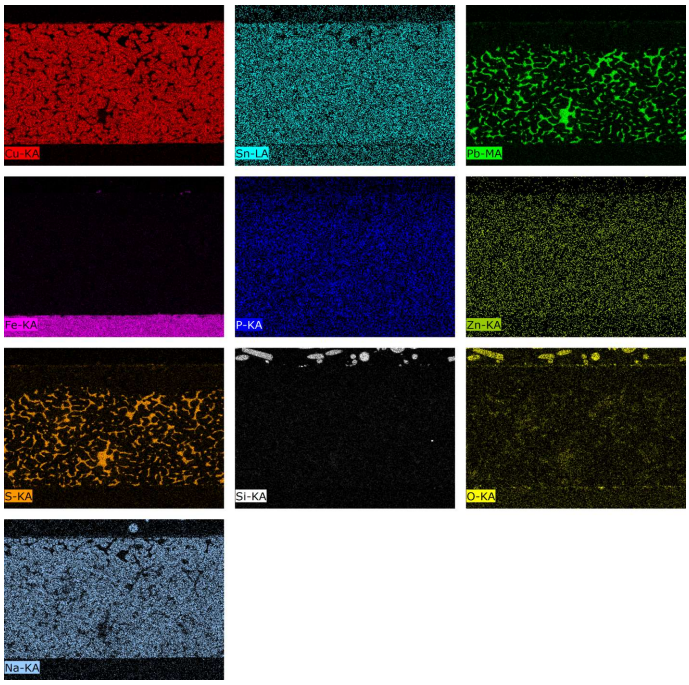

CROSS-SECTIONAL ANALYSIS (DERM119 after 50,200,500 hrs)

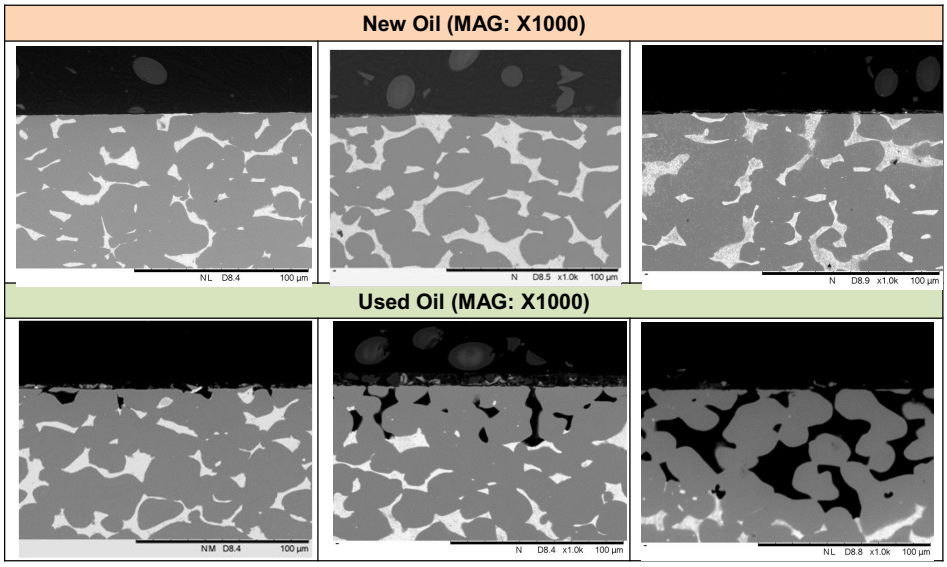

CROSS-SECTIONAL ANALYSIS (DERM119 after 50,200,500 hrs)

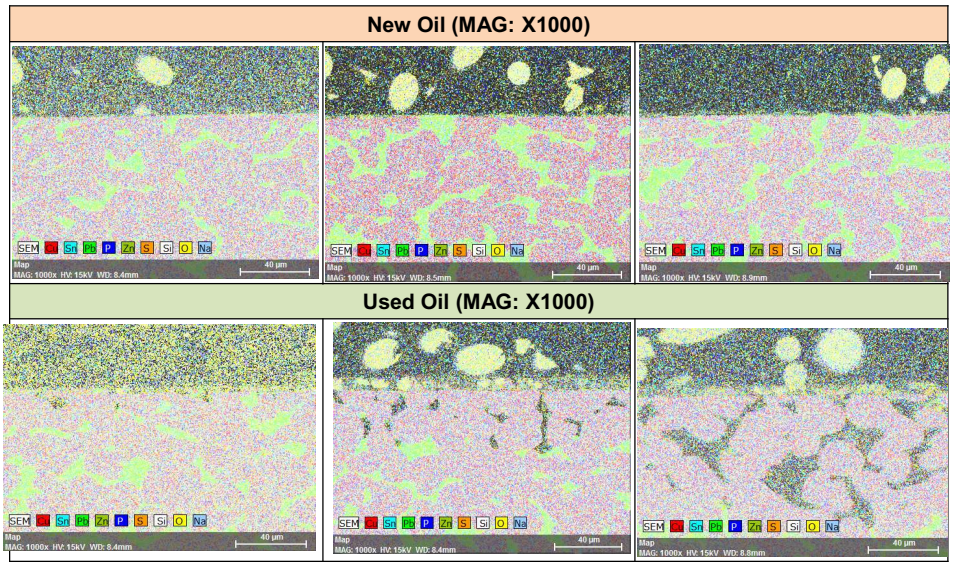

DAIDO METAL

19

DERM119 after 50,200 & 500 hrs
(NEW OIL 1000X)

DAIDO METAL

20

50 hrs

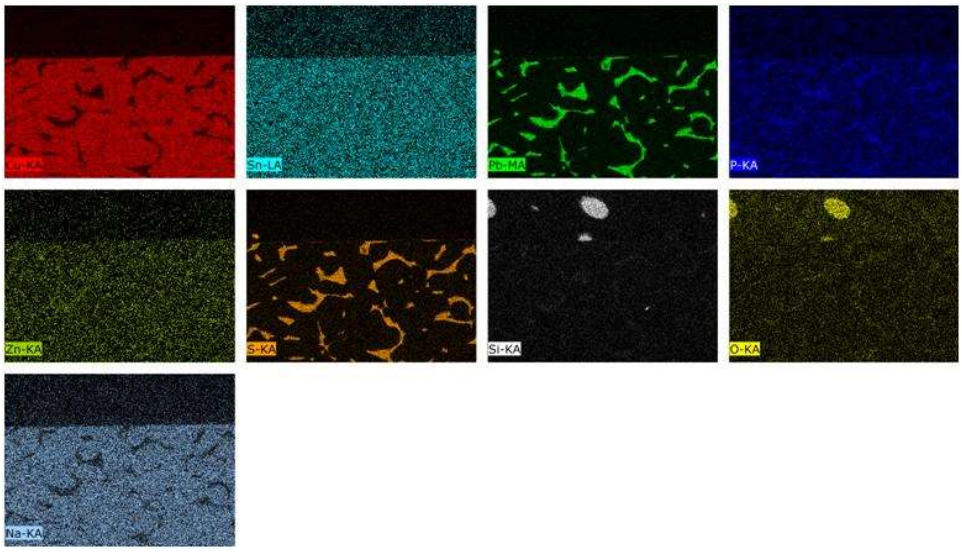

DAIDO METAL

21

200 hrs

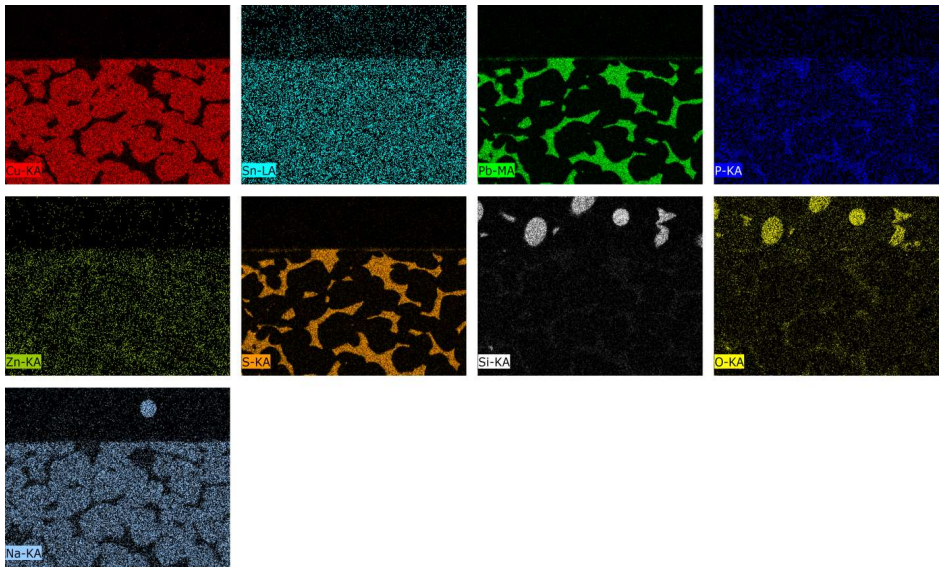

DAIDO METAL

22

500 hrs

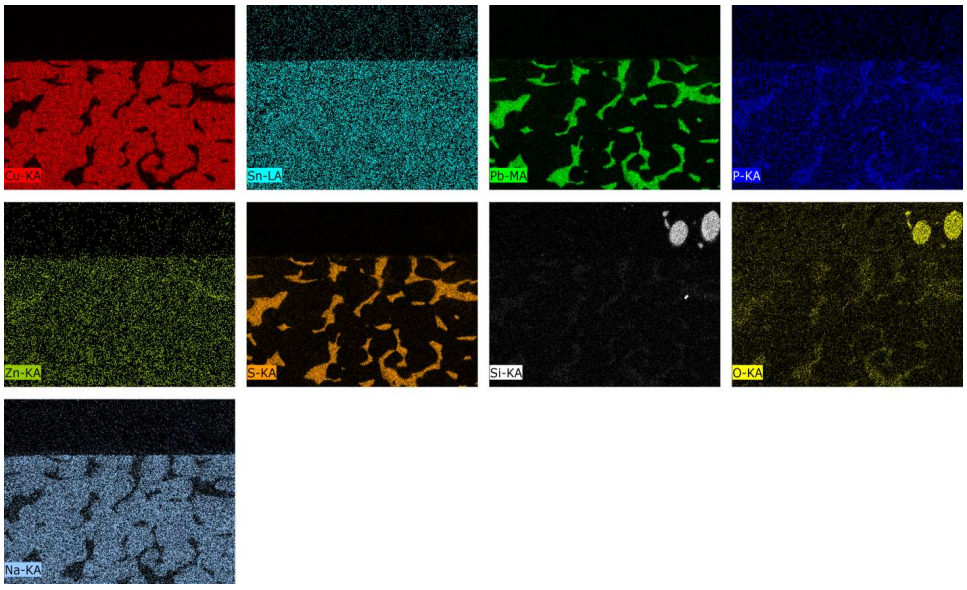

DAIDO METAL

23

DERM119 after 50,200 & 500 hrs
(USED OIL 1000X)

29-10-2020

DAIDO METAL

24

50 hrs

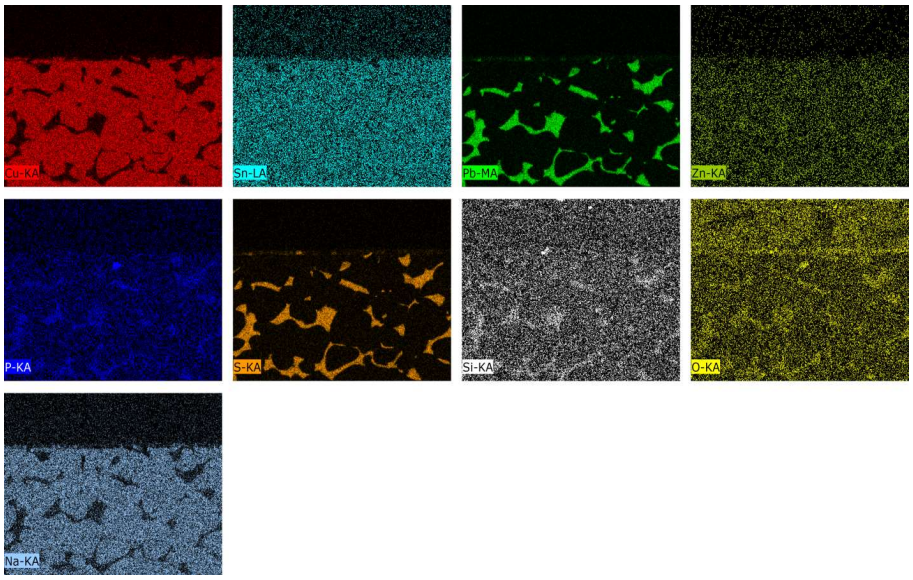

DAIDO METAL

25

200 hrs

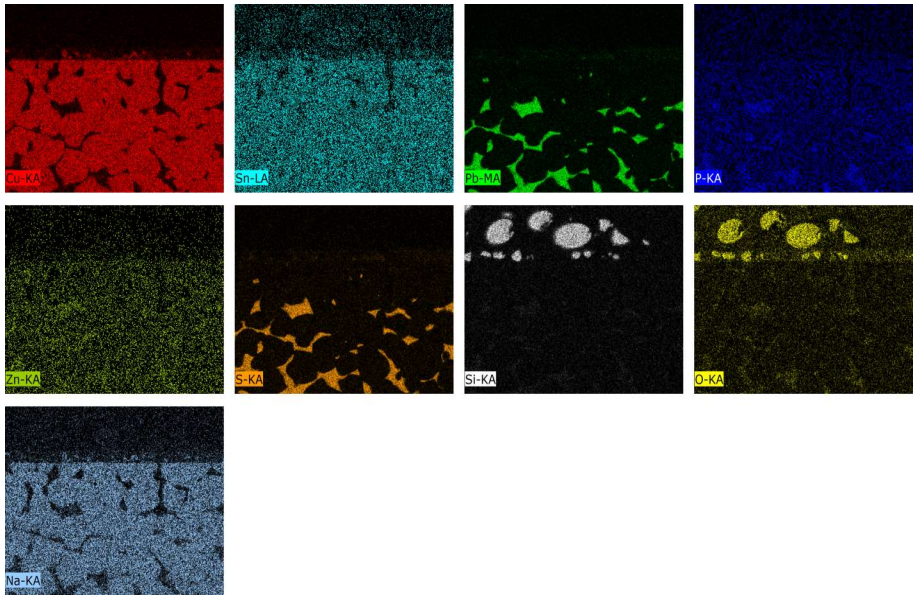

DAIDO METAL

26

500 hrs

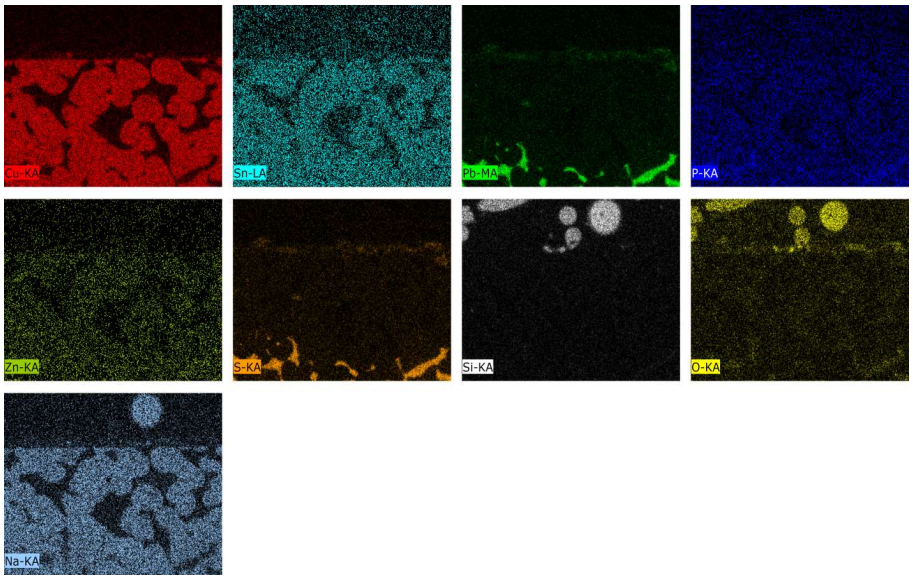

DAIDO METAL

27

CROSS-SECTIONAL ANALYSIS (DERM119 after 50,200,500 hrs)

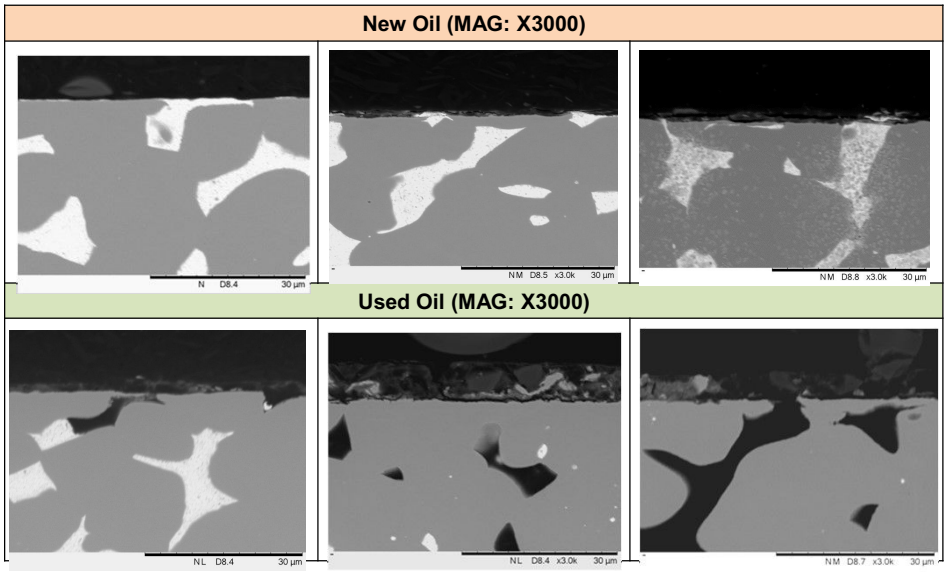

DAIDO METAL

28

CROSS-SECTIONAL ANALYSIS (DERM119 after 50,200,500 hrs)

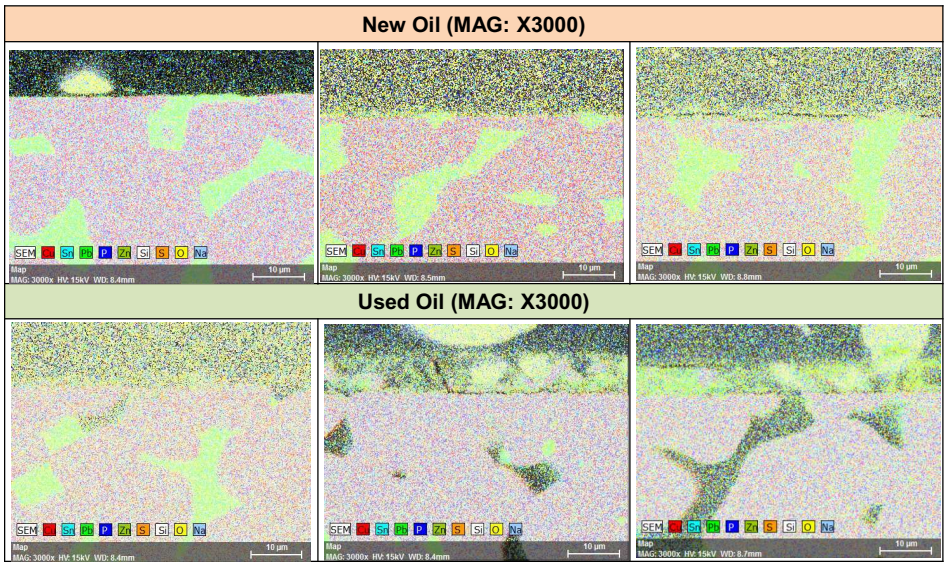

DAIDO METAL

29

DERM119 after 50,200 & 500 hrs
(NEW OIL 3000X)

29-10-2020

DAIDO METAL

30

50 hrs

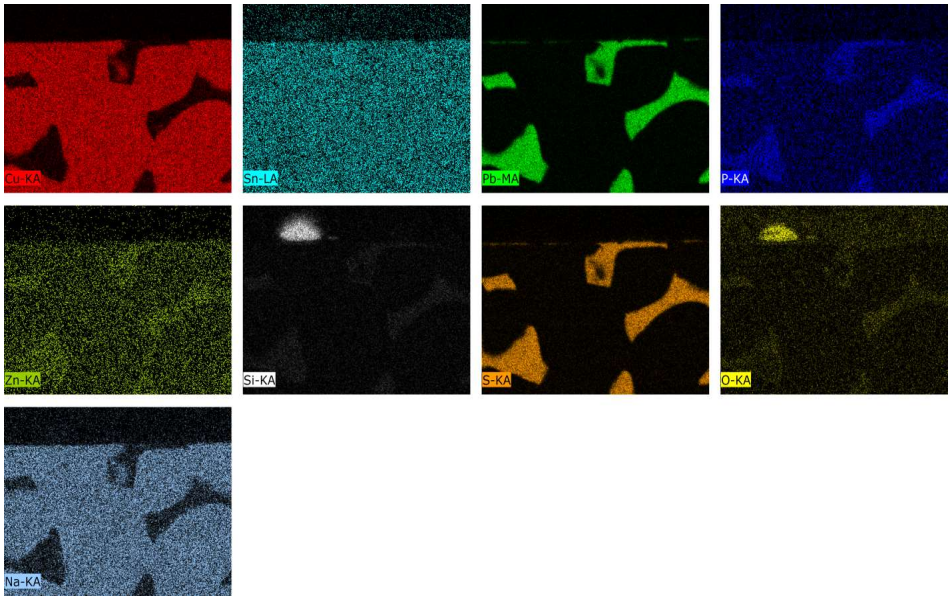

DAIDO METAL

31

200 hrs

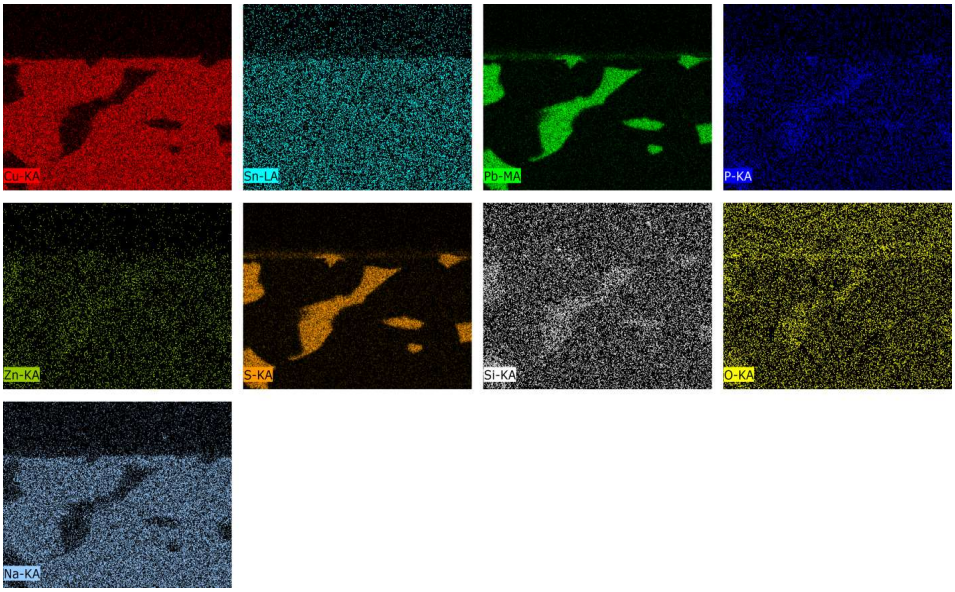

DAIDO METAL

32

500 hrs

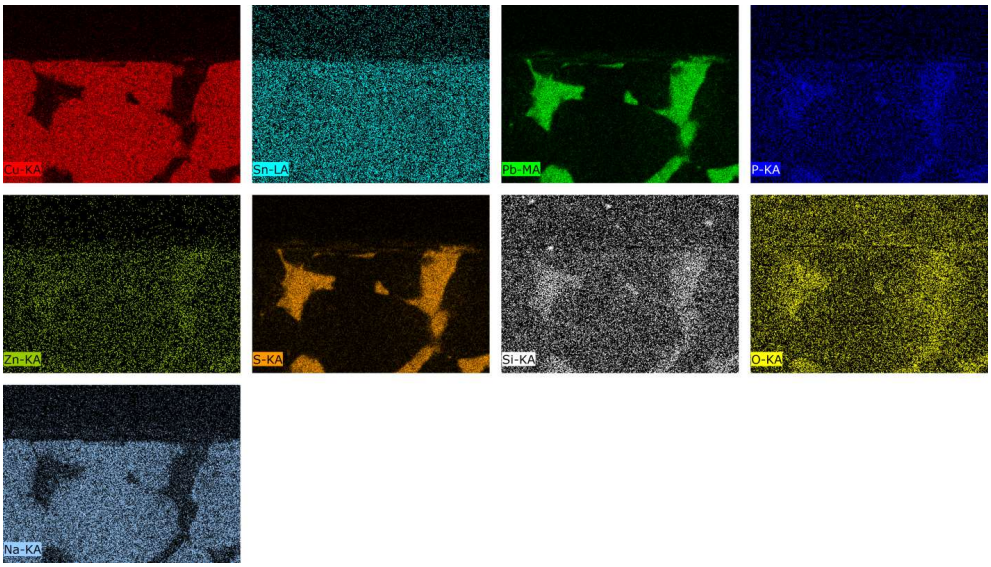

DAIDO METAL

33

DERM119 after 50,200 & 500 hrs
(USED OIL 3000X)

DAIDO METAL

34

50 hrs

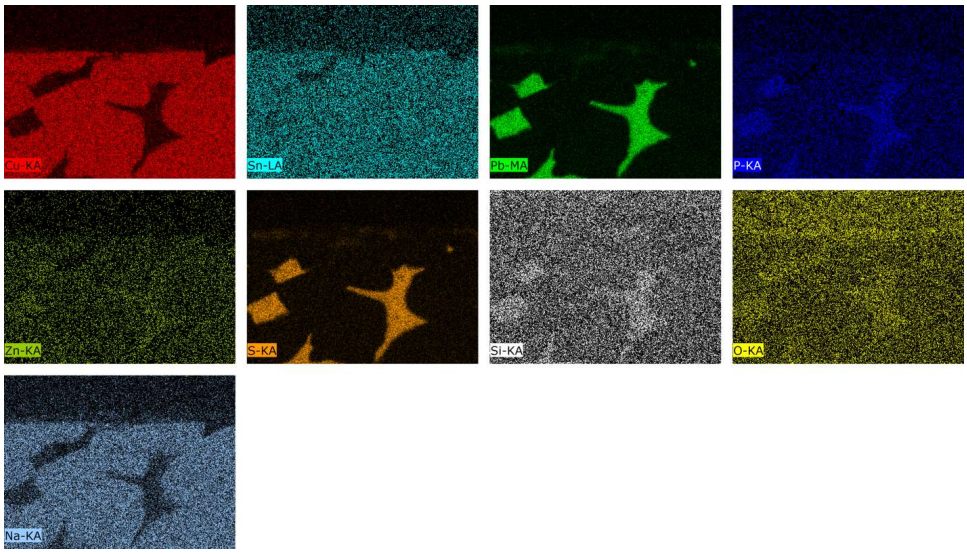

DAIDO METAL

35

200 hrs

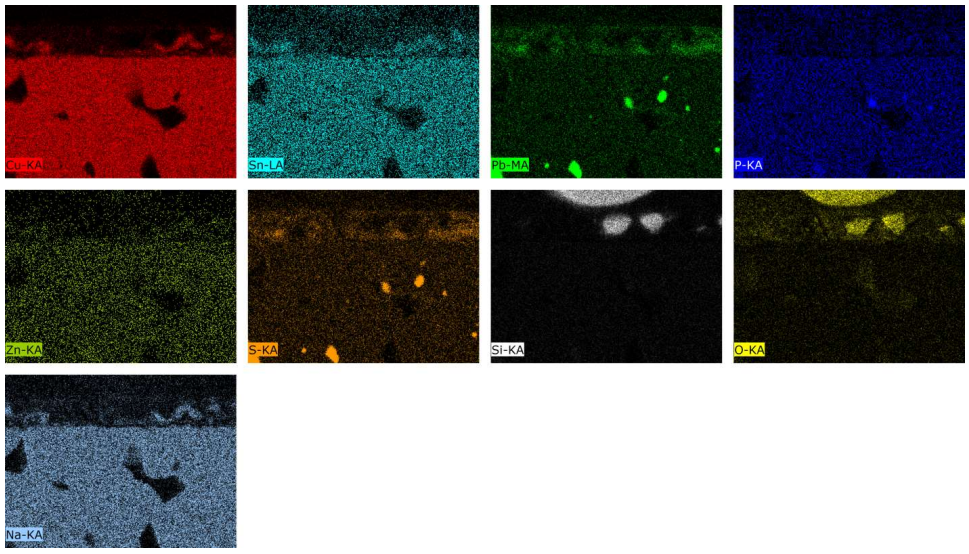

DAIDO METAL

36

500 hrs

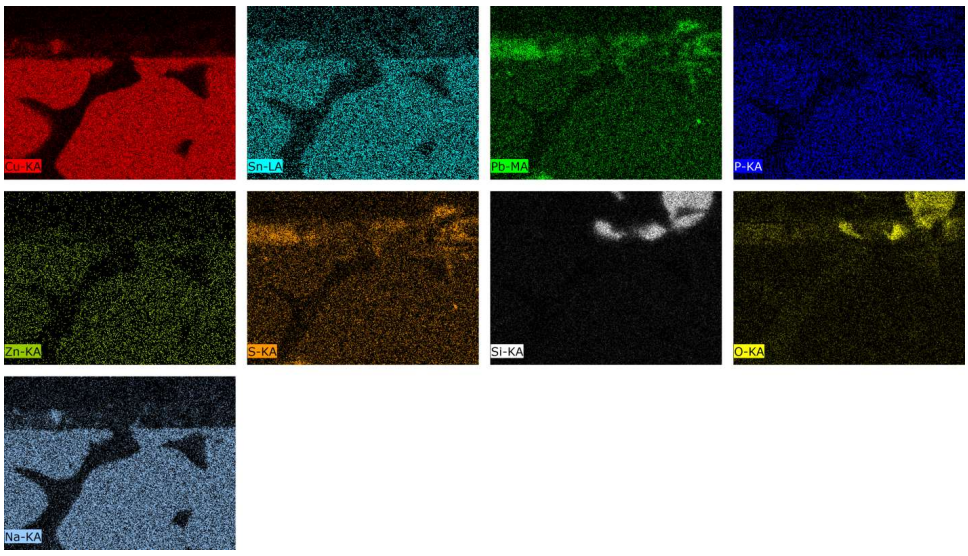

DAIDO METAL

37

DERM123

DAIDO METAL

38

APPEARANCE CHANGE (DERM123 after 50hrs)

	Before test	After test
New Oil		
Used Oil	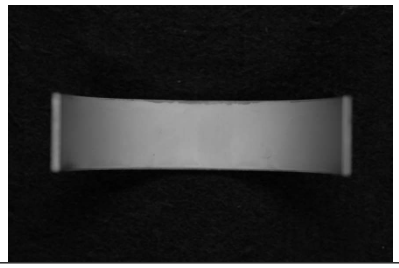	

DAIDO METAL

39

APPEARANCE CHANGE (DERM123 after 200hrs)

	Before test	After test
New Oil		
Used Oil		

DAIDO METAL

40

APPEARANCE CHANGE (DERM123 after 500hrs)

	Before test	After test
New Oil		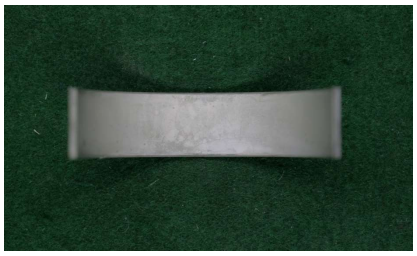
Used Oil		

DAIDO METAL

41

CROSS-SECTIONAL ANALYSIS (DERM123 after 50,200,500 hrs)

New Oil (MAG: X300)

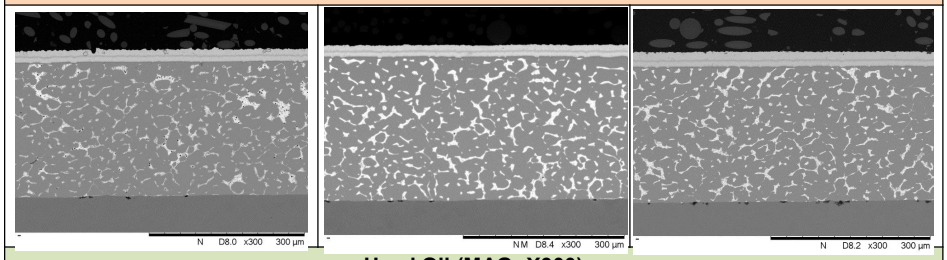

Used Oil (MAG: X300)

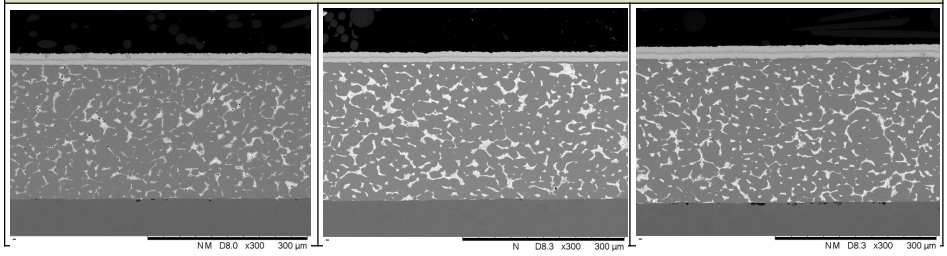

DAIDO METAL

42

CROSS-SECTIONAL ANALYSIS (DERM123 after 50,200,500 hrs)

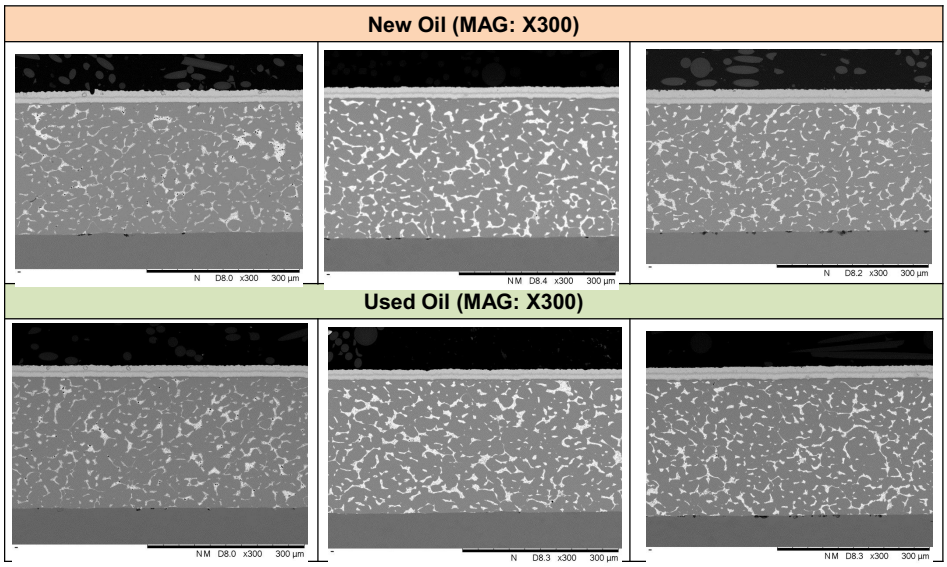

DAIDO METAL

43

DERM123 after 50,200 & 500 hrs
(NEW OIL 300X)

DAIDO METAL

44

50 hrs

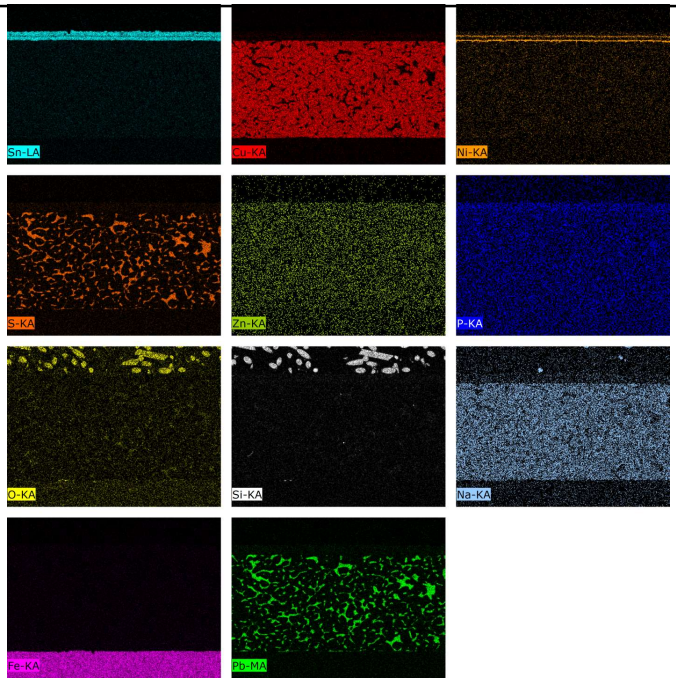

DAIDO METAL

45

200 hrs

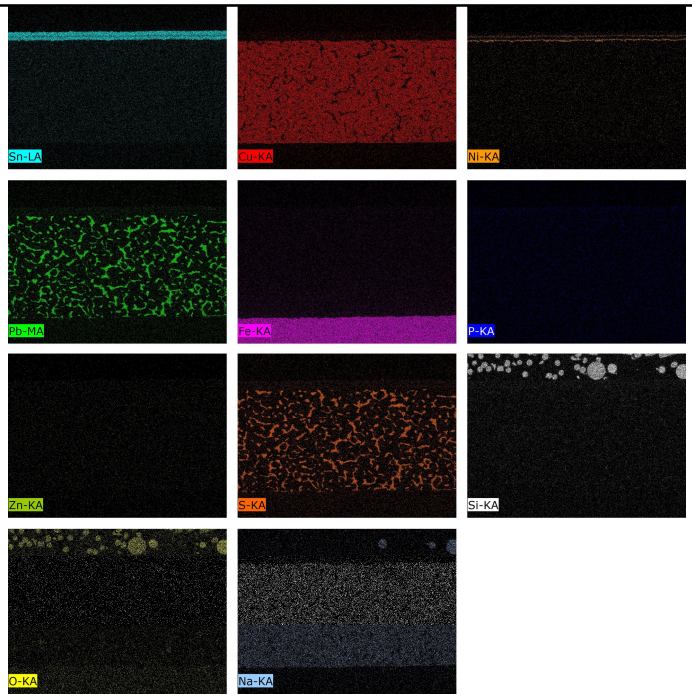

DAIDO METAL

46

500 hrs

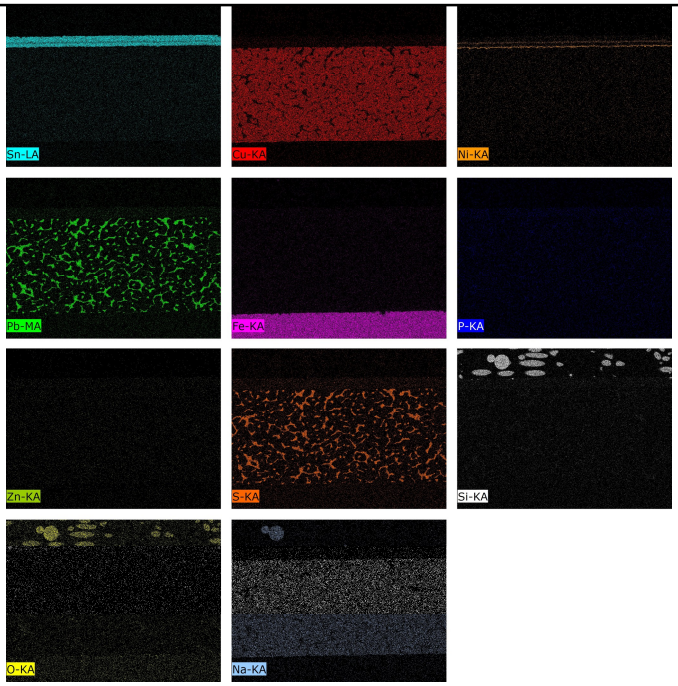

DAIDO METAL

47

DERM123 after 50,200 & 500 hrs
(USED OIL 300X)

29-10-2020

DAIDO METAL

48

50 hrs

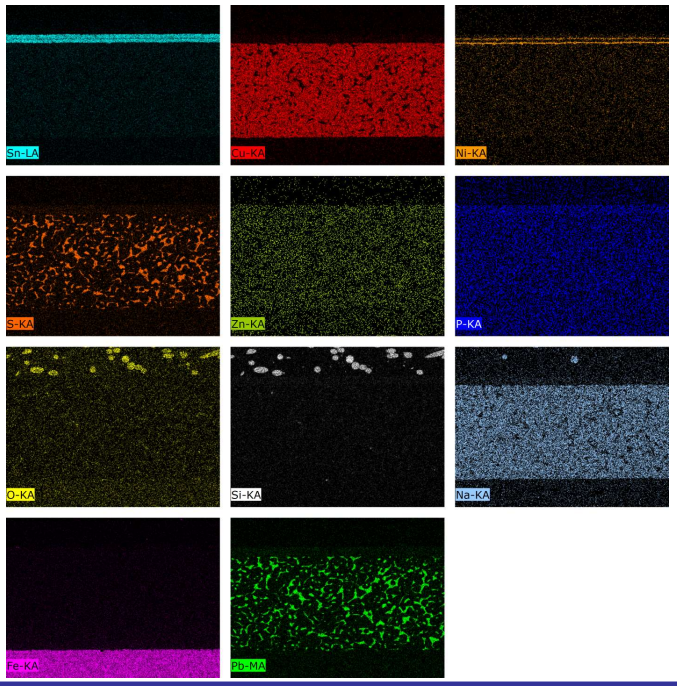

DAIDO METAL

49

200 hrs

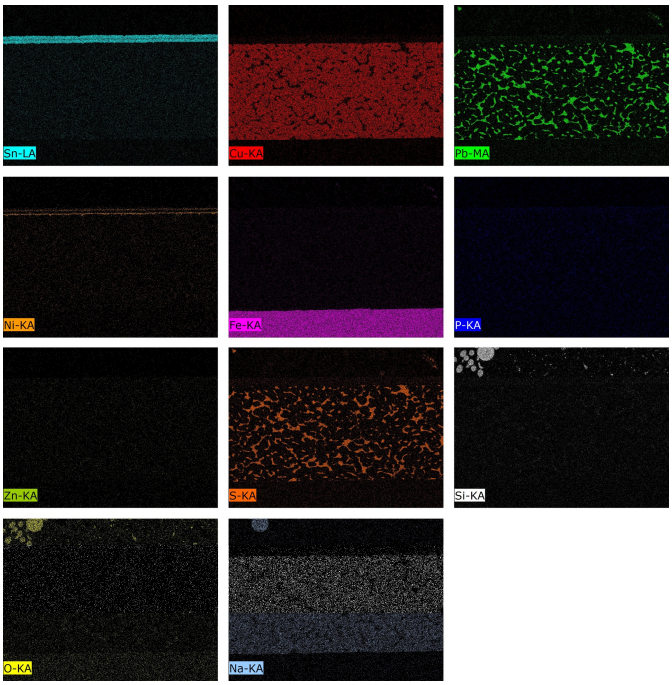

DAIDO METAL

50

500 hrs

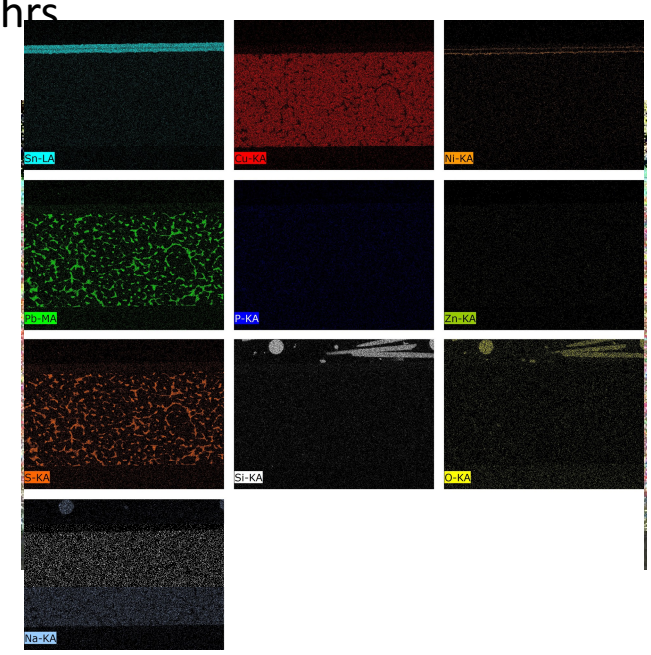

DAIDO METAL

51

CROSS-SECTIONAL ANALYSIS (DERM123 after 50,200,500 hrs)

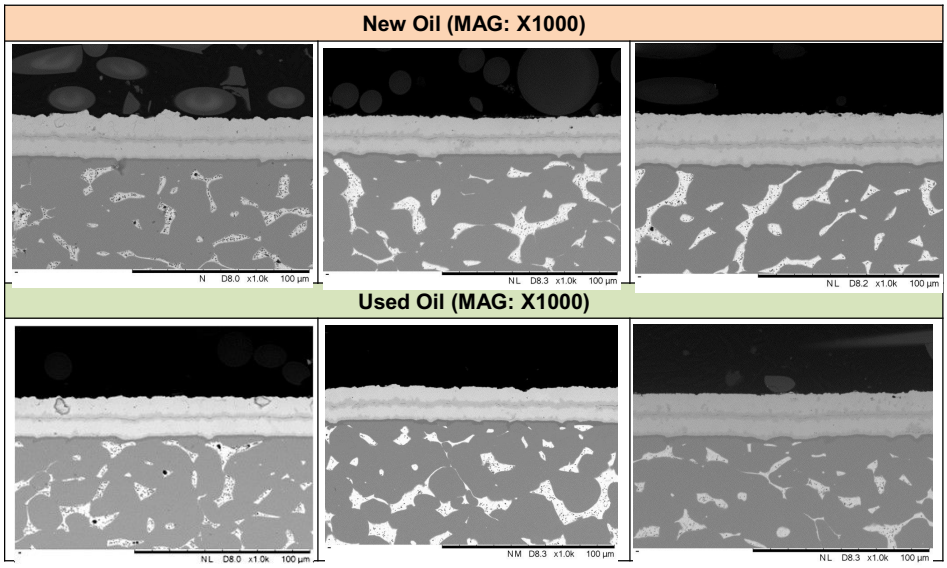

DAIDO METAL

52

CROSS-SECTIONAL ANALYSIS (DERM123 after 50,200,500 hrs)

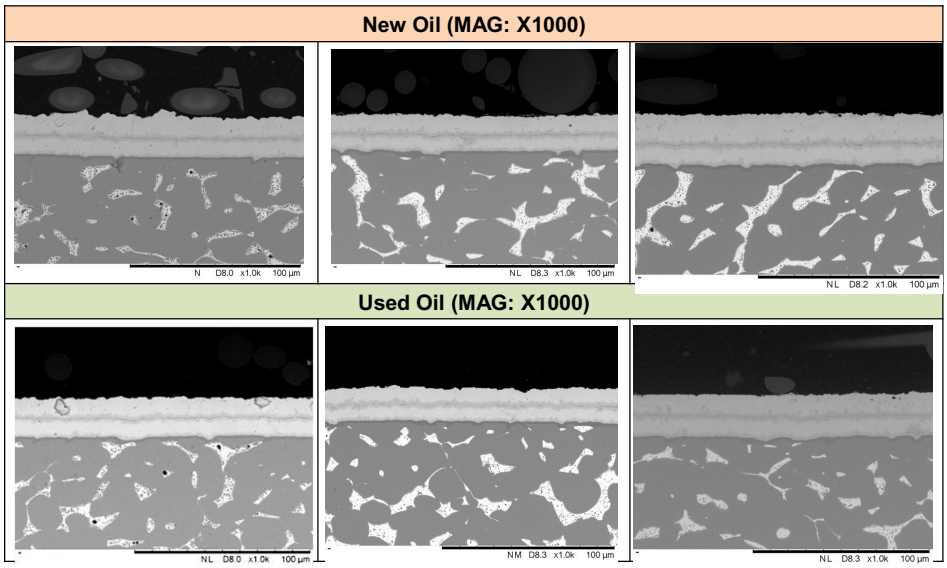

DAIDO METAL

53

DERM123 after 50,200 & 500 hrs
(NEW OIL 1000X)

29-10-2020

DAIDO METAL

54

50 hrs

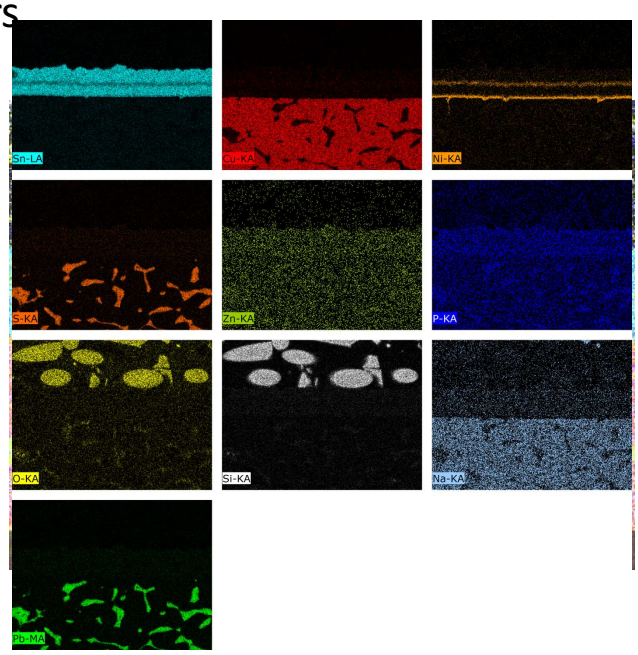

DAIDO METAL

55

200 hrs

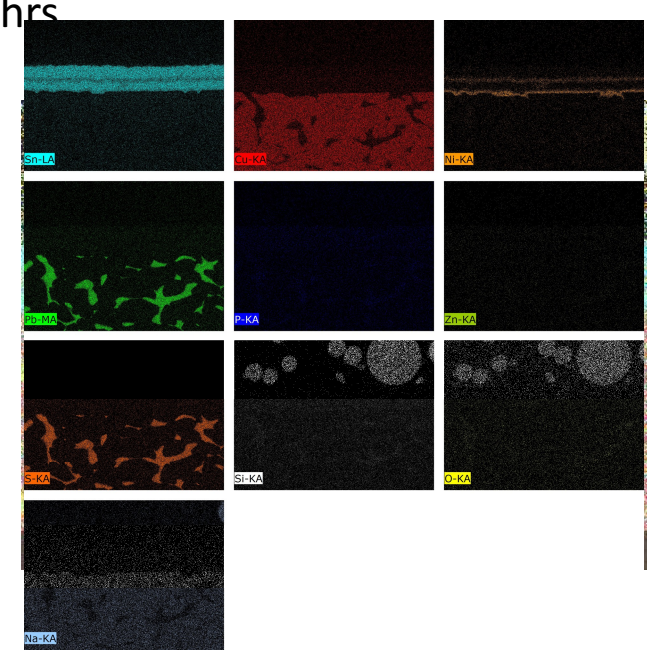

DAIDO METAL

56

500 hrs

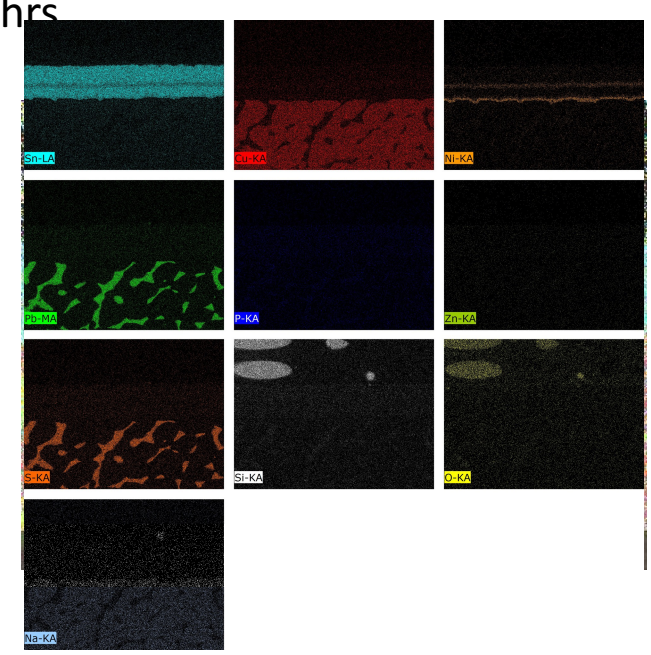

DAIDO METAL

57

DERM123 after 50,200 & 500 hrs
(USED OIL 1000X)

29-10-2020

DAIDO METAL

58

50 hrs

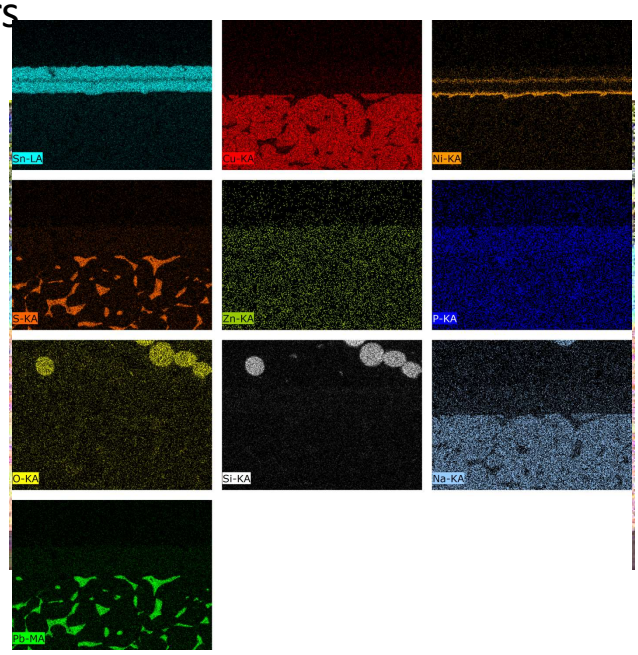

DAIDO METAL

59

200 hrs

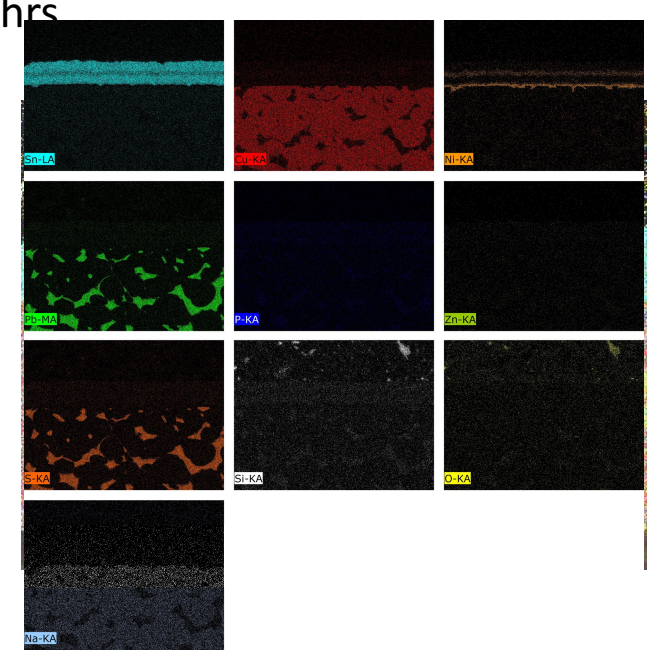

DAIDO METAL

60

500 hrs

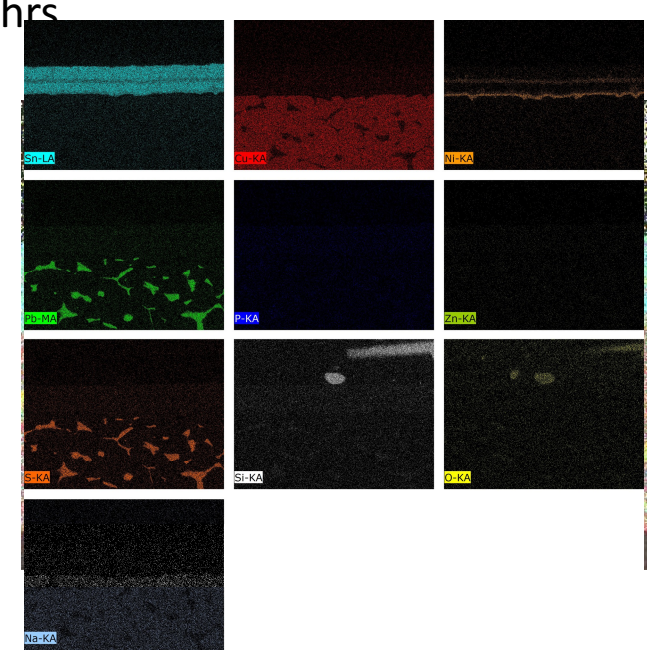

DAIDO METAL

61

CROSS-SECTIONAL ANALYSIS (DERM123 after 50,200,500 hrs)

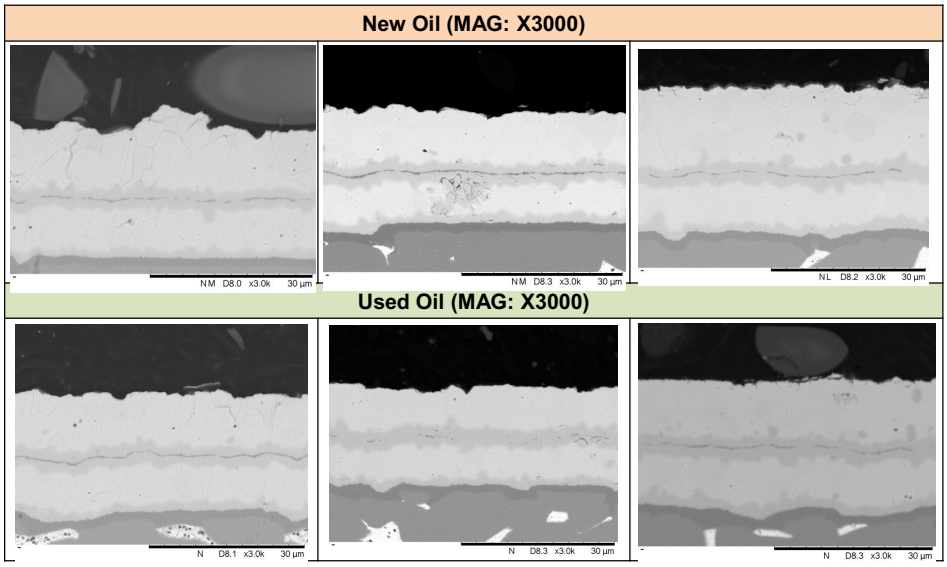

DAIDO METAL

62

CROSS-SECTIONAL ANALYSIS (DERM123 after 50,200,500 hrs)

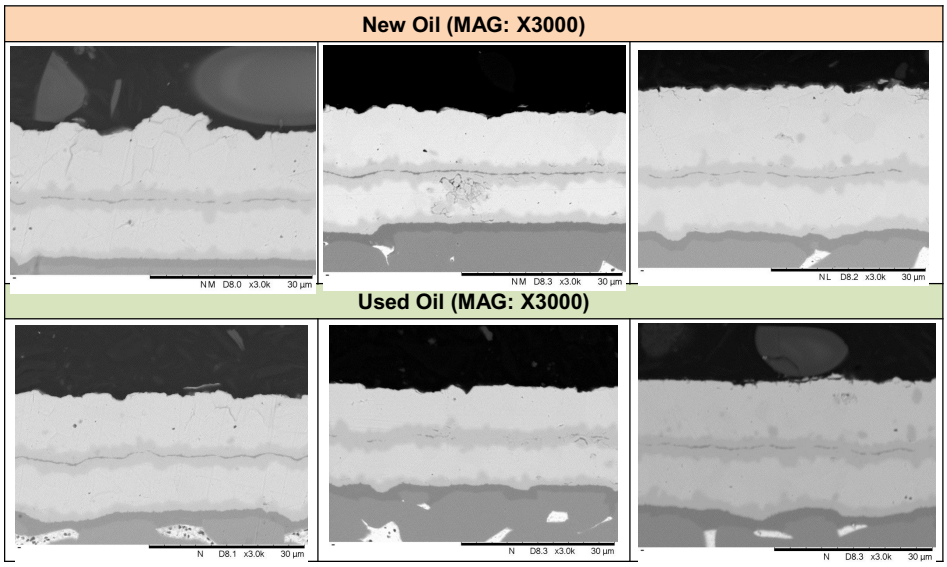

DAIDO METAL

63

DERM123 after 50,200 & 500 hrs
(NEW OIL 3000X)

DAIDO METAL

64

50 hrs

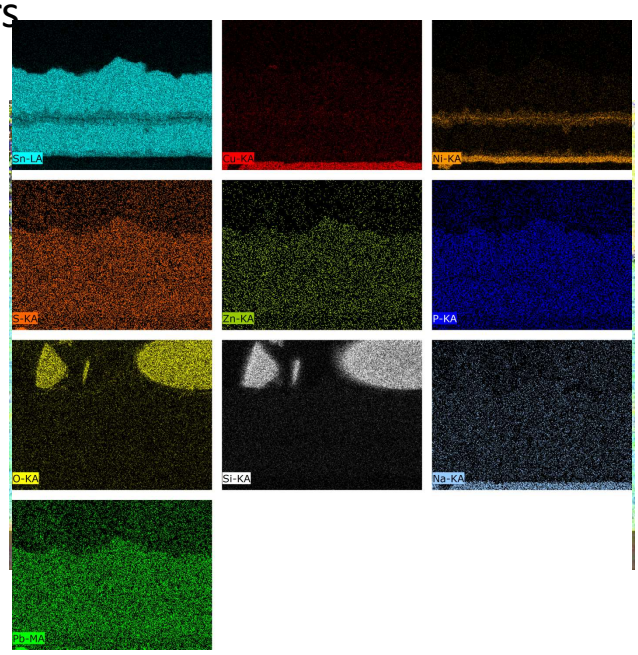

DAIDO METAL

65

200 hrs

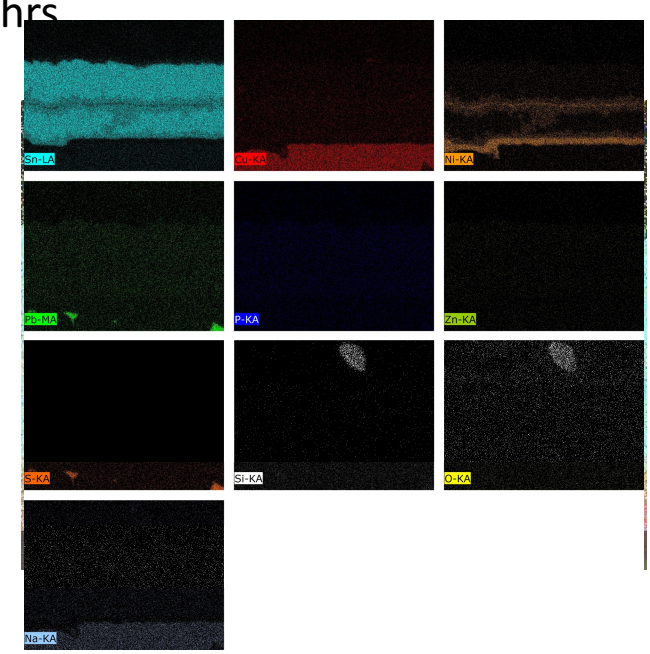

DAIDO METAL

66

500 hrs

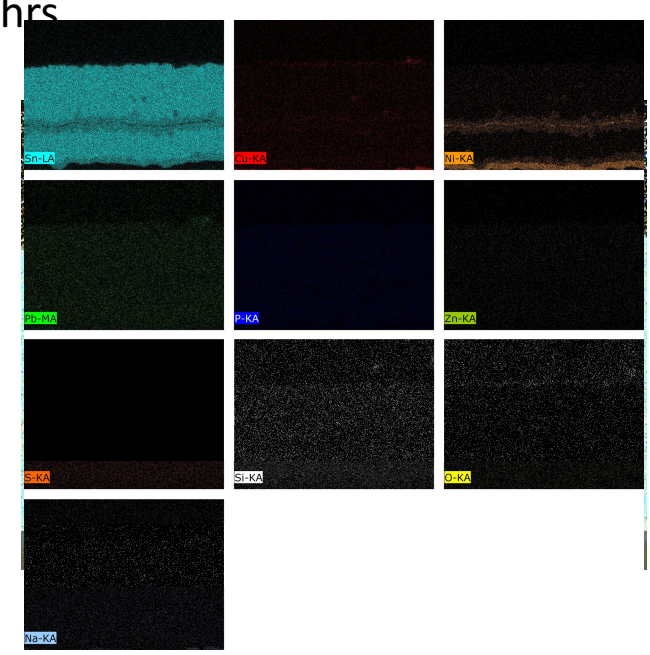

DAIDO METAL

67

DERM123 after 50,200 & 500 hrs
(USED OIL 3000X)

DAIDO METAL

68

50 hrs

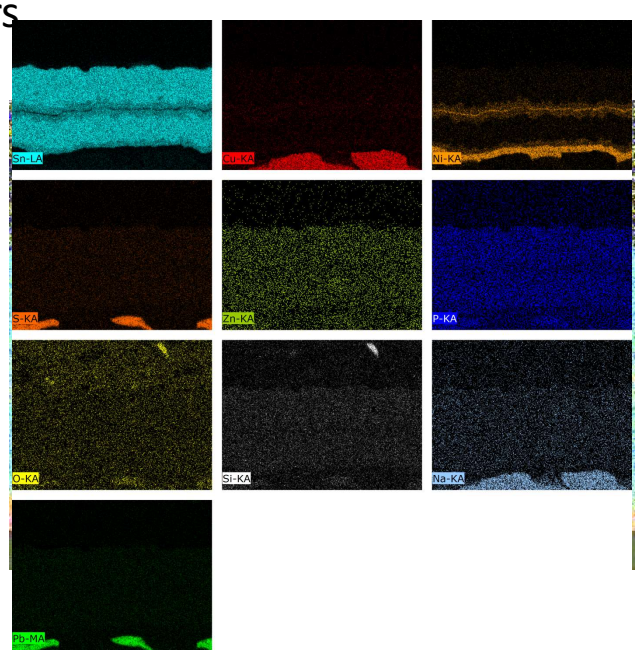

DAIDO METAL

69

200 hrs

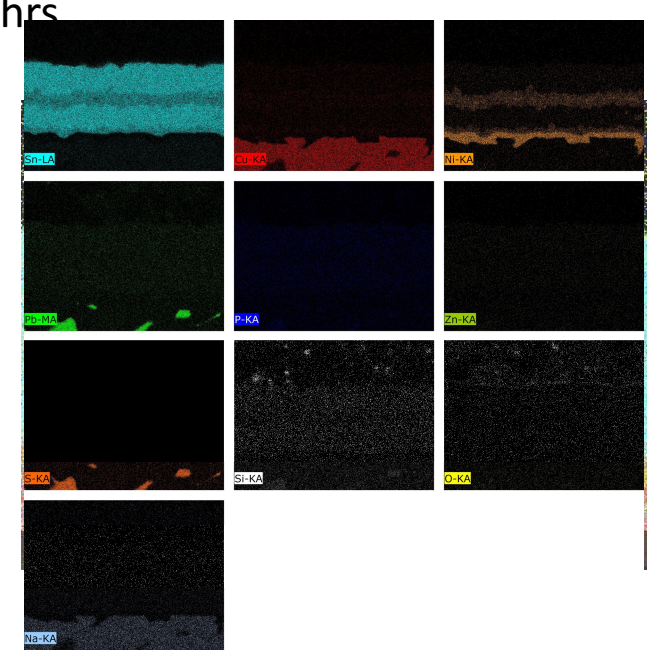

DAIDO METAL

70

500 hrs

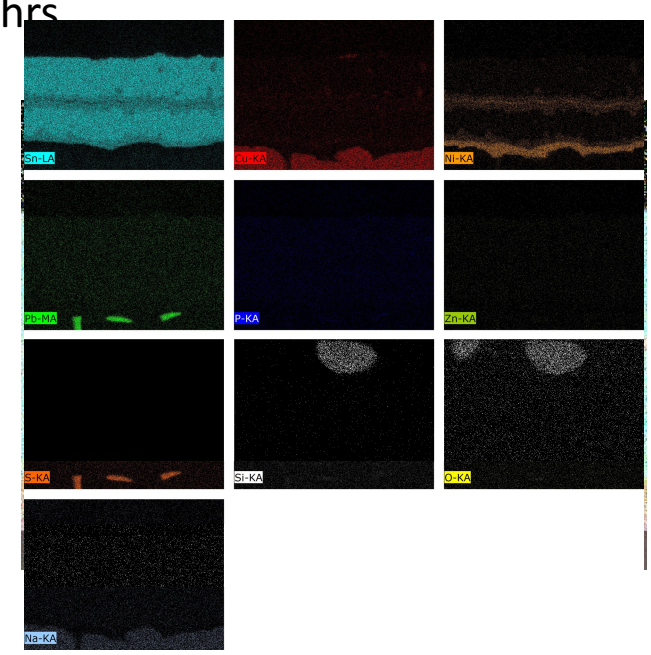

DAIDO METAL

71

DERM122

DAIDO METAL

72

APPEARANCE CHANGE (DERM122 after 50hrs)

	Before test	After test
New Oil		
Used Oil		

DAIDO METAL

73

APPEARANCE CHANGE (DERM122 after 200hrs)

	Before test	After test
New Oil		
Used Oil	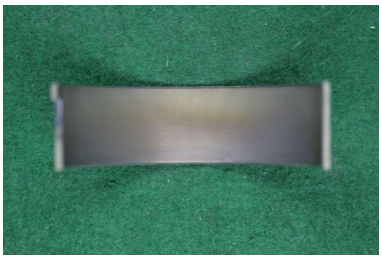	

DAIDO METAL

74

APPEARANCE CHANGE (DERM122 after 500hrs)

	Before test	After test
New Oil		
Used Oil		

AIDO METAL

75

CROSS-SECTIONAL ANALYSIS (DERM122 after 50,200,500 hrs)

New Oil (MAG: X300)

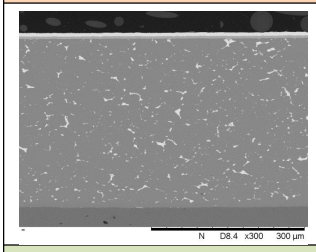

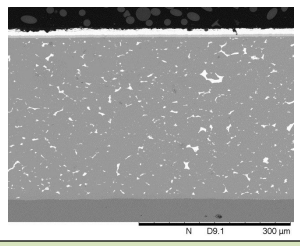

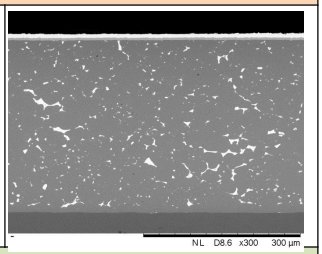

Used Oil (MAG: X300)

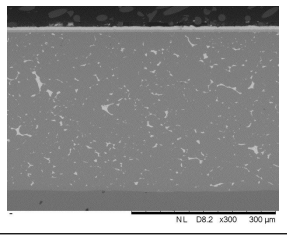

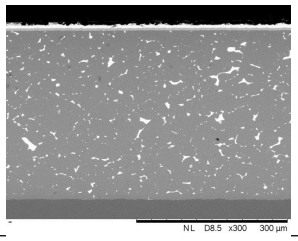

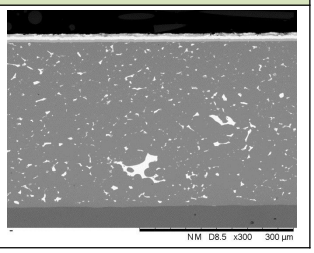

AIDO METAL

76

CROSS-SECTIONAL ANALYSIS (DERM122 after 50,200,500 hrs)

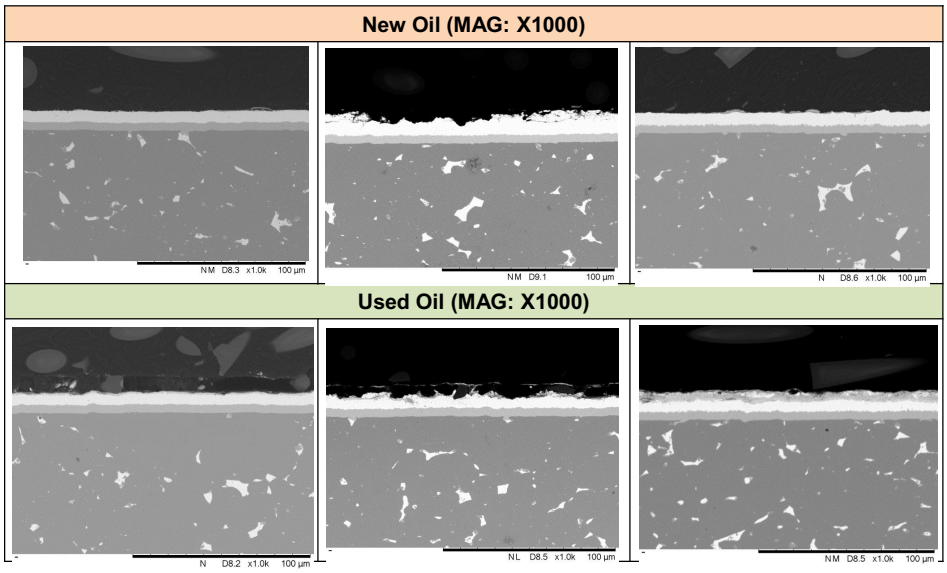

DAIDO METAL

77

CROSS-SECTIONAL ANALYSIS (DERM122 after 50,200,500 hrs)

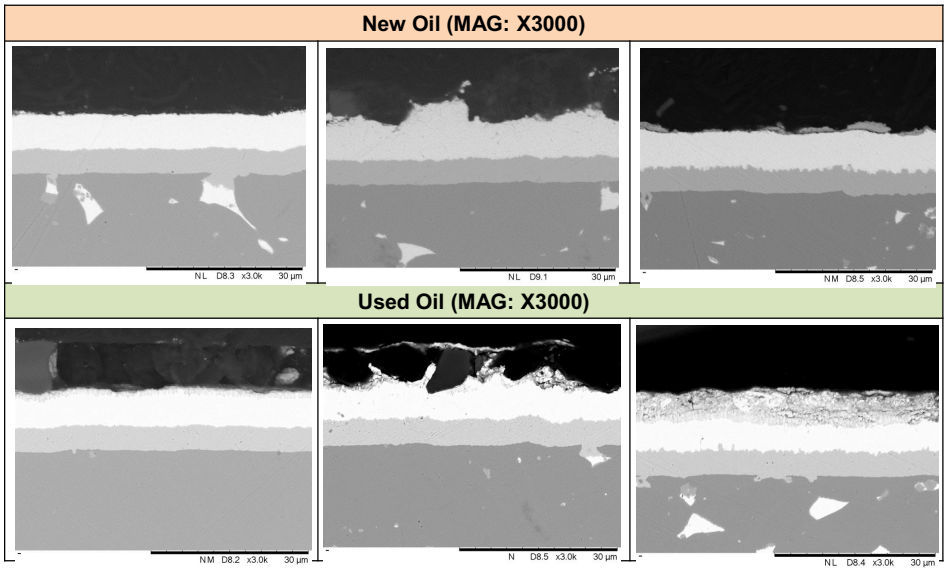

DAIDO METAL

78

CROSS-SECTIONAL ANALYSIS (DERM122 after 50,200,500 hrs)

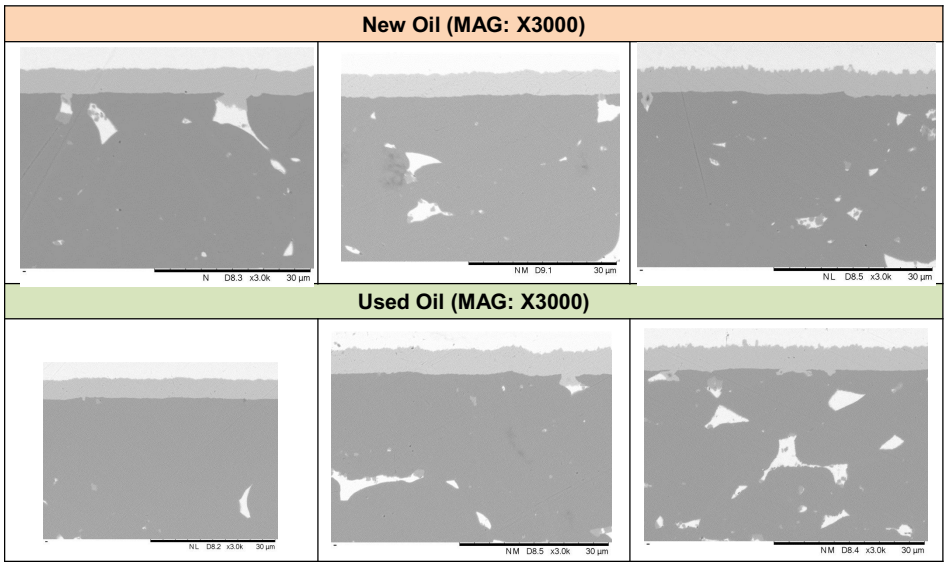

DAIDO METAL

79

CROSS-SECTIONAL ANALYSIS (DERM122 after 50,200,500 hrs)

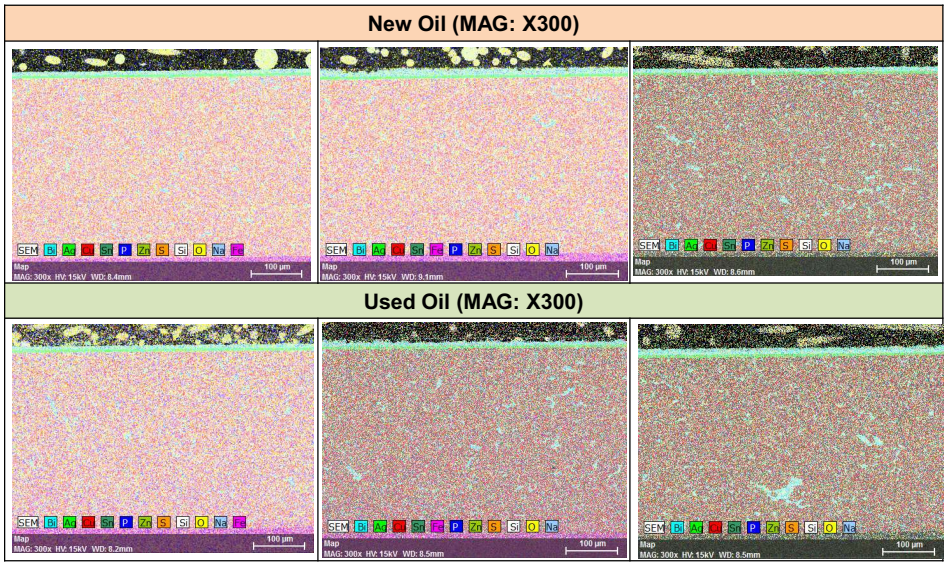

DAIDO METAL

80

CROSS-SECTIONAL ANALYSIS (DERM122 after 50,200,500 hrs)

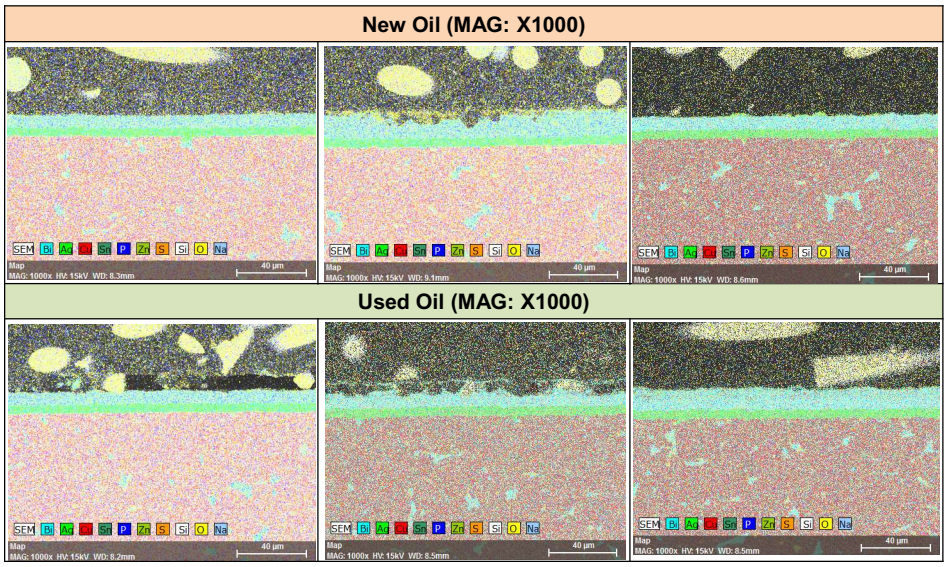

DAIDO METAL

81

CROSS-SECTIONAL ANALYSIS (DERM122 after 50,200,500 hrs)

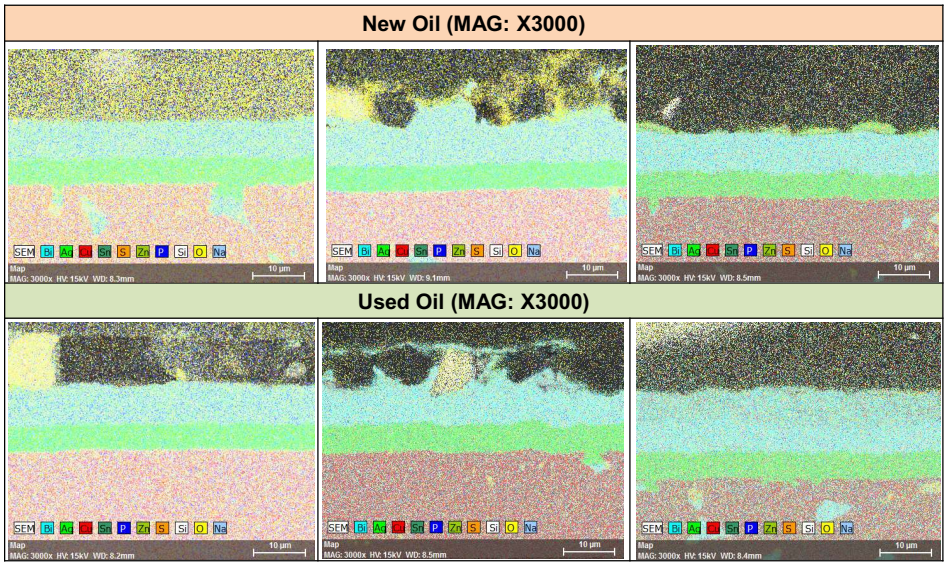

DAIDO METAL

82

CROSS-SECTIONAL ANALYSIS (DERM122 after 50,200,500 hrs)

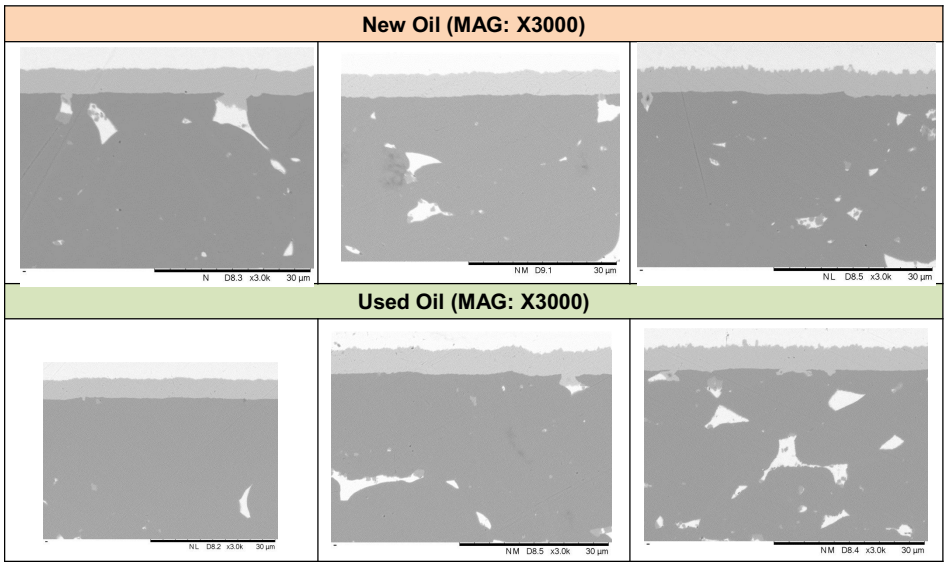

DAIDO METAL

83

DERM122 after 50,200 & 500 hrs
(NEW OIL 300X)

29-10-2020

DAIDO METAL

84

50 hrs

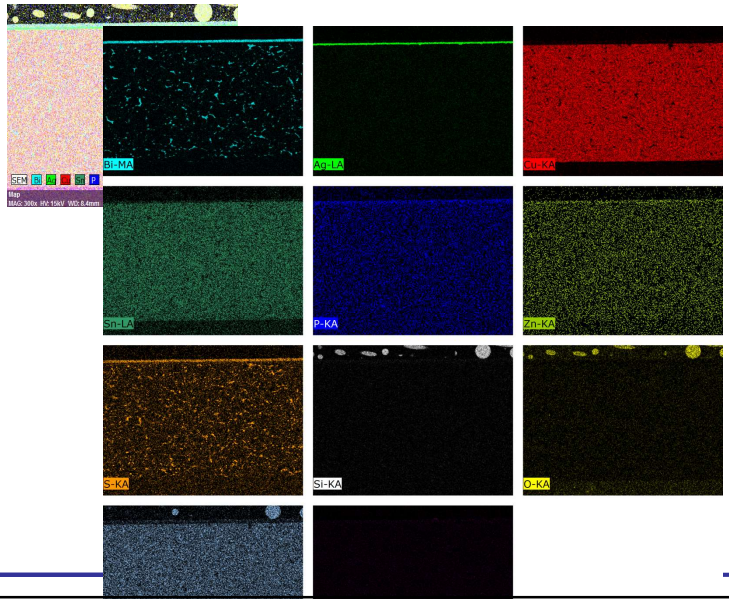

DAIDO METAL

85

200 hrs

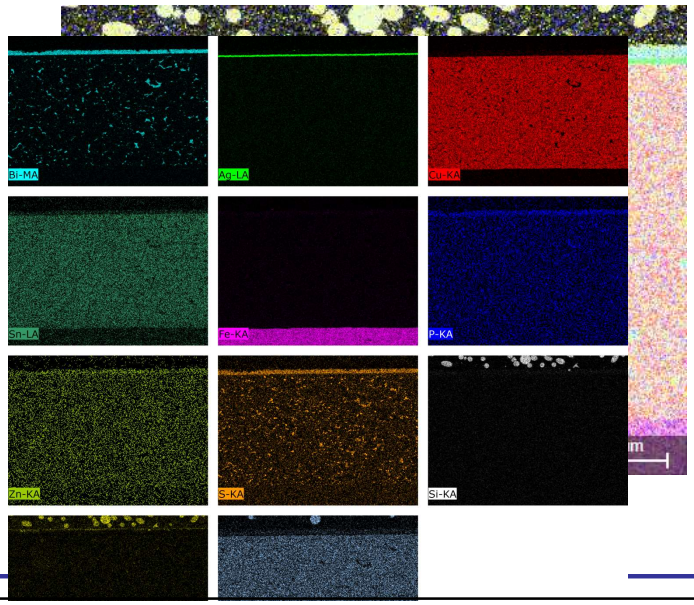

DAIDO METAL

86

500 hrs

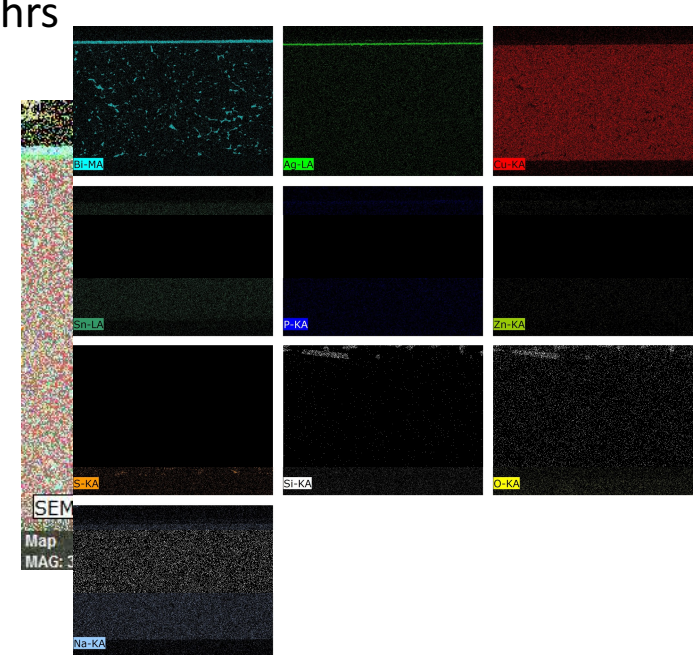

DAIDO METAL

87

DERM122 after 50,200 & 500 hrs
(USED OIL 300X)

29-10-2020

DAIDO METAL

88

50 hrs

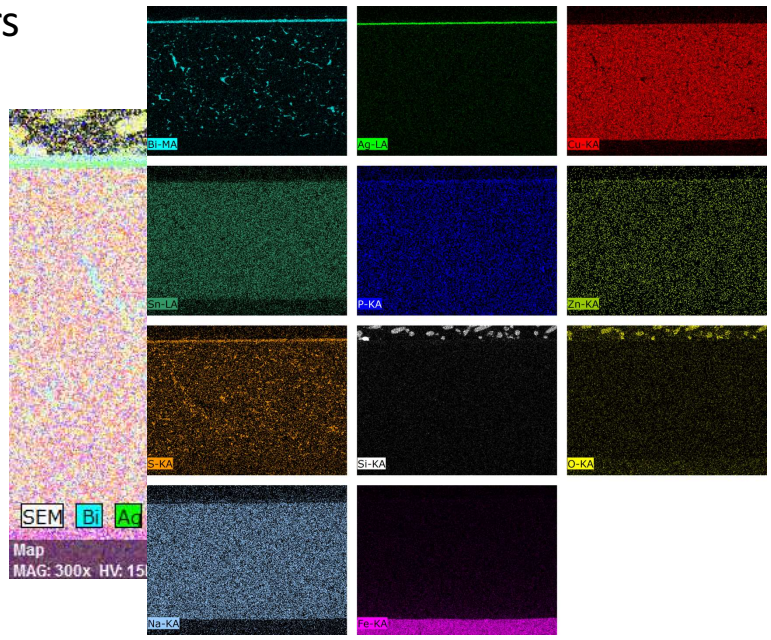

DAIDO METAL

89

200 hrs

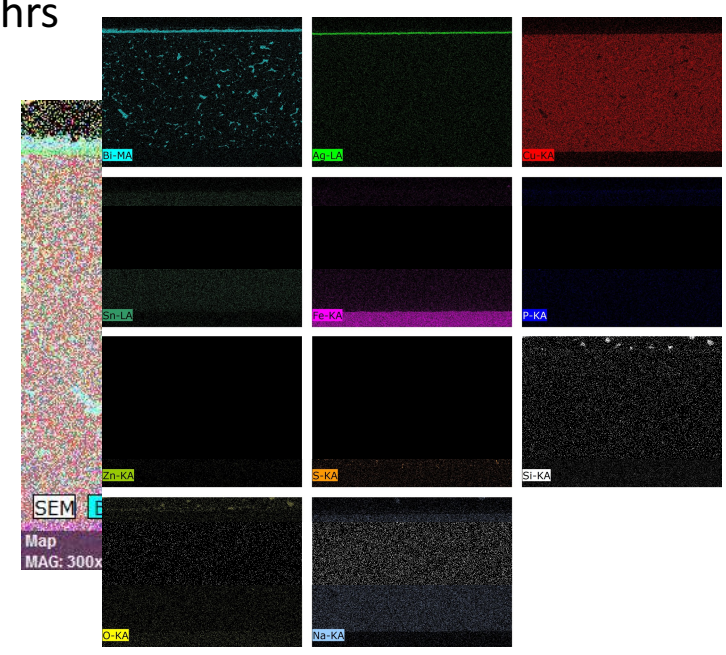

DAIDO METAL

90

500 hrs

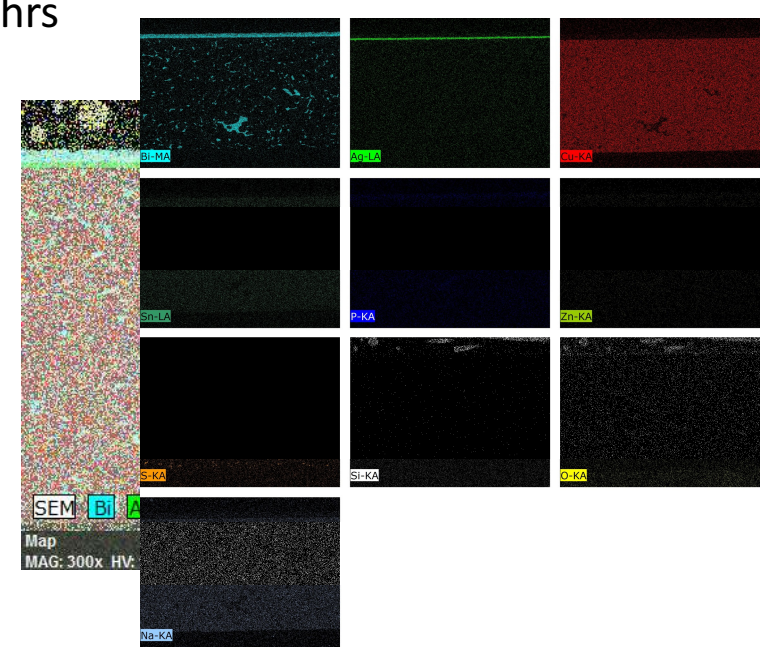

DAIDO METAL

91

DERM122 after 50,200 & 500 hrs
(NEW OIL 1000X)

29-10-2020

DAIDO METAL

92

50 hrs

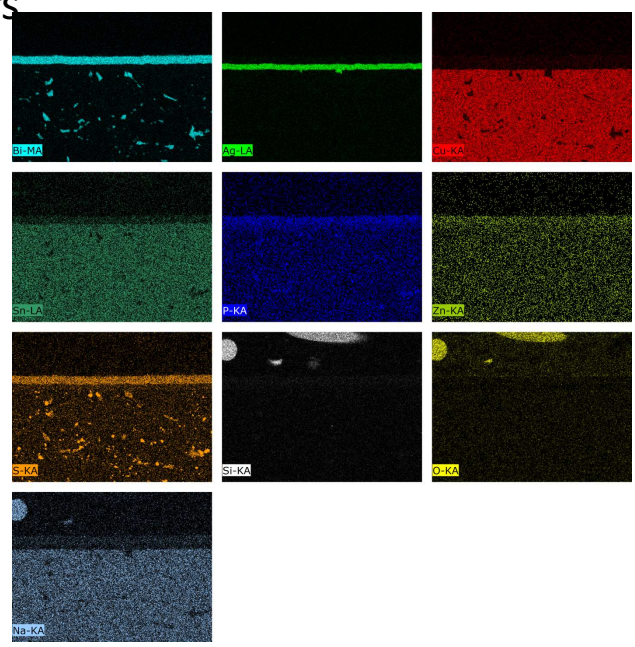

DAIDO METAL

93

200 hrs

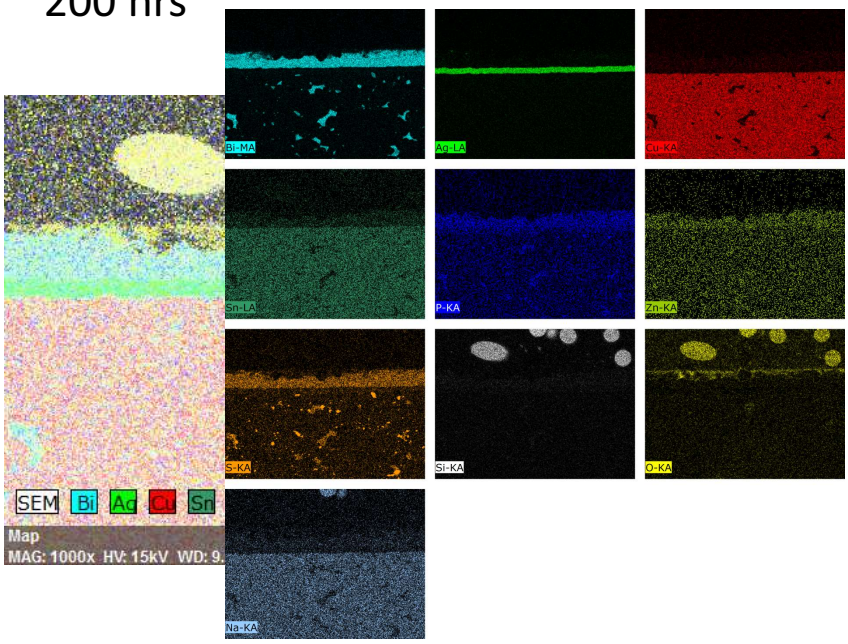

DAIDO METAL

94

500 hrs

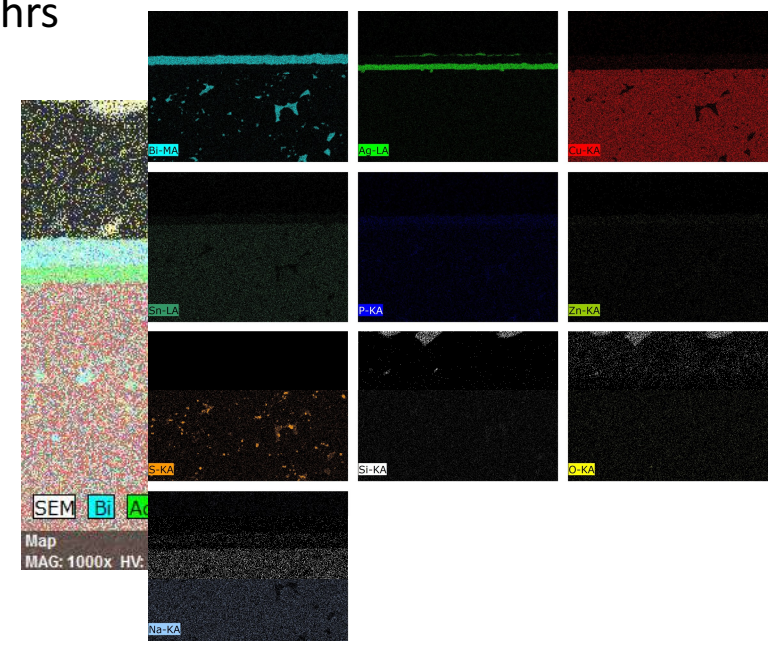

DAIDO METAL

95

DERM122 after 50,200 & 500 hrs
(USED OIL 1000X)

29-10-2020

DAIDO METAL

96

50 hrs

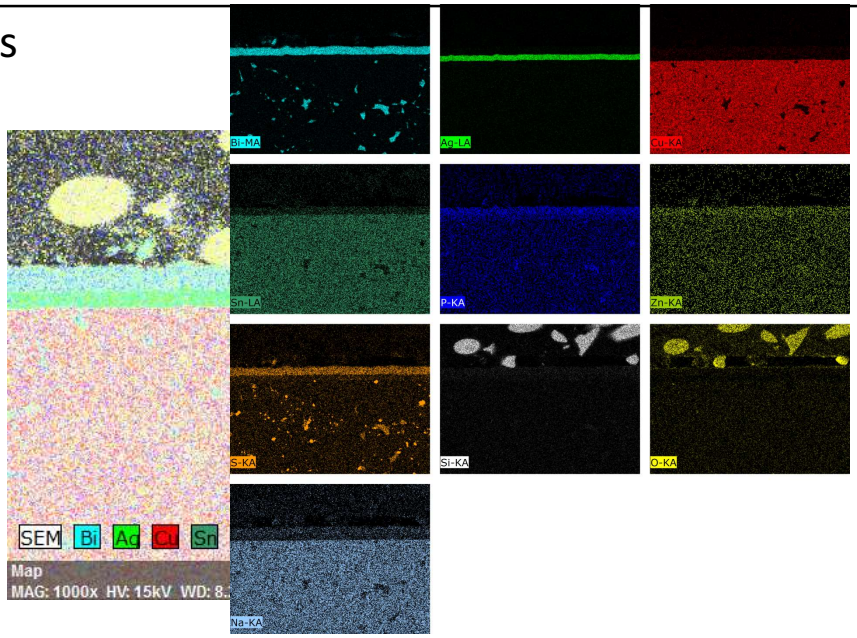

DAIDO METAL

97

200 hrs

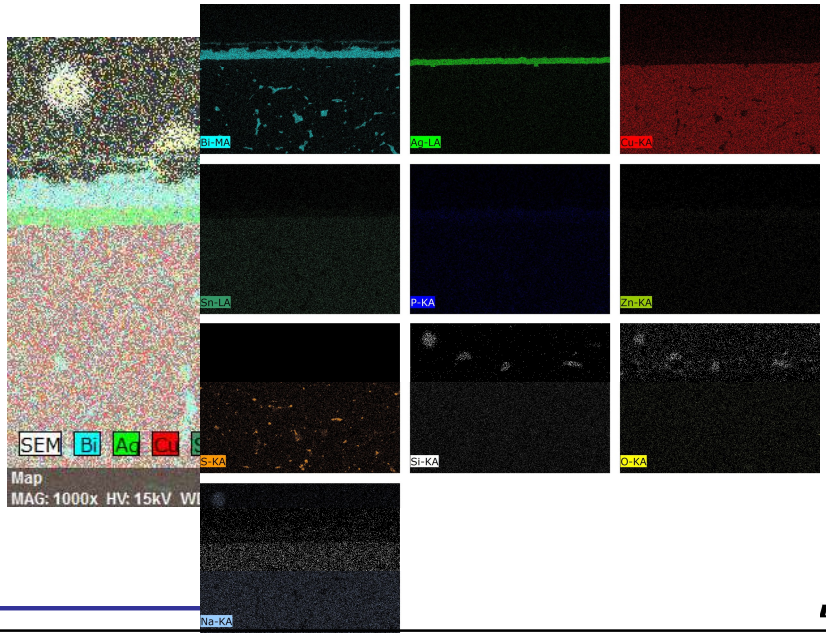

DAIDO METAL

98

500 hrs

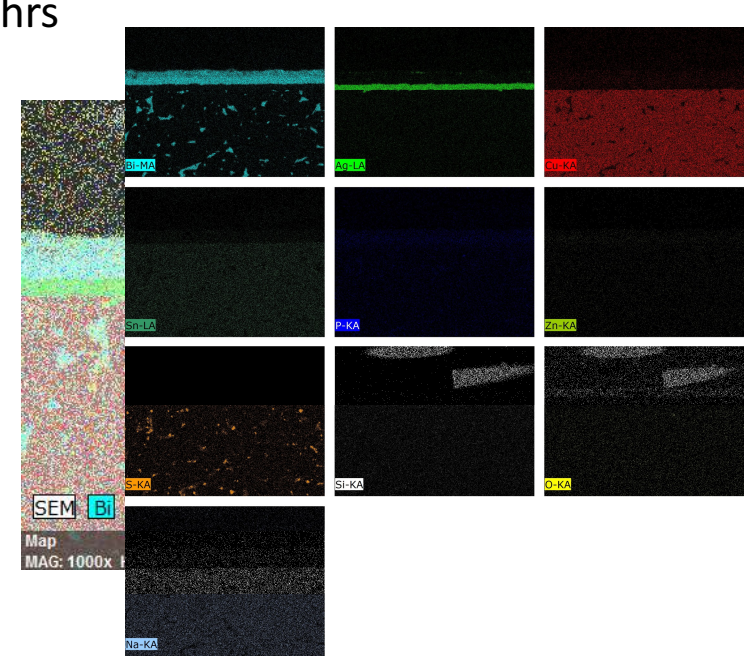

DAIDO METAL

99

DERM122 after 50,200 & 500 hrs
(NEW OIL 3000X)

29-10-2020

DAIDO METAL

100

50 hrs

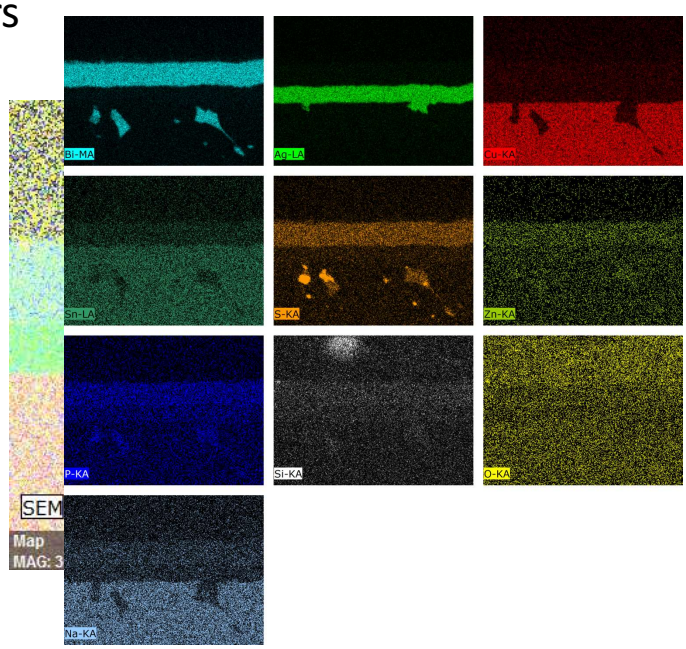

DAIDO METAL

101

200 hrs

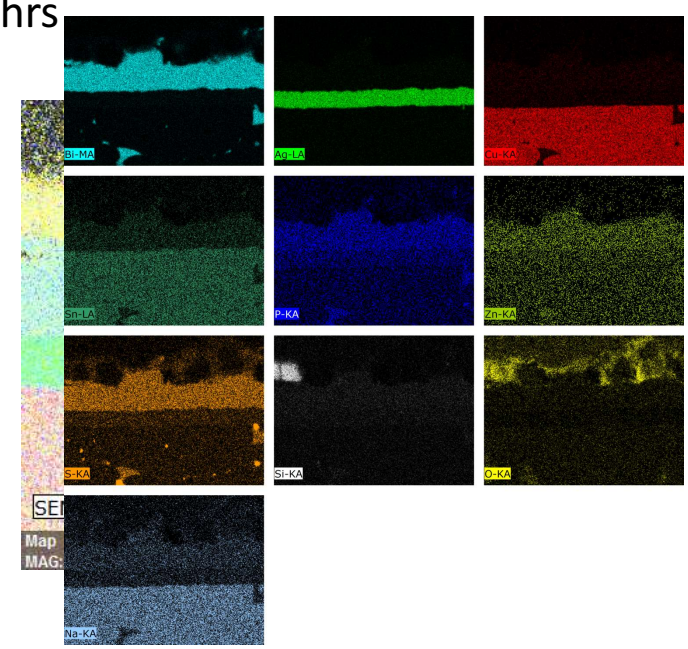

DAIDO METAL

102

500 hrs

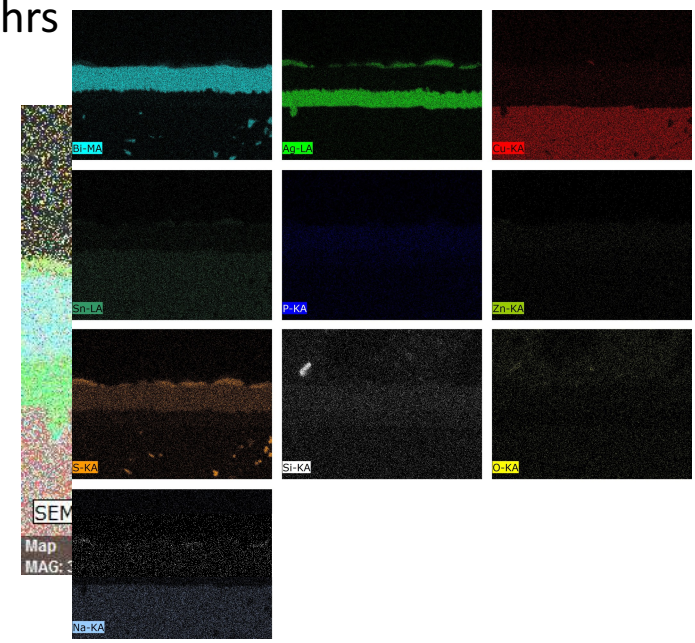

DAIDO METAL

103

DERM122 after 50,200 & 500 hrs
(USED OIL 3000X)

29-10-2020

DAIDO METAL

104

50 hrs

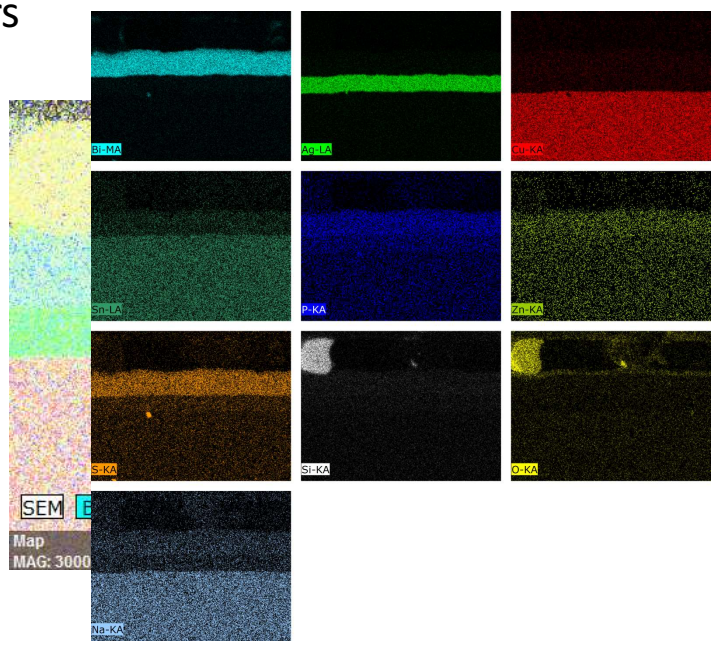

DAIDO METAL

105

200 hrs

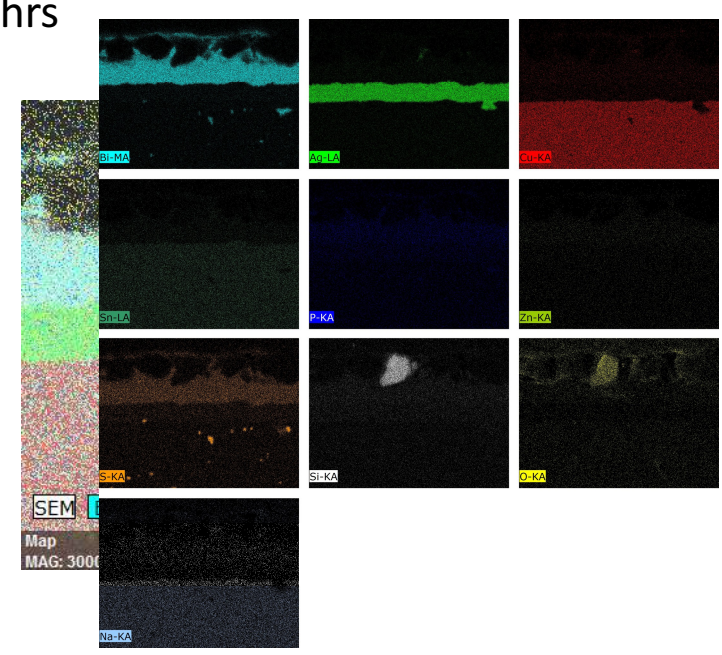

DAIDO METAL

106

500 hrs

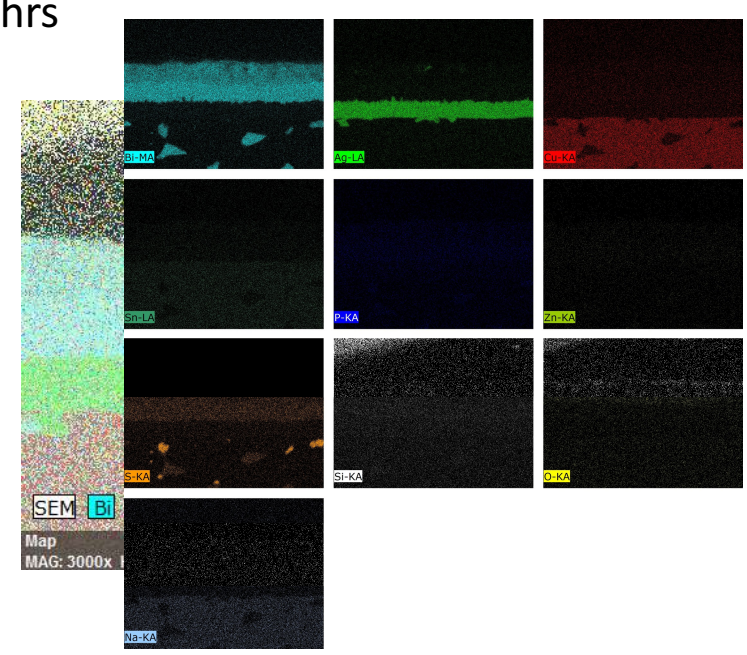

DAIDO METAL

107

DERM120

DAIDO METAL

108

APPEARANCE CHANGE (DERM120 after 50hrs)

	Before test	After test
New Oil	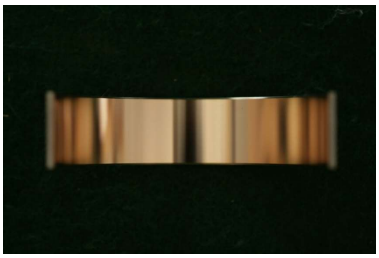	
Used Oil	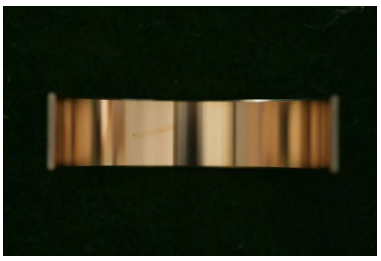	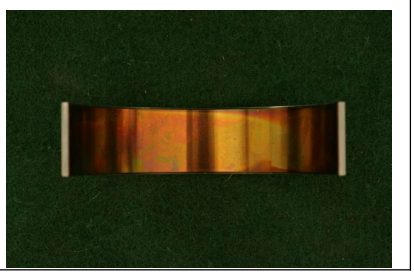

DAIDO METAL

109

APPEARANCE CHANGE (DERM120 after 200hrs)

	Before test	After test
New Oil	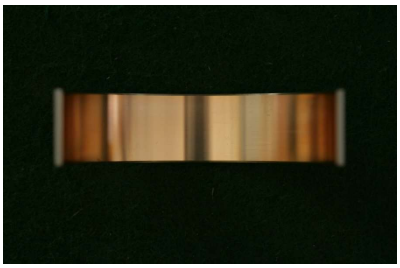	
Used Oil	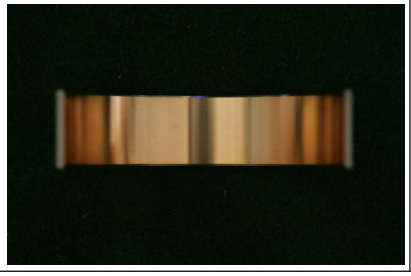	

DAIDO METAL

110

APPEARANCE CHANGE (DERM120 after 500hrs)

	Before test	After test
New Oil		
Used Oil		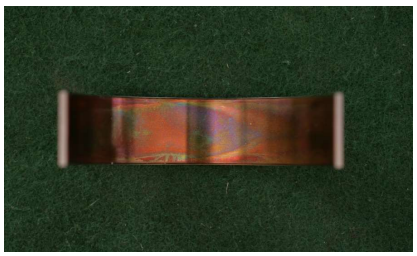

DAIDO METAL

111

CROSS-SECTIONAL ANALYSIS (DERM120 after 50,200,500 hrs)

New Oil (MAG: X300)

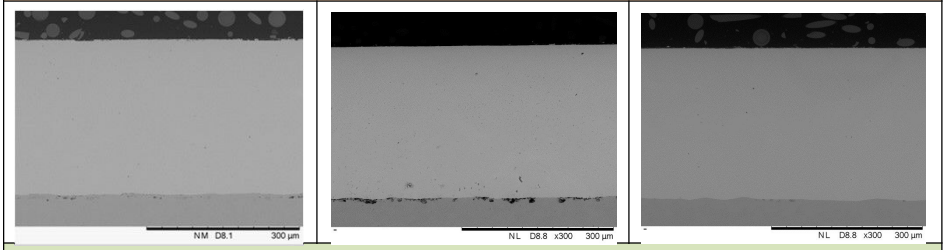

Used Oil (MAG: X300)

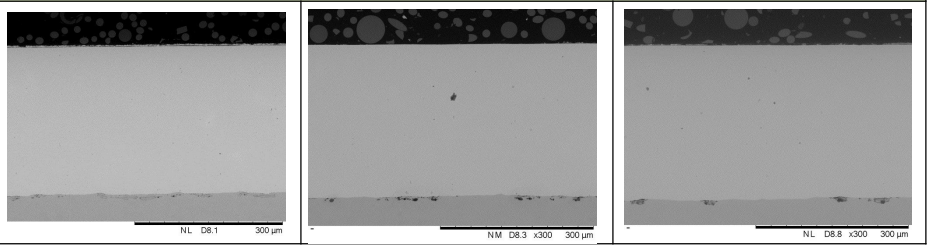

DAIDO METAL

112

CROSS-SECTIONAL ANALYSIS (DERM120 after 50,200,500 hrs)

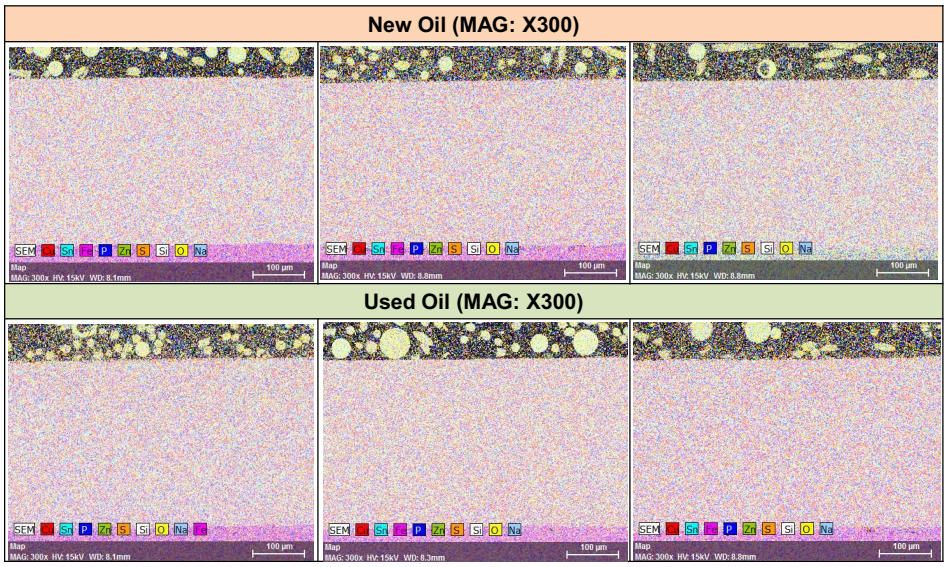

DAIDO METAL

113

DERM120 after 50,200 & 500 hrs
(NEW OIL 300X)

DAIDO METAL

114

50 hrs

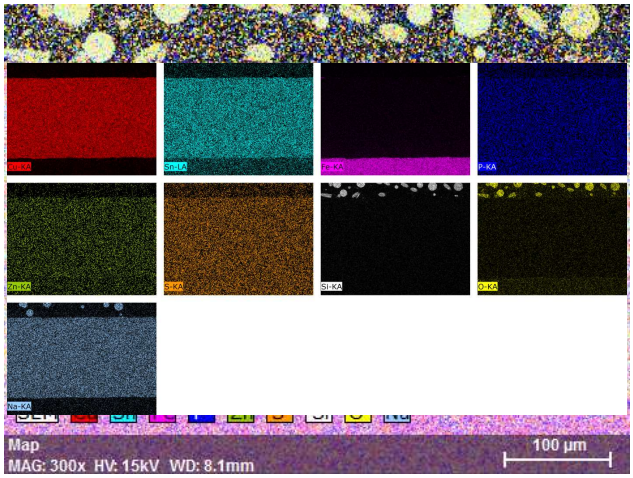

DAIDO METAL

115

200 hrs

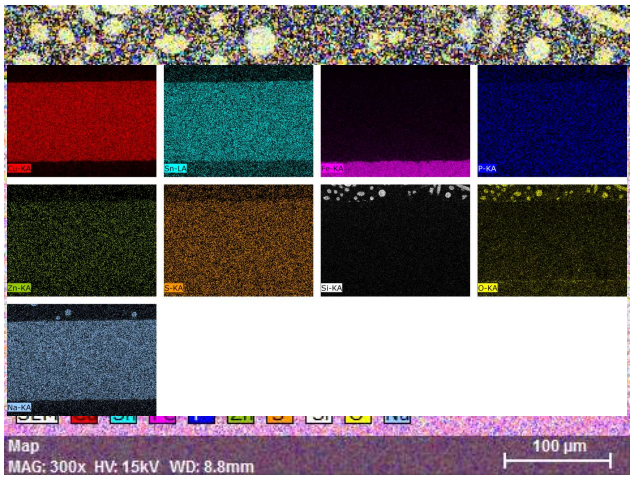

DAIDO METAL

116

500 hrs

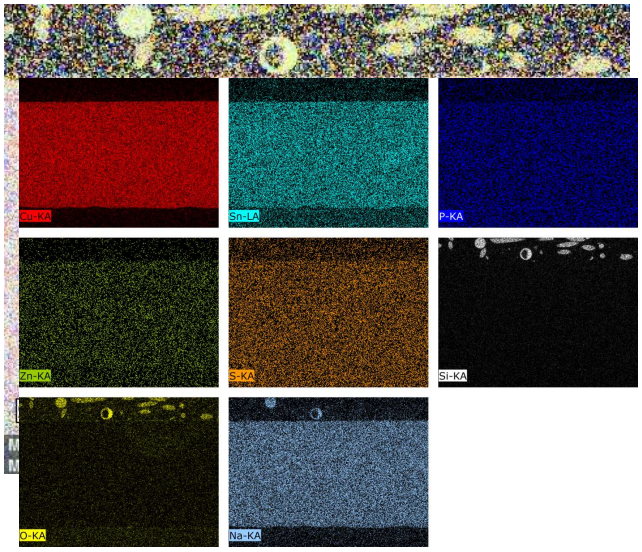

DAIDO METAL

117

DERM120 after 50,200 & 500 hrs
(USED OIL 300X)

29-10-2020

DAIDO METAL

118

50 hrs

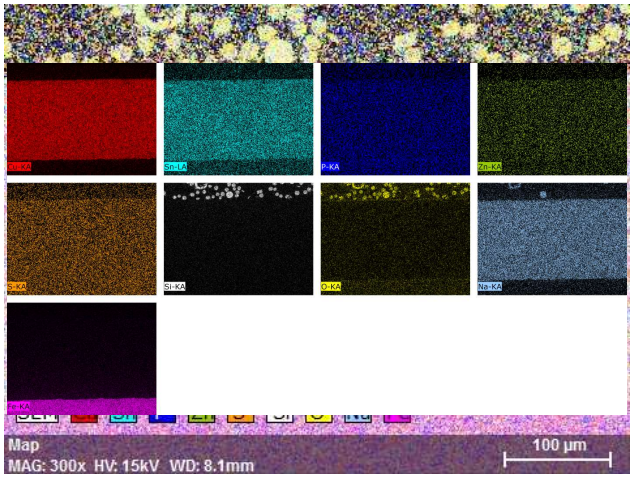

DAIDO METAL

119

200 hrs

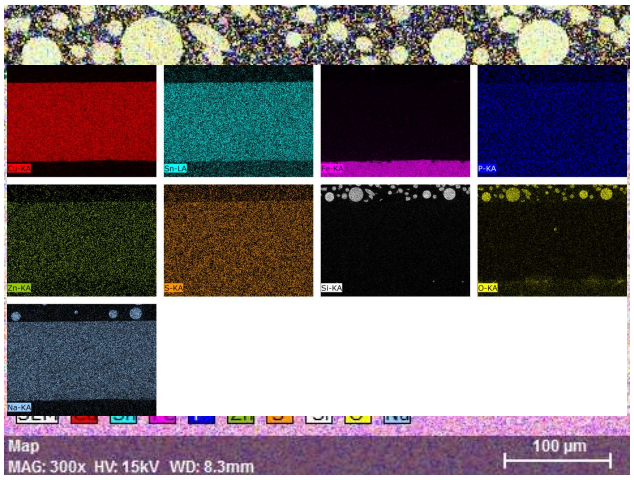

DAIDO METAL

120

500 hrs

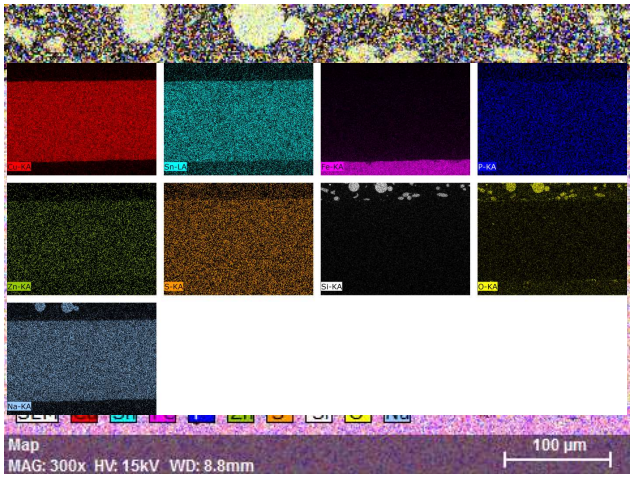

121

CROSS-SECTIONAL ANALYSIS (DERM120 after 50,200,500 hrs)

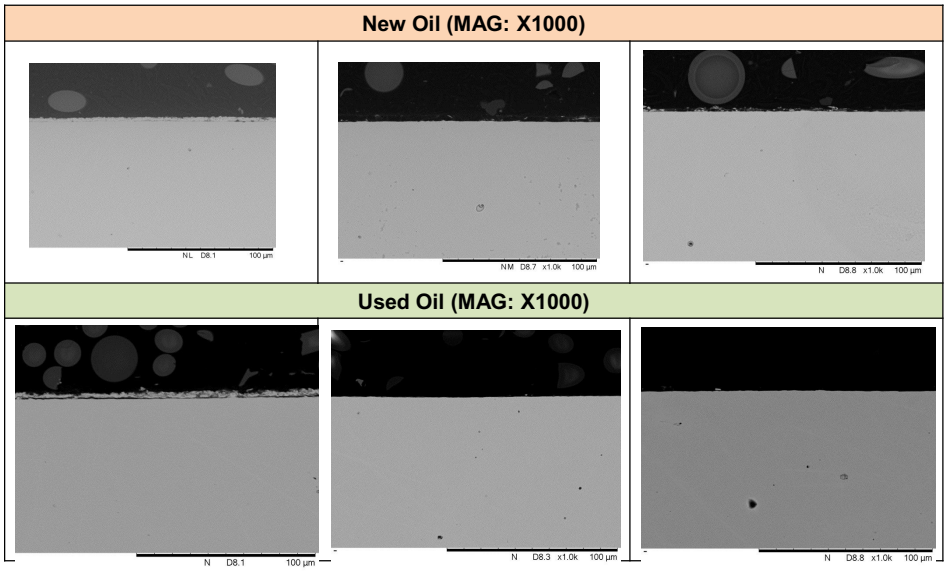

122

CROSS-SECTIONAL ANALYSIS (DERM120 after 50,200,500 hrs)

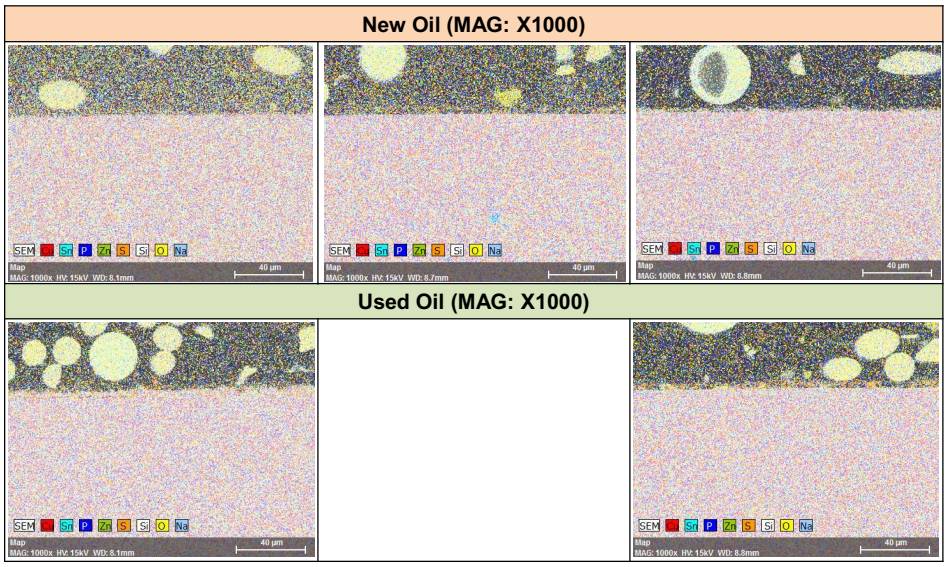

DAIDO METAL

123

DERM120 after 50,200 & 500 hrs
(NEW OIL 1000X)

DAIDO METAL

124

50 hrs

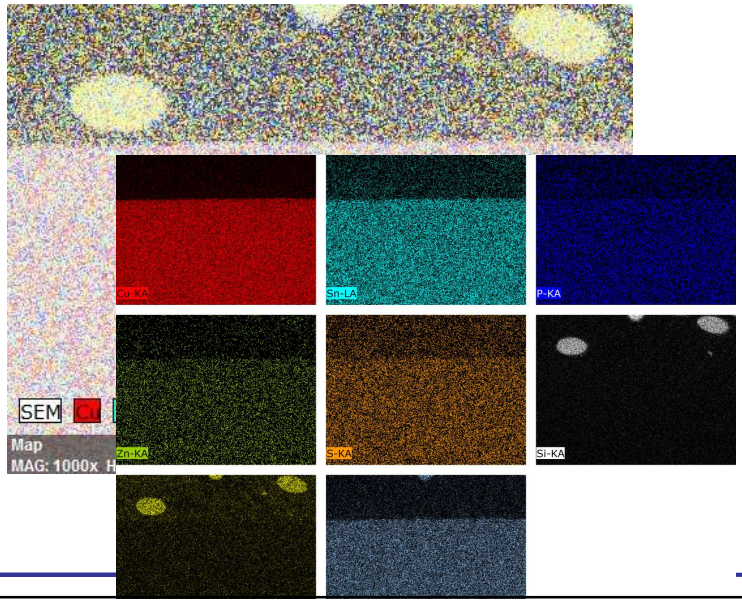

125

200 hrs

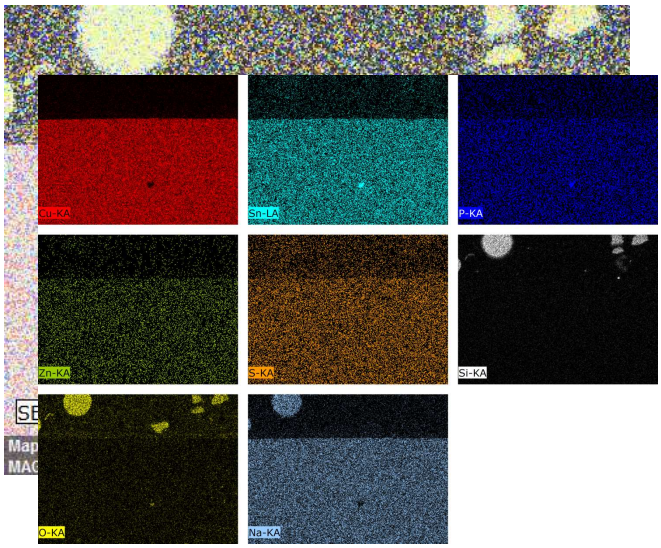

126

500 hrs

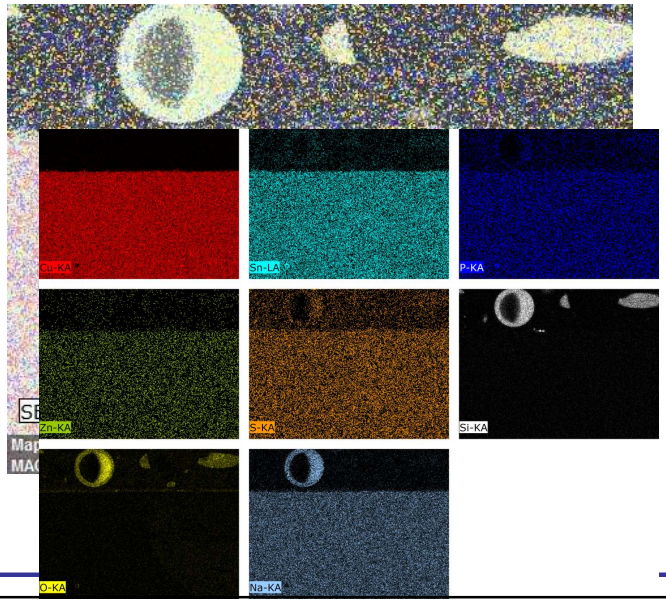

DAIDO METAL

127

DERM120 after 50,200 & 500 hrs
(USED OIL 1000X)

DAIDO METAL

128

50 hrs

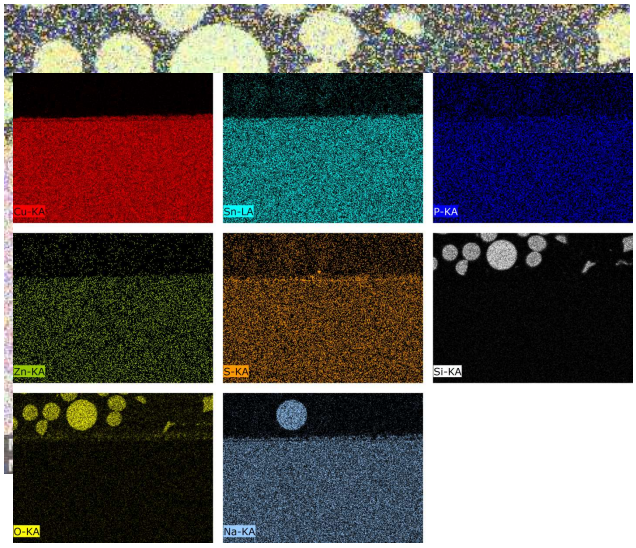

DAIDO METAL

129

500 hrs

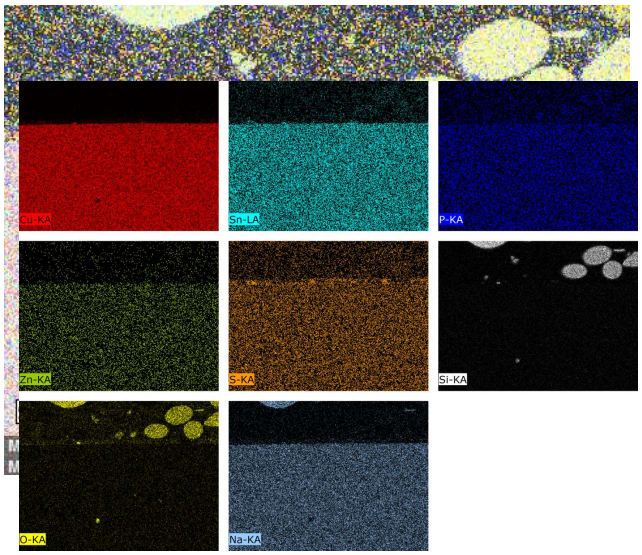

DAIDO METAL

130

CROSS-SECTIONAL ANALYSIS (DERM120 after 50,200,500 hrs)

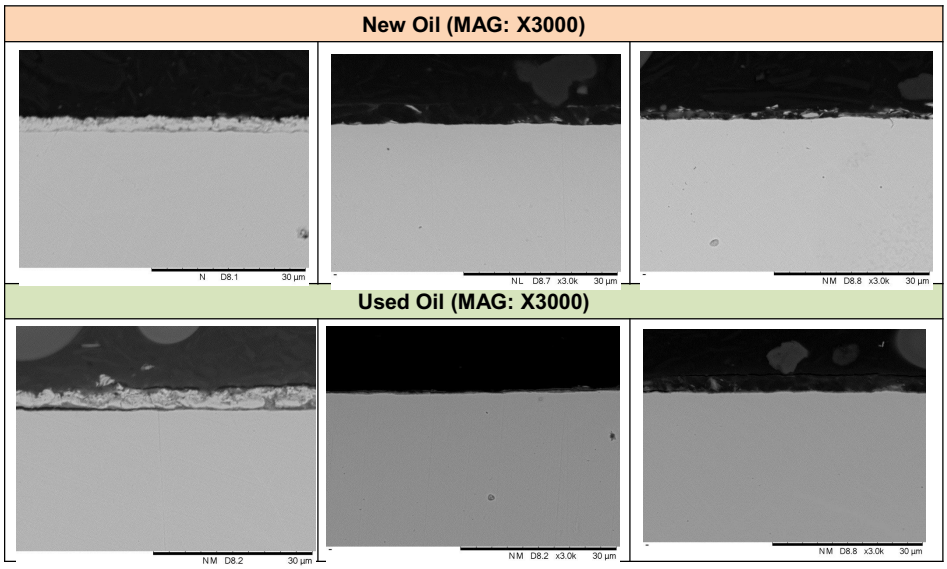

DAIDO METAL

131

CROSS-SECTIONAL ANALYSIS (DERM120 after 50,200,500 hrs)

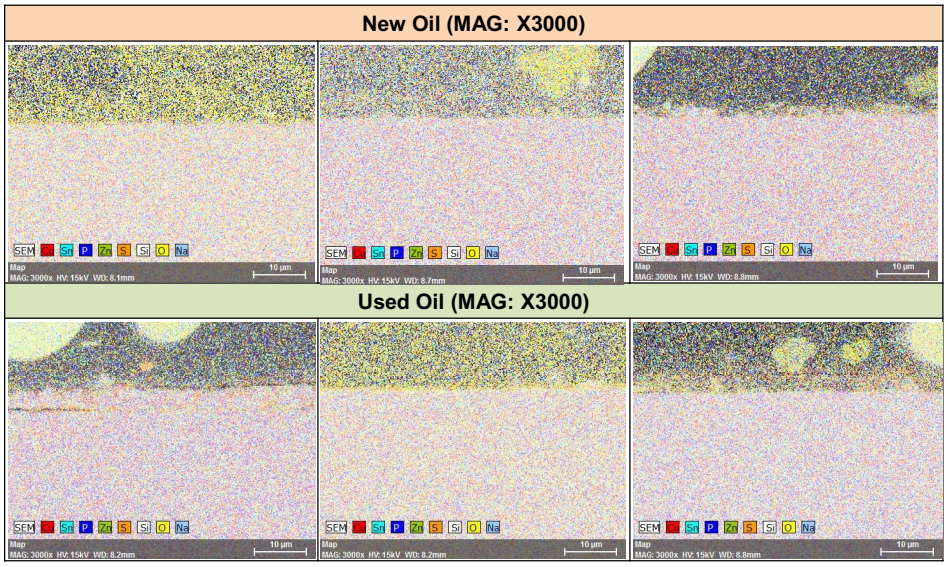

DAIDO METAL

132

50 hrs

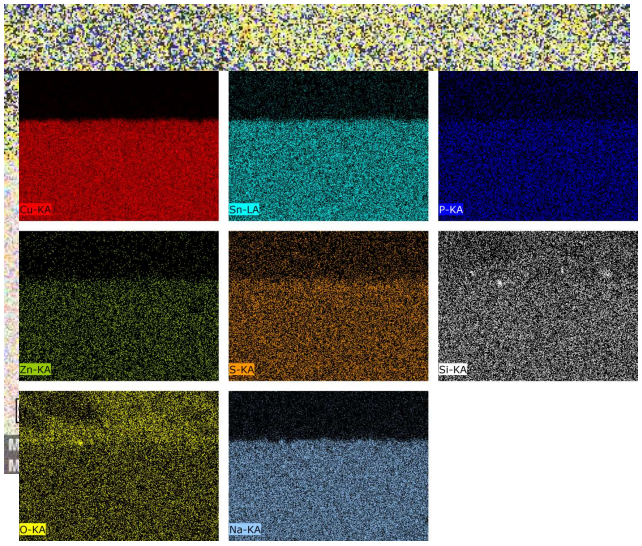

DAIDO METAL

133

200 hrs

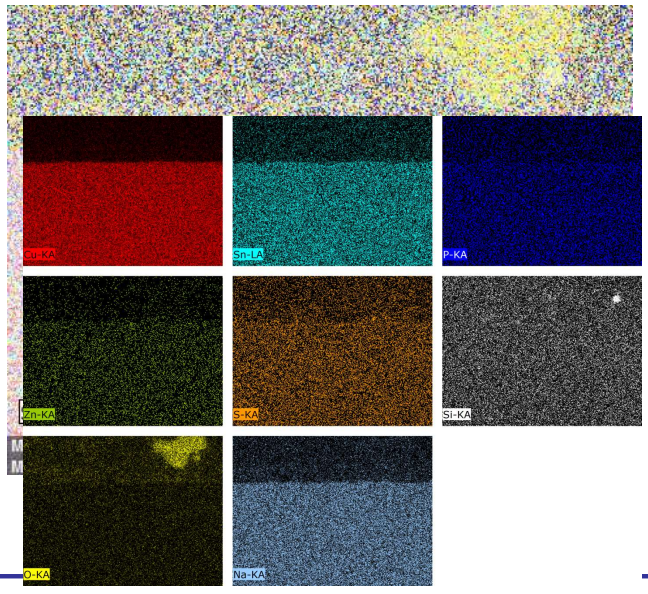

DAIDO METAL

134

500 hrs

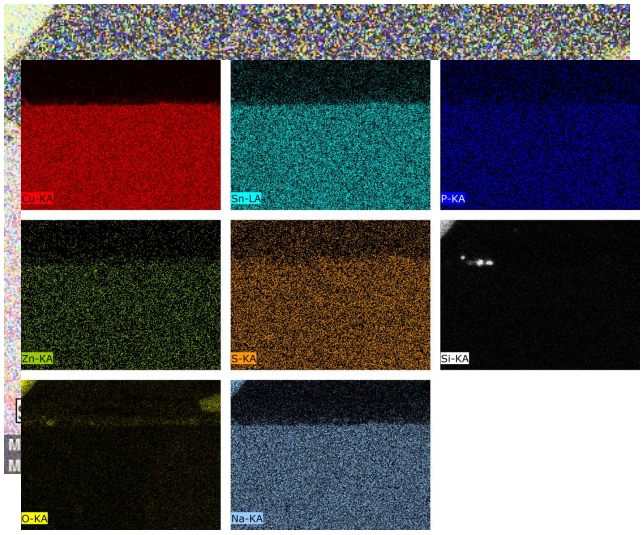

DAIDO METAL

135

DERM120 after 50,200 & 500 hrs
(USED OIL 3000X)

DAIDO METAL

136

50 hrs

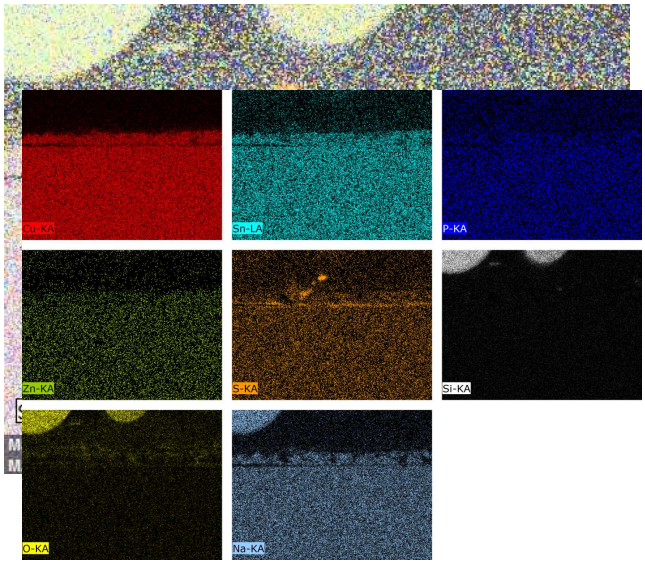

DAIDO METAL

137

200 hrs

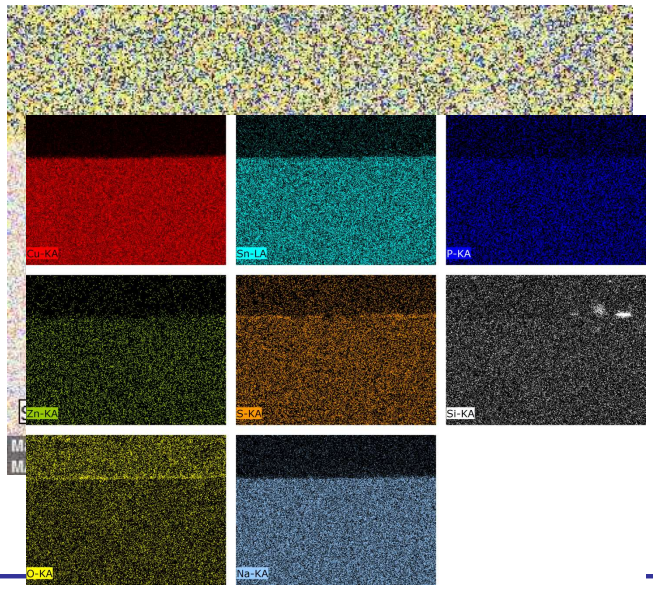

DAIDO METAL

138

500 hrs

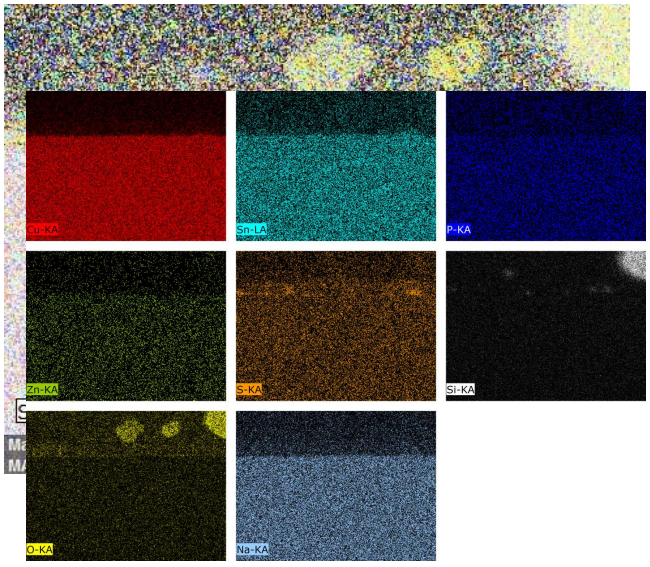

DAIDO METAL

139

WEIGHT LOSS MEASUREMENTS

Coatings	Pb-free		Pb-free		Pb-based	
µg	P2M (DERM 123)		PK1 (DERM 122)		P8(DERM 121)	
	New oil	Used oil	New oil	Used oil	New oil	Used oil
50h	-4	-45	-43	-186	-18	54
200h	-28	-30	-7	-130	90	148
500h	-32	-58	152	-139	75	240

DAIDO METAL

140

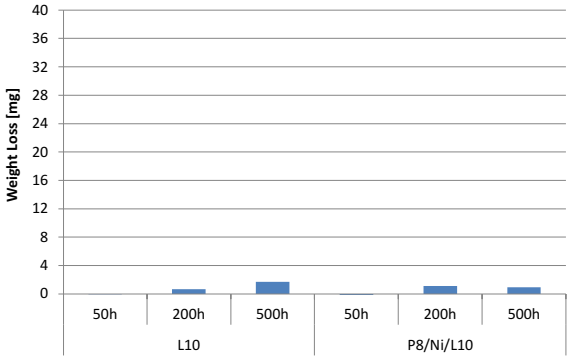

CROSS-SECTIONAL ANALYSIS (DERM123 after 50,200,500 hrs)

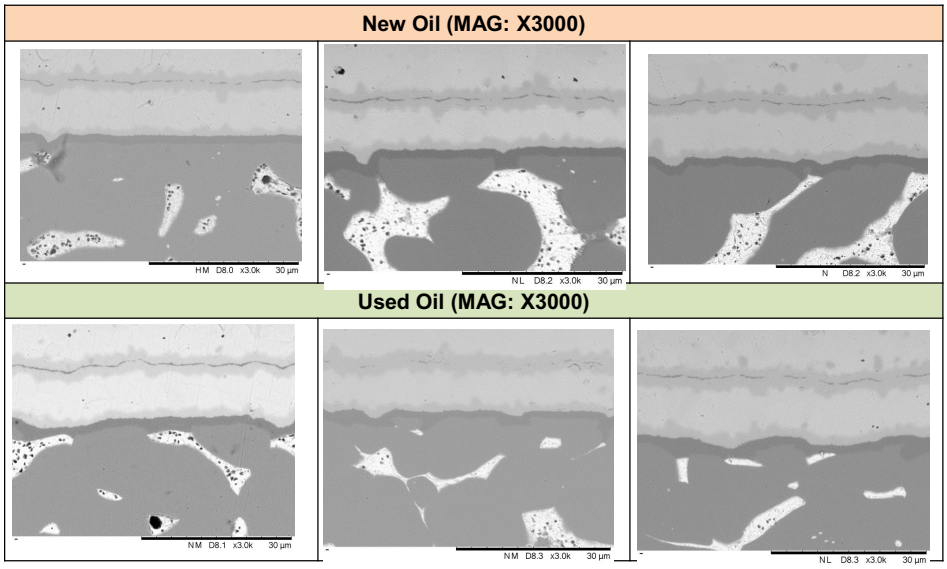

CROSS-SECTIONAL ANALYSIS (DERM123 after 50,200,500 hrs)

New Oil (MAG: X3000b)

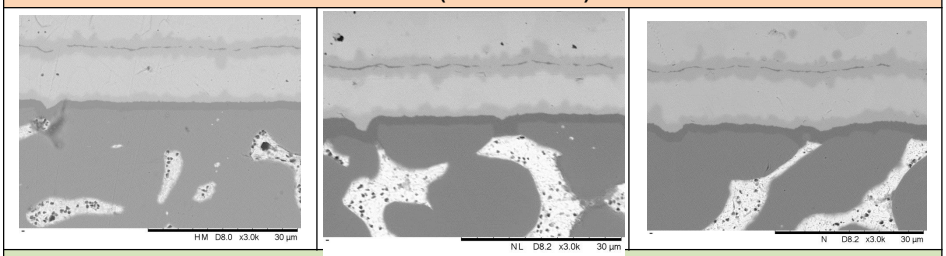

Used Oil (MAG: X3000)

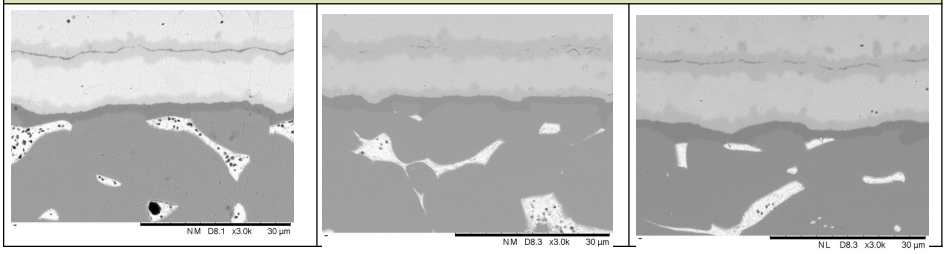

DAIDO METAL

143

Appendix 2 Test rig Pictures

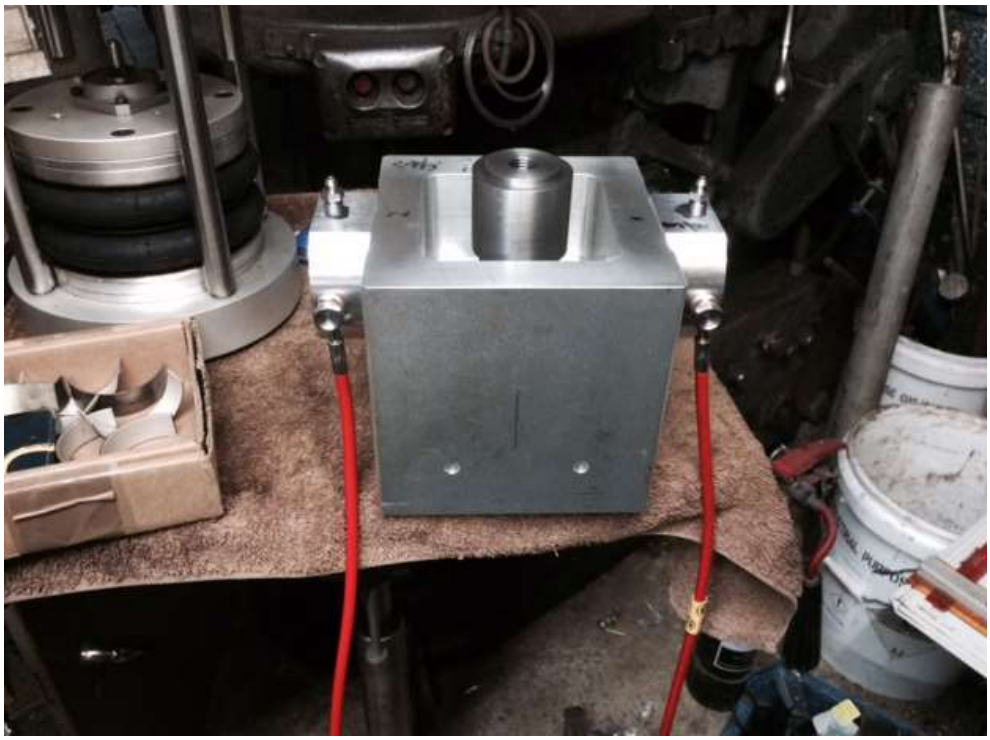

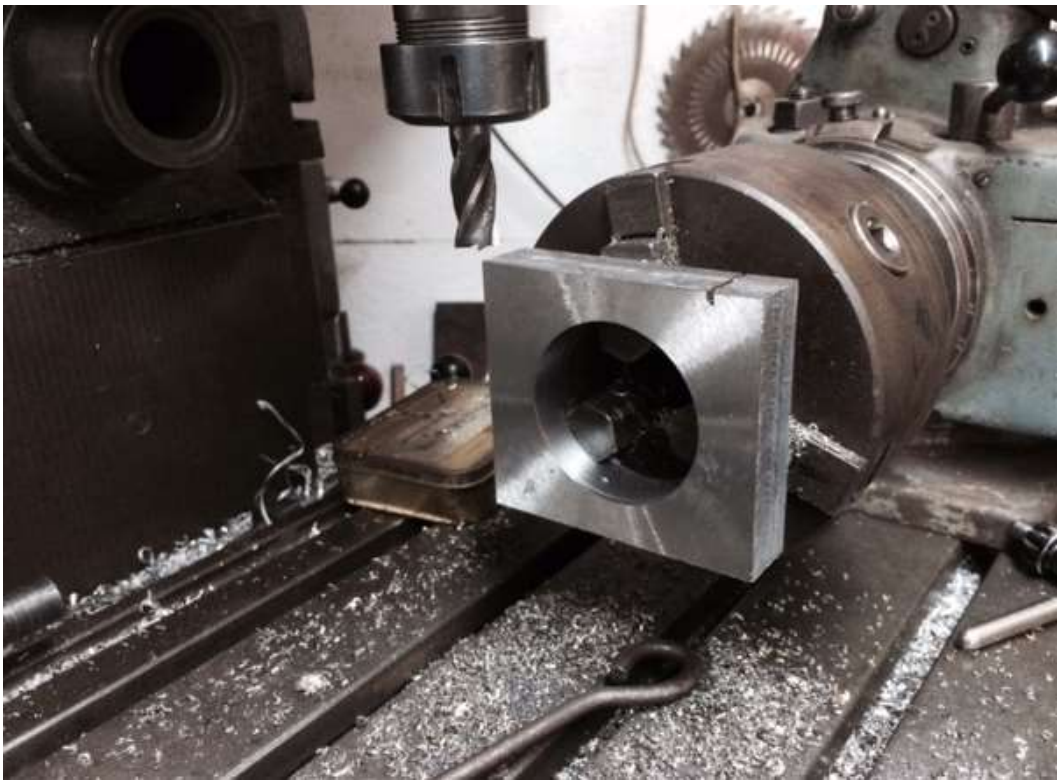

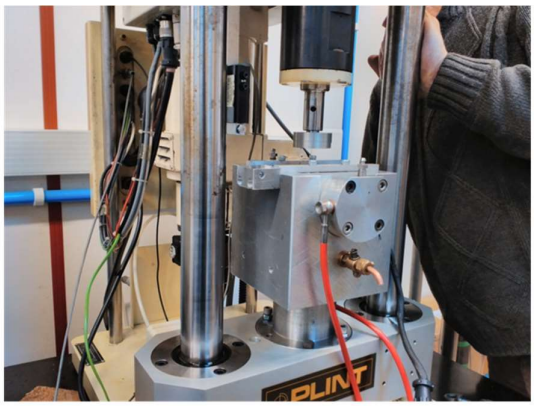
PLINT

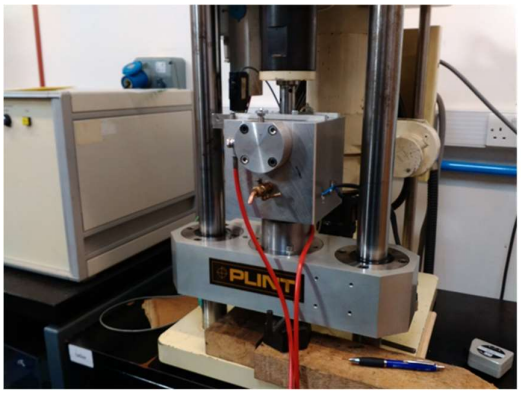
PLINT

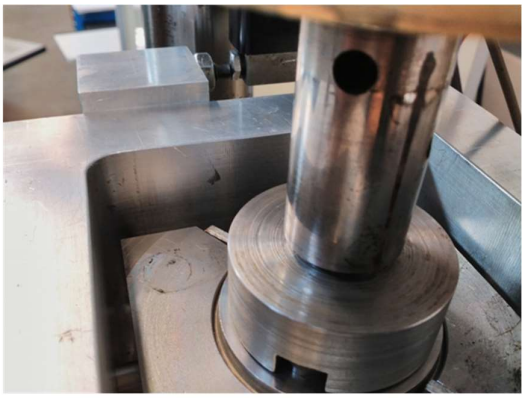

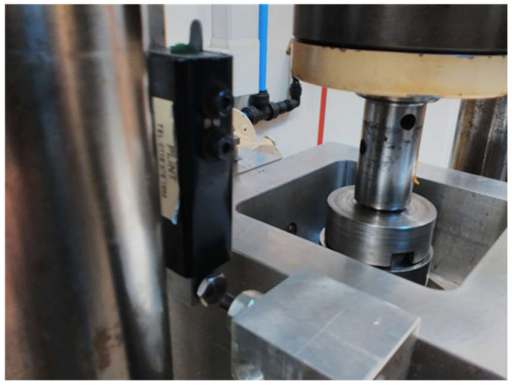

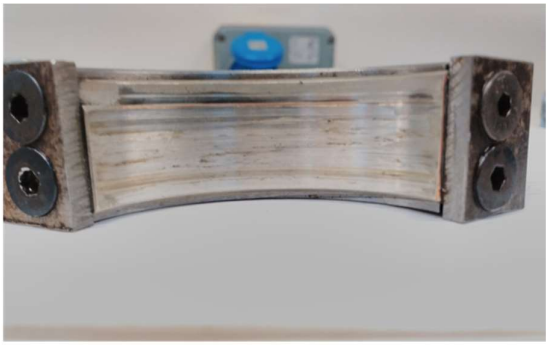

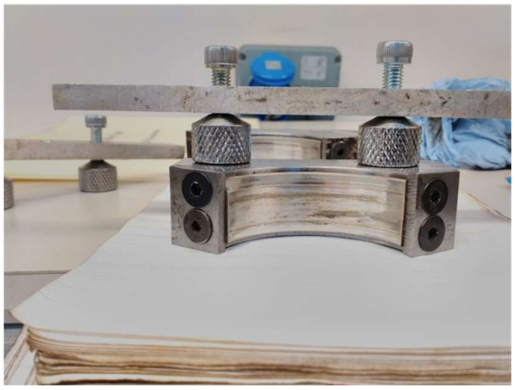


ERS LTD.
WOKINGHAM, ENG

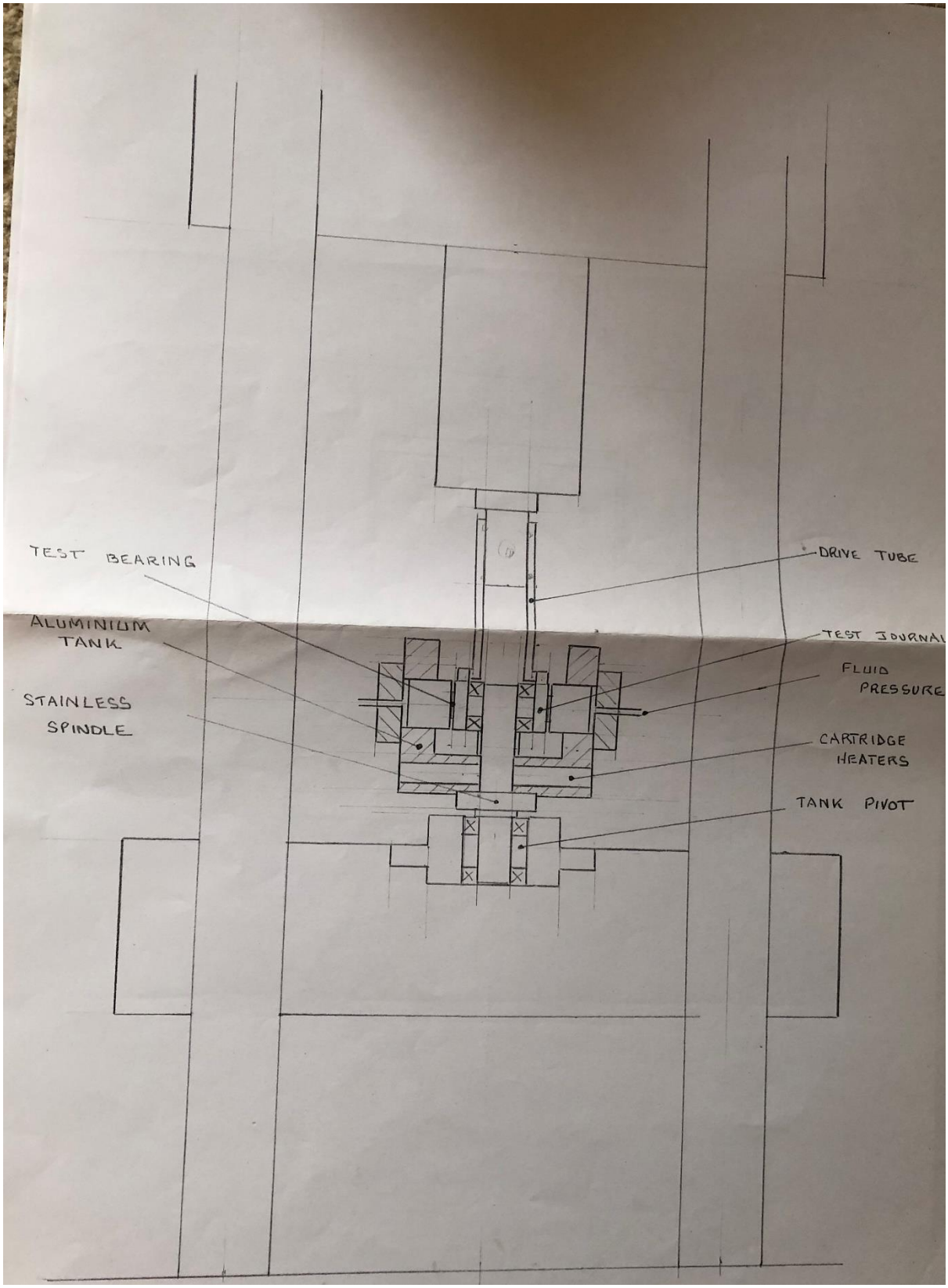
TEST BEARING
DRIVE TUBE
ALUMINIUM TANK
TEST JOURNAL
FLUID PRESSURE
STAINLESS SPINDLE
CARTRIDGE HEATERS
TANK PIVOT

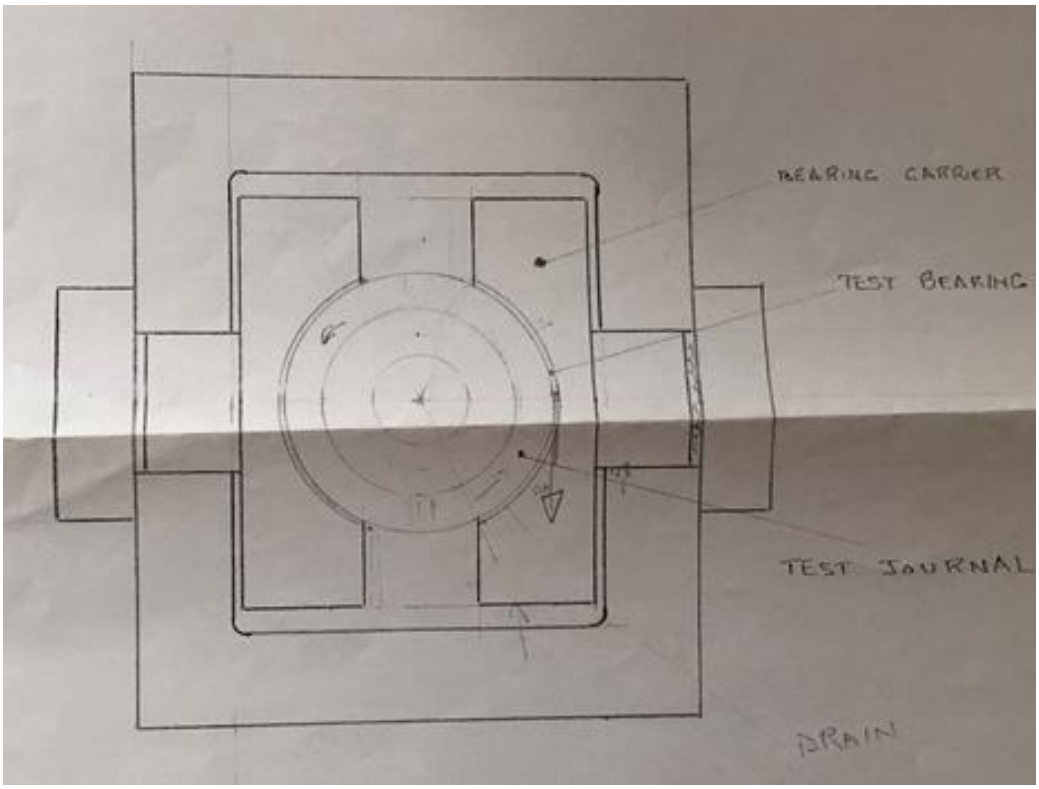
BEARING CARRIER
TEST BEARING
TEST JOURNAL
DRAIN

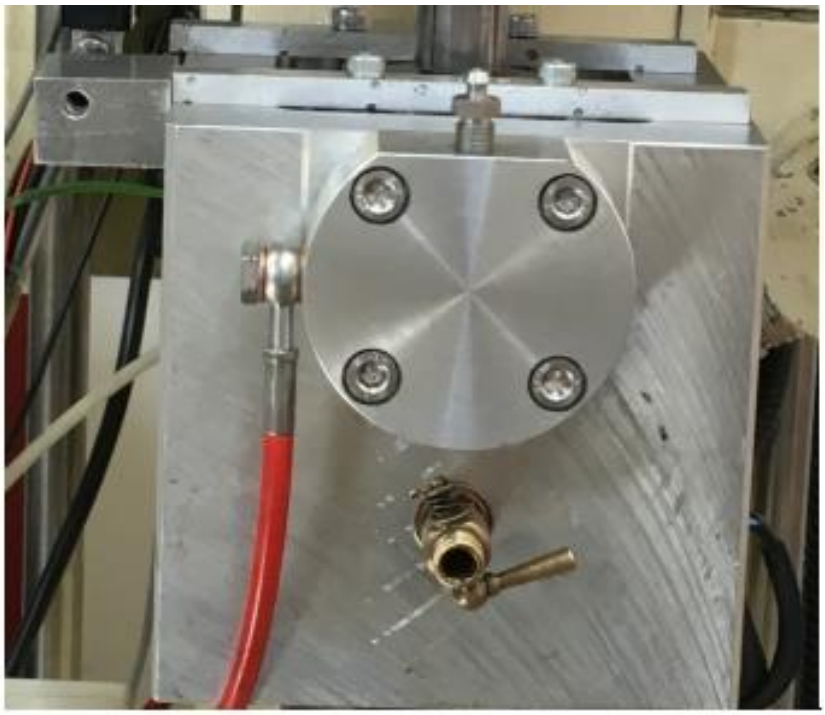

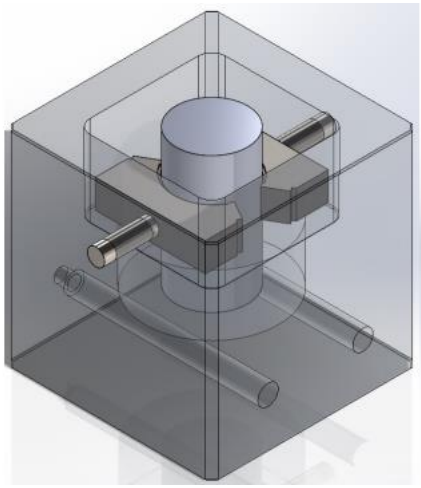

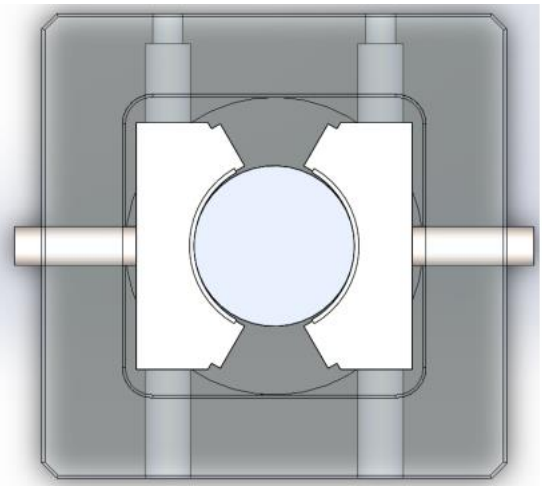

Appendix 3 Tribotest trials

1

Test -1

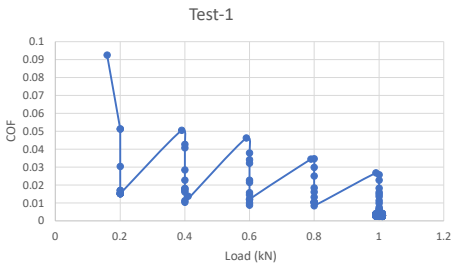

- Temperature: 120^{O}C
- Load : 1 kN (0.2 kN, 0.4 kN, 0.6 kN, 0.8 kN, 1 kN)
- Speed : 1068 rpm

2

Test -2

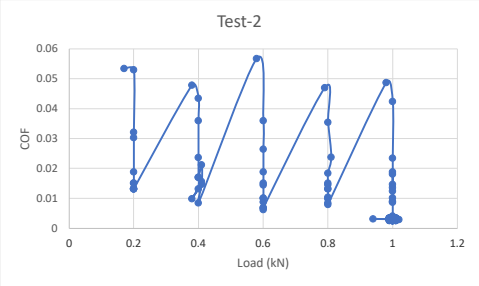

- Temperature-120^{O}C
- Load : 1 kN (0.2 kN, 0.4 kN, 0.6 kN, 0.8 kN, 1 kN)
- Speed : 1068 rpm

3

Test -3

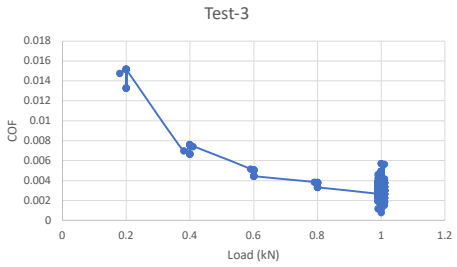

- Temperature : 80^{O}C
- Load : 1 kN (0.2 kN, 0.4 kN, 0.6 kN, 0.8 kN, 1 kN)
- Speed : 1068 rpm

4

Test-4

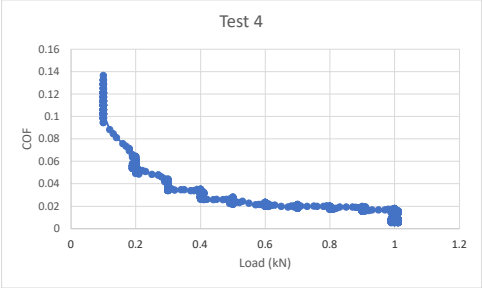

- Temperature : 100^{O}C
- Load : 1 kN (0.1 kN, 0.2 kN, 0.3 kN, 0.4 kN, 0.5 kN, 0.6 kN, 0.7 kN, 0.8 kN, 0.9 kN, 1 kN)
- Speed : 1068 rpm

5

Test -5

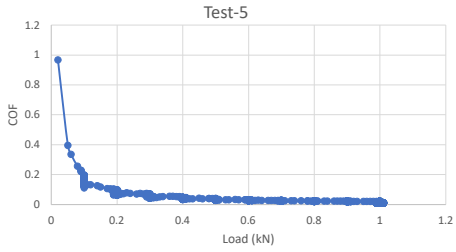

- Temperature : 120^{O}C
- Load : 1 kN (0.1 kN, 0.2 kN, 0.3 kN, 0.4 kN, 0.5 kN, 0.6 kN, 0.7 kN, 0.8 kN, 0.9 kN, 1 kN)
- Speed : 1068 rpm

6

Test-10

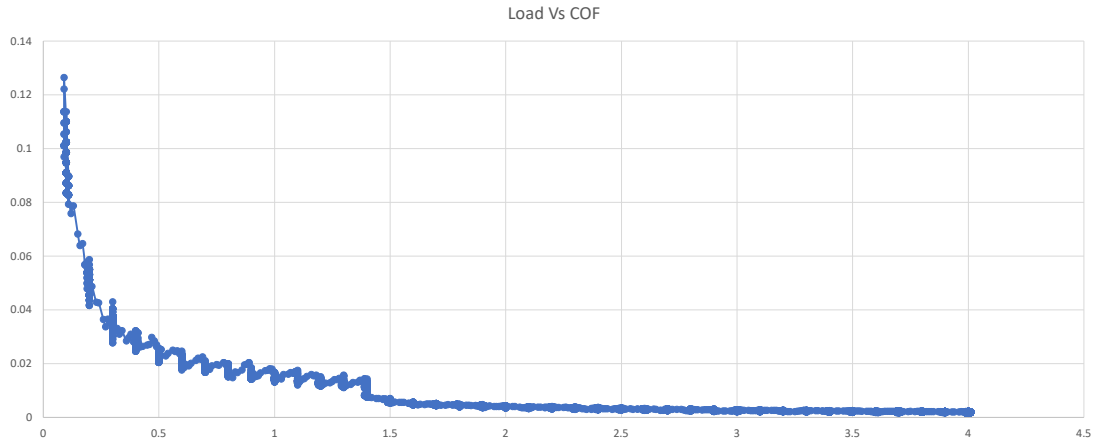

7

Time Vs Torque

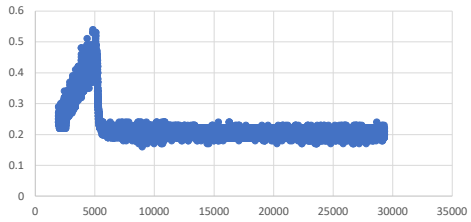

Time Vs Temperature

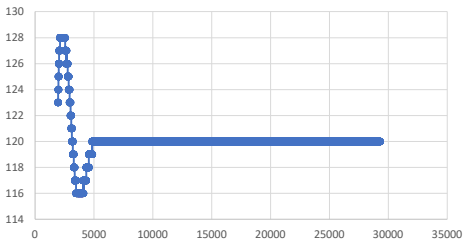

8

Test-9

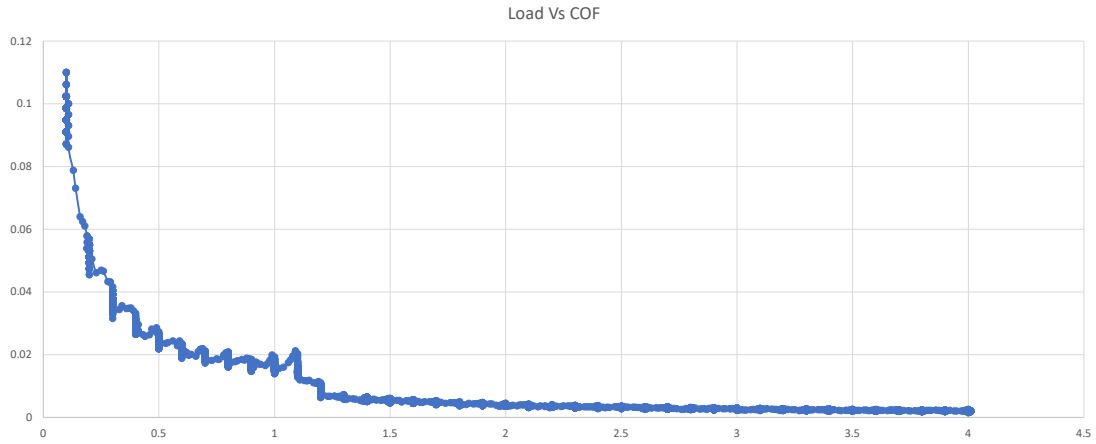

9

Time Vs Torque

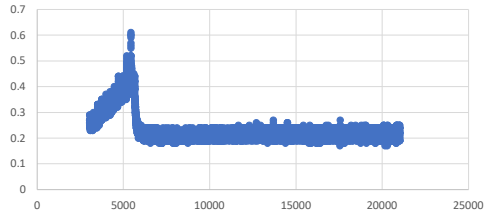

Time Vs Temperature

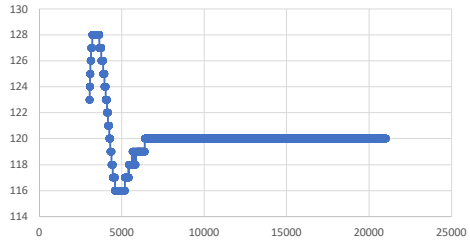

10

Test-6

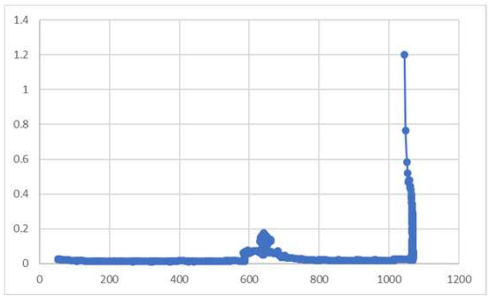

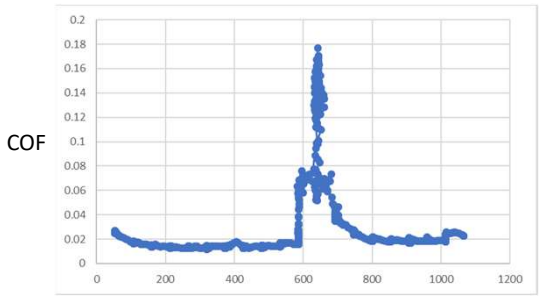

11

Test-6

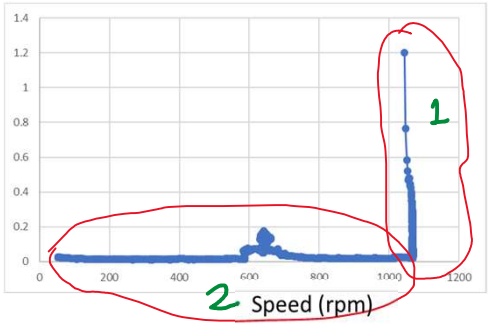

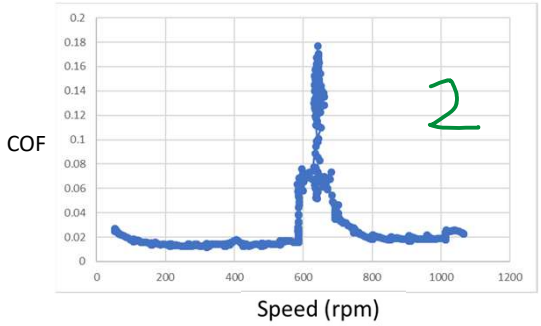

1.

Load	100 N to 1 kN (100 N,200 N, 300 N, 400 N, 500 N, 600 N, 700 N, 800 N, 900 N, 1 kN)
Speed	1000 rpm
Temperature	120°C

2.

Load	1 kN
Speed (rpm)	1000 to 50 rpm (1000, 950, 900, 850, 800, 750, 700, 650, 600, 550, 500, 450, 400, 350, 300, 250, 200,150, 100, 50)
Temperature	120°C

12

Test-7

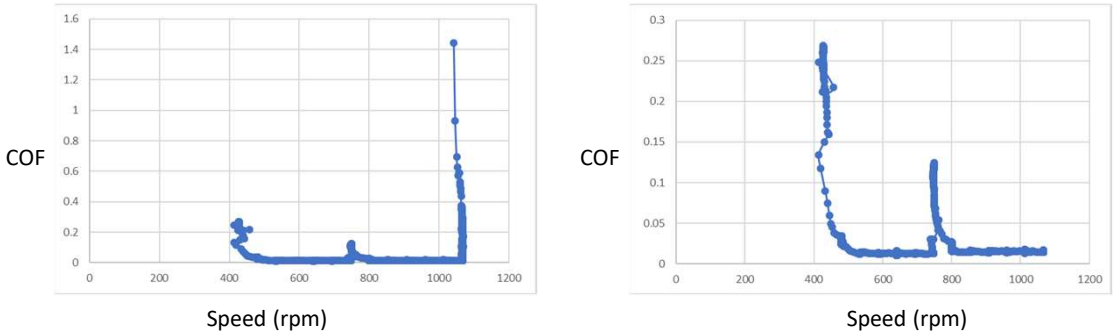

13

Test-7

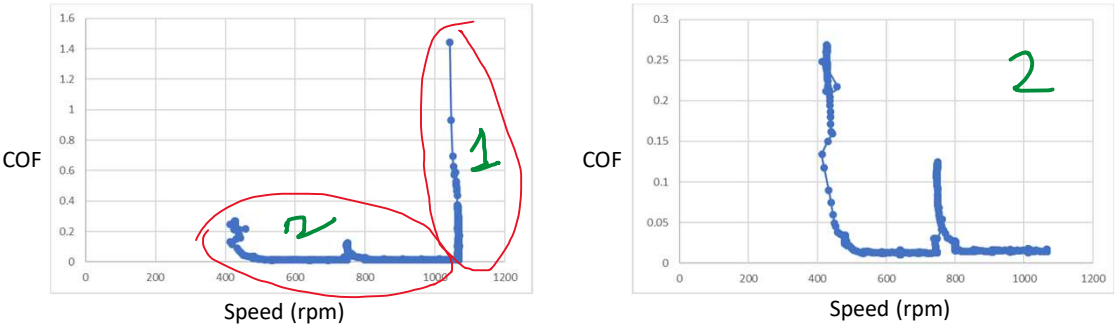

1.

Load	**100 N to 1 kN (100 N,200 N, 300 N, 400 N, 500 N, 600 N, 700 N, 800 N, 900 N, 1 kN)**
Speed	1000 rpm
Temperature	120°C

2.

Load	**1 kN**
Speed (rpm)	1000 to 400 rpm (1000, 950, 900, 850, 800, 750, 700, 650, 600, 550, 500, 450, 400, seized at 400 rpm)
Temperature	120°C

14

Tribotest-SEM images of unloaded and loaded material

DERM121 Pb based overlay

Unloaded material

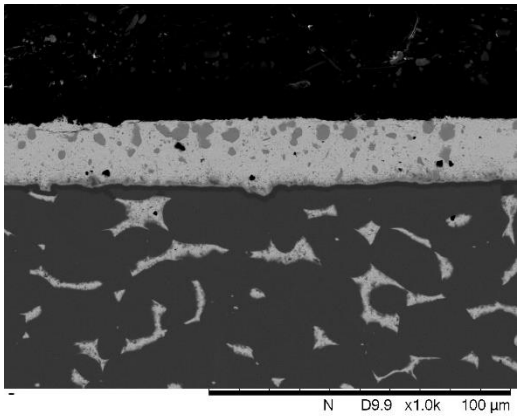

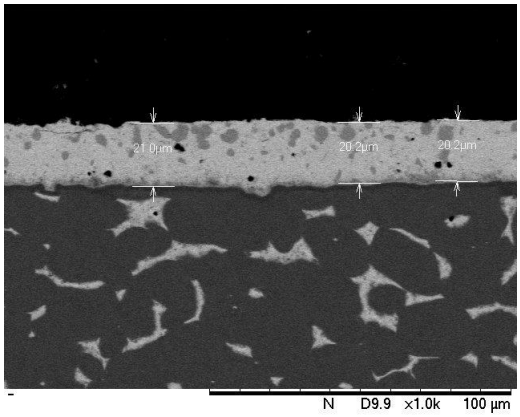

Loaded material

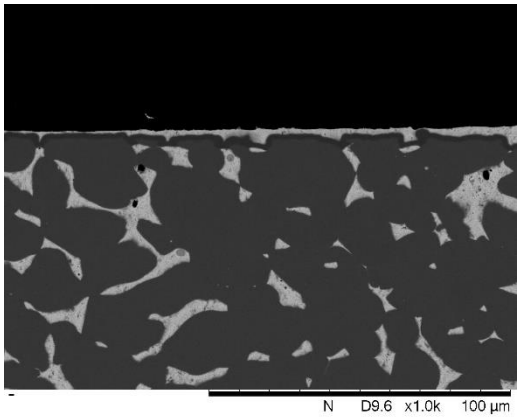

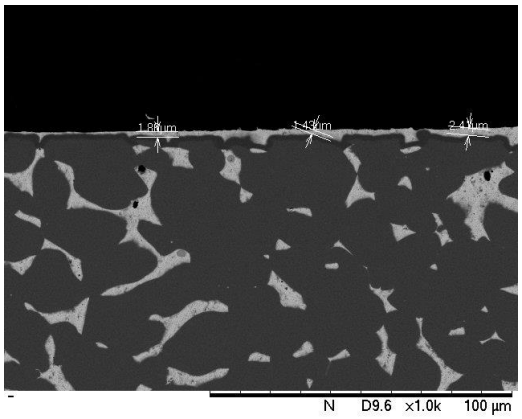

DERM123 -Lead free overlay

Unloaded material

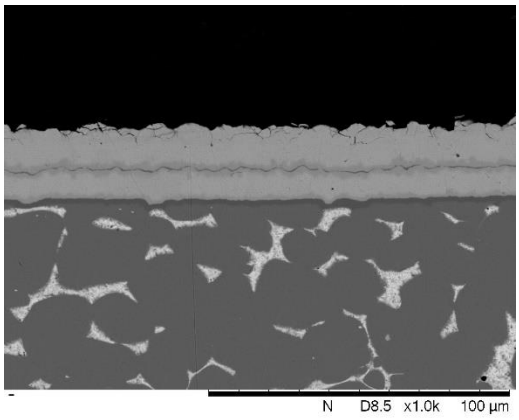

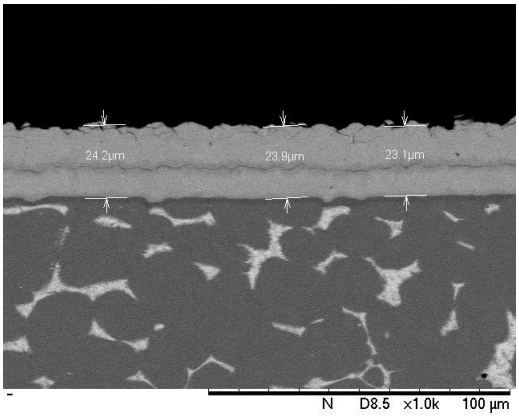

Loaded material